國立臺灣大學醫學院轉譯醫學博士學位學程

博士論文

Ph.D. Program of Translational Medicine

College of Medicine

National Taiwan University

Doctoral Dissertation

以分子影像探討神經母細胞瘤的腫瘤行為特徵

Characterization of Neuroblastoma Tumor Behavior by Molecular Imaging

劉彥麟

Yen-Lin Liu

指導教授： 林凱信教授　Kai-Hsin Lin, MD

Advisors　　許文明教授　Wen-Ming Hsu, MD, PhD

廖永豐博士　Yung-Feng Liao, PhD

中華民國 105 年 6 月

June 2016

國立臺灣大學（碩）博士學位論文
口試委員會審定書

論文中文題目

以分子影像探討神經母細胞瘤的腫瘤行為特徵

論文英文題目

Characterization of Neuroblastoma Tumor Behavior
by Molecular Imaging

本論文係劉彥麟君（學號 D99456003）在國立臺灣大學 轉譯醫學博士學位學程 完成之博士學位論文，於民國 105 年 6 月 8 日承下列考試委員審查通過及口試及格，特此證明

口試委員：

_____（簽名）

（指導教授）

系主任、所長 _____（簽名）

（是否須簽章依各院系所規定）

Acknowledgement 誌謝

中文摘要

神經母細胞瘤（neuroblastoma；NB）起源於交感神經，好發於嬰幼兒。過半病童診斷時已有多處轉移，預後不佳。因此，臨床上需使用多種影像檢查來進行診斷、分期與追蹤。本研究欲以分子影像探討神經母細胞瘤的腫瘤行為特徵。首先，我們運用氟多巴正子造影（^{18}F-FDOPA PET）在身體各部位診斷神經母細胞瘤；其敏感度達 97.6%（95%信賴區間 87.4%–99.9%），特異性 87.5%（47.3%–99.7%），可與目前黃金標準的 MIBG 核子醫學掃描（^{123}I-MIBG scintigraphy）或去氧葡萄糖正子造影（^{18}F-FDG PET）互補。接下來，由 2007 年至 2014 年新診斷神經母細胞瘤的個案中，分析主要腫瘤 FDG 與 FDOPA 正子影像的最大標準吸收值（SUV_{max}），發現年齡較大、分期較嚴重、MYCN 放大等較惡性特徵者，皆具有 FDG 吸收值較高、FDOPA 吸收值較低的現象（所有 P 值 < 0.02）。利用接收者操作特徵曲線（receiver operating characteristics）統計，我們將 FDG 吸收值 ≥ 3.31 及 FDOPA 吸收值 < 4.12 定義為「正子影像極高危險群（PET ultra-high-risk）」，可區分出節段性染色體變化或 *MYCN* 致癌基因放大等高度惡性的基因體類型，為無事件存活率較差的獨立預測因子（多變數分析之風險比值 [HR] = 4.9 [1.9–30.1]，P = 0.012），且較不易以外科手術完整切除（gross total resection；切除率 46%相對於 100%，P = 0.04）。此外，FDG 與 FDOPA 吸收值的比值（G:D）與糖解作用 *HK2* 激酶基因表現呈正相關（Spearman's ρ = 0.86，P < 0.0001）、與多巴代謝酵素 *DDC* 基因表現呈負相關（ρ = -0.58；P = 0.02），表示 PET-UHR 腫瘤很可能具有較強的糖解作用活性及較差的神經代謝分化。最後，我們整合小動物超音波與正子造影，以 Th-*MYCN* 基因轉殖小鼠發展臨床前試驗平臺，發現其腫瘤 75%為 FDG 吸收值較高、FDOPA 吸收值較低，與人類神經母細胞瘤帶有 *MYCN* 放大者相似。利用此影像評估與追蹤平臺，我們驗證了 BRD4 表觀基因標靶藥物可強力抑制 Th-*MYCN* 小鼠腫瘤生長，但維他命 A 酸分化治療則無效。總結來說，FDG 與 FDOPA 功能性分子影像可評估神經母細胞瘤的腫瘤行為、補強現有的危險群分類系統、發展為重要的臨床前評估工具，未來可望轉譯為運用分子影像發展個人化標靶治療的新穎治療策略。

關鍵詞：兒童癌症、神經母細胞瘤、正子造影、分子影像、^{18}F-FDOPA、^{18}F-FDG、TH-MYCN 基因轉殖鼠

Abstract

Neuroblastoma (NB) is a devastating tumor that usually occurs in young children. More than 50% of patients are diagnosed with metastatic diseases or other high-risk features, who suffer from a dismal prognosis. Therefore, a multitude of imaging studies are required for the staging and surveillance of NB. This study aims to characterize NB tumor behavior using molecular imaging modalities. First, we showed that positron emission tomography (PET) with ^{18}F-fluoro-dihydroxyphenylalanine (FDOPA), a radiolabeled amino acid targeting catecholamine metabolism, had a sensitivity of 97.6% (87.4%–99.9%) and a specificity of 87.5% (47.3%–99.7%) and may compliment current ^{123}I-metaiodobenzylguanidine (^{123}I-MIBG) and ^{18}F-fluorodeoxyglucose (FDG) PET scans. Next, NB patients undergoing paired FDG and FDOPA PET scans at diagnosis during 2007–2014 (N = 42; median age, 2.0 years; 28 boys and 14 girls;) were evaluated for the maximum standardized uptake value (SUV$_{max}$) of FDG or FDOPA by the primary tumor, revealing that NB with older age, advanced stages, or *MYCN* amplification showed higher FDG and lower FDOPA SUV$_{max}$ (all P < 0.02). Receiver operating characteristics analysis identified FDG SUV$_{max}$ ≥ 3.31 and FDOPA SUV$_{max}$ < 4.12 as an ultra-high-risk feature (PET-UHR) that distinguished the most unfavorable genomic types, *i.e.* segmental chromosomal alterations and/or *MYCN* amplification, at a sensitivity of 81.3% (54.4%–96.0%) and a specificity of 93.3% (68.1%–99.8%). Considering with age, stage, *MYCN* status, and anatomical image-defined risk factor, PET-UHR was an independent predictor of inferior event-free survival (multivariate hazard ratio, 4.9 [1.9–30.1]; P = 0.012) and was associated lower likelihood of gross total resection of the main tumor (46% *vs*. 100%; P = 0.04). Meanwhile, the ratio between FDG and FDOPA SUV$_{max}$ (G:D) correlated positively with hexokinase 2 (*HK2*; Spearman's ρ = 0.86, P < 0.0001) and negatively with DOPA decarboxylase (*DDC*; ρ =

-0.58, $P = 0.02$) gene expression levels, suggesting higher glycolytic activity and less catecholaminergic differentiation in NB tumors taking up higher FDG and lower FDOPA. Finally, we incorporated small-animal ultrasound screening and PET imaging to build up a preclinical trial platform. We characterized the tumor latency and progression in the hemizygous Th-*MYCN* mice, a genetically-engineered mouse model of NB. In parallel to human NB with *MYCN* amplification, the majority (75%) of Th-*MYCN* murine NB tumors showed higher uptake of FDG and lower uptake of FDOPA. Using the imaging platform, We have validated the potent therapeutic effect of epigenetic inhibition of MYCN transcription by targeting the bromodomain BRD4 reader protein, while 13-*cis*-retinoic acid showed no anti-tumor activity in this model. In conclusion, the functional FDG and FDOPA PET imaging characterizes the NB tumor behavior; complements the current risk stratification systems of NB; and serves as an important part of preclinical trails. The results of this study can be translated into critical clinical knowledge of molecular imaging of NB, and may pave the way of individualized target therapy through molecular imaging.

Key Words: Childhood cancer; neuroblastoma; positron emission tomography; molecular imaging; ^{18}F-FDG; ^{18}F-FDOPA; TH-*MYCN* transgenic mice

Table of Contents 目錄

Table Contents 表目錄

Figure Contents 圖目錄

1. Introduction 緒論

Neuroblastoma (NB) is a devastating disease that mostly occurs in infants and young children.[1] Local invasion or distant metastases of NB causes life-threatening crisis in children. As an embryonal tumor originating from the precursor cells of the sympathetic nervous system, primary NB may arise from the adrenal medulla, preaortic ganglia, or the paraspinal ganglia in the posterior neck, chest, abdomen, or pelvis, causing nerve root compression, vessel encapsulation, and/or vital organ infiltration.[2] In addition, NB may metastasize to lymph nodes, bones, bone marrow, and/or liver, which further jeopardizes the patients' hematopoiesis and metabolism.[2]

The clinical course of NB is highly heterogeneous and dependent on the age at diagnosis. The spectrum of neuroblastic tumors (NTs) include NB (accounting for more than 80%), the more differentiated ganglioneuroblastoma (GNB), and the benign ganglioneuroma (GN)[3]. While NB in infants usually show spontaneous regression or differentiation into benign GN, NB in toddlers and older children frequently develops metastatic disease with high risk of recurrence.[3] This variability correlates to the cellular heterogeneity and different extent of maturation, and probably corresponds to malignant transformation of cells at various stages of tissue maturation within the sympathoadrenal lineage of neural crest.[4]

1.1. Epidemiology of neuroblastoma

The age-standardized incidence rate (ASIR) of NB can be generally considered as approximately 10 per million children per year across the world (**Figure 1**). Higher incidence rates of NB may be seen in westernized societies; in countries with large-scale NB screening programs (such as Japan[5] and Canada[6]); or in studies that used

an older version of World Standard Population[7], which is enriched with more children aged 0–4 years, to adjust the ASIR. Recent evidence from Children's Oncology Group in the United States have also revealed racial and ethnic disparities in prognosis of NB even with uniform treatment: African, Native, and Asian Americans have higher prevalence of high-risk features and worse event-free survival rate.[8]

In our recent study on childhood cancer epidemiology[9] performed with colleagues from the Taiwan Cancer Registry, the ASIR of NB is 8.1 per million children aged 0–14 years, accounting for 6% of all childhood cancers (ASIR of all cancers, 125.0/million/year; **Figure 2**). NB is the 5th commonest childhood cancer in Taiwan, ranked after acute lymphoblastic leukemia (24%), germ cell tumors (9%), acute myeloid leukemia (8%), and non-Hodgkin lymphoma (7%). Boys were more commonly diagnosed than girls (male:female ratio = 1.4); median age at diagnosis is 937 days (2 year and 6 months), while 79% of cases were diagnosed at age 0–4 years.

After the implementation of National Health Insurance in Taiwan in 1995, the year-on-year incidence-trend of NB seemed to be stable with wide fluctuations (annual percentage change, 1.5%; 95% confidence interval [95%CI], -1.6%–4.7%). In average, there were 31 newly diagnosed NB patients per year during 1996–2010. However, pooled analysis of incidence data based on 3-year intervals revealed that the incidence rate of NB has been increasing at a speed of 5.8% (1.4%–10.4%) every 3 years, especially in the latest 3-year interval (2008–2010) (**Figure 3**). Whether the common practice of using abdominal ultrasound to screen the newborn babies for congenital structural anomalies[10] has contributed to the recent raise of NB incidence remains to be investigated.

1.2. Diagnostic modalities and treatment stratification of NB

In a child with newly diagnosed NB, staging and risk stratification are mandatory to help to choose the most appropriate treatment. A combination of bone marrow studies, urinary catecholamine levels, and multiple imaging modalities have been recommended to accurately define the extensiveness of disease, *i.e.* to detect occult metastasis in bones, bone marrow, lymph nodes, liver, and, rarely, lungs and brain.[11]

Because the clinical course of NB is variable, it is also mandatory to tailor the treatment plan based on prognostic factors. This risk stratification process has been coined "tumor biology-based therapy assignment".[12] Traditionally, the tumor biology of NB has been defined by age, stage, histopathology, DNA ploidy, and *MYCN* status.[13] Patients with older age (≥18 months)[14], more advanced stage (stages 3 and 4), higher mitosis and karyorrhexis index (unfavorable Shimada histology), diploidy, and/or *MYCN* amplification have worse prognosis. More recently, overall genomic patterns were proven to have independent prognostic value.[15,16] In addition, CT or MR image-defined risk factors (IDRFs) such as tumor encasement of major structures[17] predict lower likelihood of gross total resection (GTR) of NB, at the range of 46.5%–51%.[18-20] Whether modern diagnostic tools, such as molecular imaging, can help to predict tumor biology, completeness of surgical resection, or treatment outcome has been less studied.
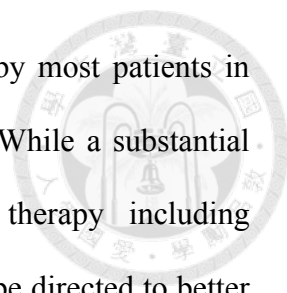
State-of-the-art treatment protocols for NB usually stratify patients into 3–4 "risk groups", based on their different risks of death or developing an event (*i.e.* relapse, progression, or secondary malignancy).[13] The patients can be generally divided into two clusters with very different outcomes: the curable low-risk (LR) or intermediate-risk (IR) groups, and high-risk (HR) group including those with *MYCN*-amplification (MNA$^+$) with a much lower cure rate (**Figure 4**). Such a striking dichotomy not only underscores

3

the importance of risk-directed therapy but also demonstrates that there are different goals of research for each risk group.[21]

The LR group includes all stage 1 patients, all stage 2 infants and children with non-amplified *MYCN*, stage 2 children with MNA$^+$ and favorable histology, and stage 4S with normal *MYCN* and favorable histology. Surgical resection alone is sufficient for the treatment of LR patients, while chemotherapy may only be needed for symptomatic children.[12] With the advent of ultrasound imaging in prenatal screening, more and more LR patients are diagnosed as an incidental finding. A subset of these incidental tumors may show spontaneous regression. Studying LR neuroblastoma may help us to understand more about the mechanisms of neuronal differentiation and maturation.

The IR group includes stage 3 or 4 infants; stage 3 children with favorable histology; and stage 4S infants with unfavorable histology and non-amplified *MYCN*. In IR patients, gross total resection of the primary tumor, either at first operation of after induction chemotherapy, may be of survival benefit. Although dose-intensive chemotherapy can achieve a high cure rate in IR, 4–8 cycles of reduced-dose chemotherapy has been proven equally effective with less toxicity.[7] Long-term follow-up of these modestly treated patients, ideally through a cancer survivorship program, is warranted.

The HR group includes stage 2 with MNA$^+$ and unfavorable histology, stage 3 with *MYCN* amplification, stage 3 children with unfavorable histology, stage 4 patients who are older than 365 days or have *MYCN* amplification, and stage 4S with *MYCN* amplification. In addition to surgery and chemotherapy, treatment for HR also includes high-dose therapy with autologous stem cell transplantation, radiation therapy, and 13-*cis*-retinoic acid.[22] More recently, immunotherapy with anti-GD2 antibody with cytokines has successfully raised the two-year survival rate for 20% in HR patients,[23]

although this high cost of immunotherapy still prevent its access by most patients in Asia. The HR patients have a 5-year survival rate less than 50%. While a substantial proportion of patients can benefit from current multimodal therapy including dose-intensive chemotherapy cycles, research for this group should be directed to better risk stratification by identifying more patients who are still at risk under current therapy. New biomarkers and an understanding of disease mechanisms are needed.

HR patients with MNA^+ may be considered at ultra-high risk of treatment failure. Even with current multimodality treatment, most HR patients are still not curable. When frontline treatment fails, these patients are ideal candidates for innovative phase 1 or 2 clinical trials and should not be precluded from the opportunity of receiving novel, experimental therapies. In addition to *MYCN* amplification, next-generation sequencing technologies have identified recurrent driver mutations from genes such as *ALK*, *PTPN11*, and *ATRX* that have also become the targets of new drug development.[24]

Surgical treatment plays a pivotal role in NB treatment, not only for obtaining the tissue sample for diagnosis and biological studies, but also for providing definitive disease control, *i.e.* GTR, in LR and IR patients. In HR NB, however, the benefit of GTR has been long debated. La Quaglia *et al.* demonstrated that GTR was associated with less local progression and better survival in stage 4 NB.[25] By contrast, a German multi-center study showed that although IDRFs significantly predicted a lower GTR rate, GTR had no prognostic impact on stage 4, non-infant NB.[18] GTR may also be affected by tumor biology. By using TrkA and MYCN protein expression to stratify patients into three molecular risk groups, Hsu *et al.* showed that GTR predicted better survival only in IR patients, while in LR patients GTR could be easily achieved and in HR patients GTR provided no additional survival benefits.[26]

5

1.3. Clinical use of molecular imaging in NB

In current practice, a multitude of imaging studies is required, including CT or MRI, bone scan, and metaiodobenzylguanidine (MIBG) scan[11]. MIBG labeled with ^{123}I or ^{131}I is the current world standard radiotracer in NTs with diagnostic, therapeutic, and prognostic implications. ^{123}I-MIBG scintigraphy is the standard molecular imaging of NB.[27,28] By targeting the norepinephrine transporter (encoded by *SLC6A2*)[29], MIBG is specifically accumulated in NB cells, not only providing diagnostic and prognostic values,[30-32] but also serving as a prelude to targeted radiotherapy with ^{131}I-MIBG in ultra-high-risk patients.[33-35] However, the commercial supply of ^{123}I-MIBG has been very limited in Taiwan, which has driven us to explore the novel application of positron emission tomography (PET) scans in NB.

Due to its increasing availability, PET with ^{18}F-fluorodeoxyglucose (FDG) has more and more been performed in NB.[36-43] By targeting aerobic glycolysis of cancer cells, known as the Warburg effect[44], FDG PET provides important information for a NB that fails to accumulate or weakly condenses MIBG[38,43], and is probably superior to ^{123}I-MIBG scan in demonstrating localized NBs and soft-tissue lesions[41]. The international guidelines for NB recommend FDG PET as an option to imaging with ^{123}I-MIBG.[27] However, major drawbacks of ^{18}F-FDG PET include false-positive finding due to inflammations or hyperactive bone marrow, and high brain uptake that easily masks cranial vault lesions[42]. Whether PET with other ^{18}F-labeled compounds[45] can perform better than the current modalities remains an open question.

1.4. Rationale for applying FDOPA PET imaging in NB

PET with L-3,4-dihydroxy-6-[^{18}F]fluorophenylalanine (FDOPA) has long been used to study the dopaminergic pathway in the brain.[46] FDOPA PET is clinically useful in neuroendocrine tumors such as pheochromcytoma and paraganglioma which also originate from the neural crest[47]. FDOPA PET targets aromatic L-amino acid decarboxylase (AADC; encoded by the *DDC* gene), a pyridoxal 5'-phosphate (active vitamin B6)-dependent enzyme catalyzing L-DOPA to L-dopamine in the catecholamine biosynthesis. In normal individuals, catecholamine production are confined to dopaminergic and noradrenergic neurons of the central nervous system (CNS), to sympathetic nerves, to adrenal and extra-adrenal chromaffin cells, and to certain non-neuronal cells of the gastrointestinal tract and kidneys. The catecholamine biosynthetic pathway in the adrenal chromaffin cells, as an example of terminal differentiation, is simply depicted as below:

$$\text{Tyrosine} \xrightarrow{TH} \text{DOPA} \xrightarrow{AADC} \text{Dopamine} \xrightarrow{DBH} \text{Norepinephrine} \xrightarrow{PNMT} \text{Epinephrine}$$

(Abbreviations: TH, tyrosine hydroxylase; DOPA, 3,4-dihydroxyphenylalanine; AADC, aromatic l-amino acid decarboxylase; DBH, dopamine β hydroxylase; PNMT, phenylehanolamine N-methyltransferase.)

In patients with NB, *DDC* gene expression serves as a specific biomarker and differentially diagnoses NB from the other pediatric small round cell malignancies at a specificity and specificity of higher than 99%.[48] The presence of DDC mRNA in bone marrow or blood samples can predict disseminated disease of NB.[49] Using R2 (r2.amc.nl)[50,51], an on-line genomic tool, we showed that in contrast to other neural tumors (*e.g.* gliomas and medulloblastoma), NB tumors express exceptionally high levels of DDC mRNA (**Figure 5**). These lines of evidence support the rationale to explore the clinical role of FDOPA PET as an NB-specific imaging tool.

7

1.5. Aims of this study

NB is a cancer of early childhood. More than 50% of cases suffer from high-risk disease with a dismal outcome. Molecular imaging study is indispensable for accurate diagnosis, staging, and surveillance of NB. While the supply of traditional [123]I- or ^{131}I-MIBG tracer is very limited in Taiwan, the clinical utility of PET imaging tracers in NB remains to be elucidated. Among the PET tracers, FDG targets the aerobic glycolysis of cancer cells and has been widely accepted as an option of NB imaging, while FDOPA, an amino acid analog of L-DOPA, targets catecholamine synthesis and has the potential to be specifically accumulated in NB tumors.

This study aims to characterize the tumor behavior of NB using FDG and FDOPA PET imaging. We hypothesize that tumor biology of NB dictates the "molecular imaging phenotype" of tumors and causes differential uptake of FDG and FDOPA on PET imaging. Specific aims of this study include:

1. To determine the diagnostic accuracy, *i.e.* sensitivity and specificity, of FDG and FDOPA PET imaging in NB;

2. To investigate the tumor uptake patterns of FDG and FDOPA across different genomic types of NB;

3. To evaluate the the impact of FDG and FDOPA uptake on surgical resection and on treatment outcome;

4. To establish a preclinical PET imaging platform using a genetically-engineered mouse model.

2. Material and Methods 材料與方法

2.1. Patient enrollment

Cohort 1: Determining the sensitivity and specificity of FDOPA PET

From August 2008 to August 2011, we recruited patients diagnosed with NTs for serial ^{18}F-FDOPA, ^{18}F-FDG, and ^{123}I-MIBG scans before therapy and during follow-ups at National Taiwan University Hospital (NTUH). When there was a clinical diagnosis of neuroblastic tumors (NTs, including NB, GNB, and GN), we arranged functional imaging studies as well as standard clinical evaluations, including CT/MRI, urinary VMA, and bone marrow smear and biopsy, for the patient, followed by tumor biopsy or resection. The scans were performed before treatment and at an interval of 3–12 months during and after therapy. The images were interpreted as positive or negative by an experienced nuclear medicine physician (Dr. Kai-Yuan Tzen, Department of Nuclear Medicine, National Taiwan University Hospital) who was blind to the clinicopathological backgrounds of patients. The method of operation was decided by the pediatric surgeon (Dr. Wen-Ming Hsu, Department of Surgery, National Taiwan University Hospital), based on preoperative anatomical imaging, resectability of the tumor, and the patient's clinical condition. Whenever possible, total resection was the first consideration. However, when the main tumor encapsulated major organs, great vessels, or nerves, a biopsy was taken from a part of the tumor with the safest accessibility, to minimize the harm to the patient. Only NT patients with concomitant ^{18}F-FDOPA imaging and tumor histology were included in this analysis.

Cohort 2: Characterizing NB tumor behavior using paired FDG and FDOPA PET

From June 2007 to July 2014, patients diagnosed with NB were enrolled. FDG and FDOPA PET scans were performed at diagnosis and during follow-up at National

Taiwan University Hospital, Taipei, Taiwan at an interval of 3–12 months with other standard evaluations. Patients with paired FDG and FDOPA PET scans performed before completion of the first chemotherapy cycle were included for analysis (**Figure 10**). The study was approved by National Taiwan University Hospital Research Ethics Committee. Informed consent was obtained from each participant's guardian.

2.2. Standard evaluations for NB patients

In addition to PET imaging, routine evaluations included complete blood count, basic biochemistry, serum lactate dehydrogenase and ferritin levels, urinary vanilylmandelic acid level, CT/MR imaging, and bone marrow smear and biopsy. The presence of CT/MR image-defined risk factor was retrospectively retrieved from patients' radiological reports at diagnosis, based on the International Neuroblastoma Risk Group staging system criteria (INRGSS).[17] All patients were staged according to International Neuroblastoma Staging System (INSS).[52] The histological classification of resected tumors was based on the International Neuroblastoma Pathology Classification (INPC).[3] *MYCN* amplification was determined by chromogenic *in situ* hybridization (CISH).[53] Urinary vanillylmandelic acid (VMA) level was measured from 12- or 24-hour urine collections, assayed by high-performance liquid chromatography (Bio-Rad Laboratories, Hercules, CA), and reported as mg/day. DNA ploidy and urinary homovanillic acid level were not routinely evaluated.

The major genomic type of each patient's tumor, *i.e.* the presence of segmental or numerical chromosomal alterations[13,14,52], was determined by array-based comparative genomic hybridization (array-CGH) [15,16,54] [15,16,52] using bacterial artificial chromosome-based (CMDX, Irvine, CA; resolution, 1 Mb) or CytoChip Oligo (BluGnome, Cambridge, UK; resolution, 60 kb) platform.

2.3. Risk-directed therapy

Patients were treated and followed according to Taiwan Pediatric Oncology Group's TPOG-N2002[21,55], a nationwide, risk-directed protocol for NB with modification of the Children's Oncology Group (COG)'s regimens[12,22]. The complete design and results of TPOG-N2002 are to be presented elsewhere (Dr. Rong-Long Chen *et al.*, manuscript in preparation). Briefly, patients were stratified into three risk groups based on age, stage, *MYCN*, and histology using a modified Children's Oncology Group (COG) definition[8] without ploidy. Briefly, the low-risk group includes all stage 1 patients, all stage 2 infants and children with normal *MYCN* copy number, stage 2 children with *MYCN* amplification and favorable histology, and stage 4S with normal *MYCN* and favorable histology. The intermediate-risk group includes stage 3 or 4 infants; stage 3 children with favorable histology; and stage 4S infants with unfavorable histology and normal *MYCN*. The high-risk group includes stage 2 with *MYCN* amplification and unfavorable histology, stage 3 with *MYCN* amplification, stage 3 children with unfavorable histology, stage 4 patients who are older than 365 days or have *MYCN* amplification, and stage 4S with *MYCN* amplification.[21]

According to their risk grouping[8,21], patients were treated with surgery alone; surgery plus 4 or 8 chemotherapy cycles, as modified from COG-A3961[12]; or multimodal therapy including surgery, chemotherapy, autologous stem cell transplantation, radiotherapy, and 13-*cis*-reticnoic acid, modified from COG-A3973[22].

2.4. Acquisition of images and data analysis

All nuclear medicine scans were obtained in random order among each other within the same admission, depending on the production schedule of the

radiopharmaceuticals. All images were acquired in 2D according to standard procedures described below. We performed a routine sedation 30 minutes before scanning if necessary.

For ^{18}F-FDOPA imaging, patients were pre-treated with 2 mg/kg of carbidopa orally an hour before injection of ^{18}F-FDOPA. Whole-body PET/CT images were acquired 90 minutes after injection of ^{18}F-FDOPA (4 MBq/kg) on a PET/CT scanner with low-dose CT (Discovery ST-16, GE Medical Systems, Milwaukee, WI). Whole-body ^{18}F-DOPA PET acquisitions included 5 to 9 bed positions (5-min emissions per bed position) and were reconstructed by using an iterative reconstruction algorithm. A non-diagnostic CT scanning (low-dose CT with 140 kV, 40–80 mA, 0.5 s per rotation) was used for attenuation correction and for anatomic localization of the hot spots of the PET study.

Before ^{18}F-FDG PET/CT study, patients were instructed to fast for at least 4 hours. ^{18}F-FDG (5 MBq/kg) supplied by the PET Center of NTUH was administered i.v. in an infusion line connected to saline. The same PET/CT scanner was used for imaging, with same setting for low-dose CT acquired first, followed by PET acquisition (4-min emissions per bed position) 45–60 min after ^{18}F-FDG injection.

For the ^{18}F-FDOPA and ^{18}F-FDG PET images, the maximum standardized uptake value (SUV$_{max}$) was determined for the lesion by manually drawing elliptical regions of interest (ROIs) around areas of abnormal uptake as delineated by PET/CT image. The SUV$_{max}$ was chosen because of its lower sensitivity to partial volume effects and higher reproducibility between observers. A large enough ROI was used to cover more than half of the lesion, meanwhile avoiding peripheral areas of the lesion to prevent partial volume effect. SUV$_{max}$ measurements from the liver were obtained in a similar fashion. The ROIs in the liver were free of visible metastatic disease and showed homogeneous

signal intensity as delineated by PET/CT. All SUV_{max} calculations were performed on the transaxial attenuation-corrected PET slices. SUV_{max} corrected for lean body mass were automatically generated with the software from GE Medical System on a Xeleris $2^®$ workstation (GE Healthcare, USA). Activity counts in the ROIs were normalized to injected doses per kilogram of patient body weight. To be more objective, we also calculated the tumor-to-liver SUV_{max} ratio (T/L).

^{123}I-MIBG was produced by the Institute of Nuclear Energy Research (Taoyuan, Taiwan)[56] and injected intravenously (IV) with an administered activity of 7.4 MBq/kg (80-370 MBq), on the third day of a 3-day course of Lugol solution. Anterior and posterior whole-body ^{123}I-MIBG scans were acquired 24 hours after tracer injection. The dual-head gamma camera (Infinia Hawkeye, GE Medical Systems, Milwaukee, WI) equipped with low-energy high-resolution parallel-hole collimators was used for scanning. The scan speed for whole-body imaging was 8 min/step/30 cm in step and shoot mode. SPECT images were obtained for some patients in specific sections of the body, according to the clinical history of the patient and tumor localization (*i.e.* thorax, abdomen, etc.). For SPECT acquisition, the following parameters were used: 60 projections, 128×128 matrix, 60s acquisition time per projection. The data were reconstructed by standard filtered back projection using a Butterworth filter.

2.5. Production of ^{18}F-FDOPA
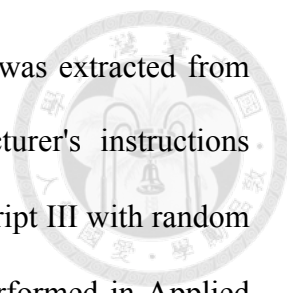
^{18}F-FDOPA was produced in-house with a commercial automatic synthesis system (TRACERlab FX$_{FE}$, GE Healthcare, USA) .[57]. Briefly, ^{18}F-fluorine was produced in the NTUH PETtrace cyclotron and then reacted with the protected trimethylstannyl precursor (N-formyl-3,4-di-tert-butoxycarbonyloxy-6-[trimethylstannyl]-L-phenyl-alanine ethyl ester; ABX, Germany) in Freon at 5°C. A deprotection step was

performed with HBr and then neutralized with NH_4OH. The product was purified with a semi-preparative high-performance liquid chromatography and followed by a sterile filtration. After a series of quality control procedure, the ^{18}F-FDOPA-containing product solution was ready for intravenous (i.v.) injection. The radiochemical yield of ^{18}F-FDOPA was 20-30 % (decay-uncorrected) in a synthesis time of 50-60 minutes from the end of bombardment. The radiochemical purity was >95% and the specific activity was >6 µCi/µg.

2.6. Real-time PCR analysis

AADC mRNA expression levels were analyzed in Cohort 1 samples by real-time PCR.[58] Only non-hepatic tumors with sufficient samples were included due to endogenous expression of AADC in liver. Briefly, fresh tumor tissue was obtained during patients' routine surgical treatment and immediately cryopreserved in liquid nitrogen, and total RNA was later extracted using TRIzol reagent (Invitrogen, Carlsbad, CA) and converted to cDNA by reverse transcriptase (SuperScript II, Invitrogen). Real-time PCR was performed by using iCycler iQ Real-Time PCR Detection System (Bio-Rad, Hercules, CA). A primer set of 5'–GAACAGACTTAACGGGAGCCTTT–3' (forward) and 5'– AATGCCGGTAGTCAGTGATAAGC–3' (reverse) were used to detect two AADC mRNA isoforms which have been reported in various NB cell lines (*24, 25*). The primer set for GAPDH were 5'–GTGGTCTCCTCTGACTTCAAC–3' (forward) and 5'-TCTCTTCCTCTTGTGCTCTTG-3' (reverse). The cycling condition was 95°C for 1.5 min, followed by 40 cycles of 95°C for 30 sec, 60°C for 30 sec, and 72°C for 30 sec. For quantification, the AADC mRNA expression level was normalized to that of GAPDH. Results from three separate experiments were averaged.

In Cohort 2 samples, an amendment was made by switching to the TaqMan system

and by using control genes validated by other groups. Total RNA was extracted from frozen tumor tissue with Trizol reagent following the manufacturer's instructions (Invitrogen). cDNA was produced from 5 μg of RNA using Superscript III with random hexamer primers (Invitrogen). Analysis of gene expression was performed in Applied Biosystems 7500 Fast Real-Time PCR System by using specific TaqMan primers (Applied Biosystems) for *HK1* (Hs00175976_m1), *HK2* (Hs00606086_m1), *TH* (Hs00165941_m1), *DDC* (Hs01105048_m1), *SLC6A2* (Hs00426573_m1), *HPRT1* (Hs99999909_m1), and *SDHA* (Hs00188166_m1). Expression levels of PET-related genes were averaged from two replicates and normalized to the geometric mean of *HPRT1* and *SDHA*, which are control genes with the least expression variability across NB samples[59].

2.7. Statistical analysis

The sensitivity and specificity of ^{18}F-FDOPA PET, ^{18}F-FDG PET, and ^{123}I-MIBG scans with 95% confidence intervals were calculated by using tumor histology as the gold standard and compared with McNemar test. Receiver operating characteristic (ROC) analysis was performed for ^{18}F-FDOPA and ^{18}F-FDG PET. The association between tumor uptake of ^{18}F-FDOPA and AADC mRNA or urinary VMA levels was evaluated by Spearman's nonparametric correlation test. Numerical data between groups were compared by Wilcoxon rank-sum test.

In Cohort 2, outcome data were frozen on October 9, 2015. The Fisher exact, Kruskal-Wallis, and Spearman's nonparametric correlation tests were used to evaluate the association across variables. The cutoff value of PET imaging parameters was determined by ROC curve analysis. Event-free survival (EFS) was calculated from diagnosis to the first occurrence of relapse, progression, secondary malignancy, or death,
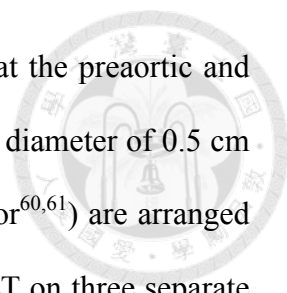
or to the last contact if no event occurred. OS was calculated until the time of death or until the last contact that the patient was alive. Kaplan-Meier curves were generated and compared by log-rank tests. Cox proportional hazard models were built to test for prognostic values.

In animal studies, we used paired *t* tests to compare tumor size, maximal diamter, radiotracer uptake (in SUV and T/L signal ratios), gene expression obtained before and after treatment in each group. A linear regression model was constructed to check the correlation between the difference of radiotracer uptake before and after treatment and the gene expression level of relevant genes.

The statistical analyses were performed with Small Stata 11.0 software (StataCorp, College Station, TX). All tests were two-sided. *P* values < 0.05 were considered statistically significant.

2.8. Transgenic NB mouse model

All mouse experiments will be performed after approval from the Institutional Animal Care and Use Committee, College of Medicine, National Taiwan University. The TH-*MYCN* mouse strain was originally designed by Dr. William A. Weiss *et al*. (University of California, San Francisco, CA, USA) and was kindly provided by Prof. Akira Nakagawara, MD, PhD (Chiba Cancer Center, Chiba, Japan). The mice have been maintained at the Transgenic Mouse Model Core, National Core Facility Programs of Biotechnology, Taipei, Taiwan. The incidence rate of NB tumor has been reported to be 100% and 33% in homozygous and hemizygous TH-MYCN mice, respectively.[60,61] Offsprings of hemizygous TH-MYCN male mice crossed with wild-type female mice are to be genotyped at age 2-3 weeks, using a modified PCR-based method developed at Chiba Cancer Center[62]. After weaning, hemizygous TH-*MYCN* mice are to be screened

with ultrasound twice a week for spontaneously growth of tumors at the preaortic and adrenal areas (n=30). Those found with tumor growth with maximal diameter of 0.5 cm or more (estimated n=10, as 33% of subjects may develop NB tumor[60,61]) are arranged for animal PET imaging with ^{18}F-FDG and ^{18}F-FDOPA, and ^{18}F-FLT on three separate days within a single week. Subsequently, animals are randomly assigned for intraperitoneal injection of all-trans retinoic acid (ATRA, 5 mg/kg, n=5) or vehicle alone (control, n=5) for 14 days and then sacrifieced for tumor harvest. The tumor growth will be traced by ultrasound biweekly. Tumor samples are to be cryopreserved and extracted for total RNA and total protein, and to be fix with 4% paraformaldehyde and checked for histopathology features.

2.9. Small animal ultrasound screening

The screening strategy was modified from Teitz *et al.*[60] Briefly, all ultrasound studies were performed using the VisualSonics VEVO-2100 High Frequency Ultrasound system (VisualSonics, Toronto, Canada). Animals were anesthetized (isoflurane 1.5% in O2 delivered at 2 liters/min; or tribromoethanol (Avertin) 1.2%) and hair covering the abdominal and thoracic area to be imaged was removed by application of hair removal cream (Nair). For scanning, animals were placed supine on the imaging stage, with ultrasound transmission gel liberally applied and the relevant transducer (RMV-706 at 40 MHz) lowered stereotactically to the surface of the animal. Tumors (characterized by irregular regions of hypoechoicity) were identified relative to normal tissue landmarks and tumor volume was determined by acquisition of high resolution images. The width, depth, and height of the tumor were measured for further estimation of tumor volume.[63]

2.10. Small animal PET study

Animal PET scans (eXplore Vista DR, GE Healthcare) will be performed TH-*MYCN* mice with ultrasound-detected tumor before and after treatment with retinoic acid. The imaging procedure is similar to that described previously.[64] In brief, 500 mCi of ^{18}F-FDOPA, ^{18}F-FDG, or ^{18}F-FLT is to be given intravenously via tail vein on an animal on separate days within the same week. Before the injection of ^{18}F-FDG, animals will be fasted for at least 4 hours. Before the injection of ^{18}F-FDOPA, animals will be premedicated with intraperitoneal injection of carbidopa and entacapone, 0.025 mg/g, respectively, to block peripheral AADC activity. Thirty minutes after the injection of a radiotracer, the animal will be imaged with PET for 60 minutes followed by low-dose CT. Fusion PET/CT images will be created and analyzed using the region of interest (ROI) method by vendor-provided software. ROIs will be drawn over the range of the tumor, and in an area of the liver without evidence of metastasis. Radioactivity within the ROI obtained by PET will be then calculated and expressed as mean nCi/cc. Ratios of the radioactivity between tumor and liver will be calculated. We will also measure the maximal standardized uptake value (SUV_{max}) for both the tumor and the liver. To be more objective, we will also calculate the tumor-to-liver tissue SUV ratio (T/L) for each tumor as a continuous variable.

3. Results 結果

3.1. Characterization of neuroblastic tumors with FDOPA PET

To determine the clinical utility of FDOPA PET in diagnosing NTs (i.e. NB, GNB, and GN), we first enrolled 34 consecutive patients with 50 tumors with paired imaging and histopathology data to determine the sensitivity and specificity of FDOPA PET *vs.* other imaging modalities, from August 2008 to August 2011. There were 20 boys and 14 girls, with a median age of 2.8 (range, 0.2–8.6) years. Most patients (26/34; 76.5%) had advanced disease (INSS stage 3 or 4). *MYCN* amplification was noted in 7 of 32 patients (21.9%) with available data. Among the 34 patients, 25 had 1 tumor, 7 had 2 tumors, 1 had 3 tumors, and 1 had 7 tumors (due to multiple relapses). Tumors from the same patients were sampled at different surgical timing. The histological types of the 50 tumors included 26 NBs (52%), 11 GNBs (22%), 5 GNs (10%), and 8 lesions without viable tumor cells (16%). Most tumors (33/50; 66%) were located in the abdomen.

In patients with active disease, FDOPA PET has successfully detected lesions in the adrenal gland, retroperitonium, mediastium, subcutaneous tissue, pleura, neck, skull, and long bones at a sensitivity of 97.6% and a specificity of 87.5% (**Figure 6**).

In patients with no evidence of disease, FDOPA uptake was noted over the basal ganglia, gallbladder, kidneys, urinary tract, and epiphyseal plates of long bones (**Figure 7**). The basal ganglia, which contain dopaminergic neurons with AADC activity, may serve as an internal positive control.

Forty-two (84%) tumors were avid on ^{18}F-FDOPA PET scan. FDOPA PET successfully detected 41 of the 42 NTs with viable tumor cells, including 25 of 26 NBs, all 11 GNBs, and all 5 GNs, with a sensitivity of 97.6% (95% confidence interval, 87.4%–99.9%). (**Table 1**)

3.2. Comparison of ^{18}F-FDOPA PET, ^{123}I-MIBG scan, and ^{18}F-FDG PET

In tumors studied with different modalities concomitantly, ^{18}F-FDOPA and ^{18}F-FDG PET scans demonstrated a higher spatial resolution and tumor delineation than did ^{123}I-MIBG scans (**Figure 8**). Although the strong physiologic FDG uptake by the brain and nasopharynx interfered the interpretation of skull lesions, FDOPA PET helped to identify lesions in the head and neck region more accurately.

In contrast to FDG PET and MIBG scan, ^{18}F-FDOPA PET successfully visualized 3 of the 4 MIBG-false-negative NTs and the 4 of the 5 FDG-false-negative NTs. The sensitivity of ^{18}F-FDOPA PET was higher than ^{123}I-MIBG scan or ^{18}F-FDG PET (P=0.0455 by McNemar test). (**Table 1**)

3.3. Correlation between tumor uptake and catecholamine markers

We also examined the relationship among tumor uptake of radiotracers, catecholamine metabolism markers, and tumor differentiation. Among 17 tumors with triplet images, MIBG-positive tumors ($n = 11$) showed significantly higher ^{18}F-FDOPA uptake (median SUV$_{max}$, 5.584 vs. 2.634, $P = 0.0348$; median tumor-to-liver uptake ratio [T/L], 3.195 vs. 1.623, $P = 0.027$) and urinary VMA (median level, 3.40 vs. 1.16 mg/day, $P = 0.0181$) than did the MIBG-negative tumors, while there was no significant difference in their ^{18}F-FDG uptake (median SUV$_{max}$, 3.316 vs. 1.834, $P = 0.107$; median T/L, 2.170 vs. 1.255, $P = 0.2677$) (**Figure 9A**). A moderately positive correlation between VMA and FDOPA uptake was also observed ($n = 47$; **Figure 9B**).

Next, we analyzed 33 NTs for AADC gene expression level by real-time PCR, using *GAPDH* as the control gene. The 25th%, 50th%, and 75th% relative AADC expression levels of the 33 tumors were 2.109, 7.166, and 23.416 $\times$ 10^{-3} folds,

respectively. In 15 non-hepatic tumors with concomitant FDOPA PET result, the median AADC gene expression level was 6.898×10^{-3} (interquartile range [IQR], 2.109–27.58×10^{-3}) folds, while their median SUV_{max} was 2.846 (IQR, 2.406–4.996), and their median T/L was 2.070 (IQR, 1.895–3.465). There was a strong correlation between AADC gene expression and FDOPA uptake (SUV_{max}, Spearman's $\rho = 0.8179$, $P = 0.0002$; T/L, $\rho = 0.8929$, $P < 0.0001$; **Figure 9C**).

Comparing NTs by histopathology, PDNB and DNB showed higher FDOPA uptake and AADC gene expression levels than the more differentiated GNB and GN and the least differentiated UNB (**Figures 9D-9E**), while urinary VMA levels showed no significant difference across histologic types (**Figure 9F**). These results suggested that in NTs, higher uptake of FDOPA is associated with MIBG avidity, less but not the least tumor differentiation, and a more "catecholaminergic" phenotype.

3.4. FDG and FDOPA PET imaging features at initial diagnosis of NB

To further evaluate the impact of NB tumor biology on FDG and FDOPA imaging, we analyzed patients with newly diagnosed NB with paired FDG and FDOPA PET scans. From June 2007 to July 2014, 88 patients with the clinical diagnosis of NB were enrolled for PET scans. Forty-six patients were excluded from analysis: Forty-two patients had PET scans performed after receiving the second chemotherapy cycle or during post-treatment follow-up only; two patients only had FDG PET at diagnosis; one patient only had FDOPA PET at diagnosis; one patient had gross total resection (GTR) of primary NB tumor prior to PET imaging. The rest 42 patients who had paired FDG and FDOPA imaging performed on different days at initial diagnosis were eligible for analysis (**Figure 10**). There were 28 boys and 14 girls. The median age at diagnosis was 2.0 years (interquartile range [IQR], 0.5–4.9 years). Most patients were diagnosed at >

21

18 months (n = 24; 57%), stage 4 (n = 25; 60%), and HR group (n = 30; 71%).

Reading the FDG and FDOPA PET images of NB, we noted that primary NB tumors frequently took up FDG and FDOPA at different intensity. The maximum standardized uptake value (SUV$_{max}$) of each primary tumor was measured as the indicator of tumor uptake of FDG or FDOPA, because of its lower sensitivity to partial-volume effects and higher reproducibility between observers.

Table 2 shows the tumor uptake values compared by clinical characteristics. The SUV$_{max}$ of FDG and the ratio between FDG and FDOPA uptake (G:D) were significantly higher in patients with high-risk features, including older age, stage 4, *MYCN* amplification, and anatomical image-defined risk factors (IDRFs)[17] (all P < 0.05). By contrast, the SUV$_{max}$ of FDOPA was significantly higher in patients with younger age, lower stage, and low- or intermediate-risk groups (all P < 0.02).

3.5. Distribution of FDG and FDOPA uptake by primary NB tumors

The distribution of FDG, FDOPA, or G:D values is skewed with a right tail (**Figure 11A**). On scatter plot, the FDG and FDOPA uptake follows an "L"-shaped distribution (**Figure 11B**; Spearman's ρ = -0.33, P = 0.22) which can be divided into two clusters by the G:D value that distinguishes the major genomic types of NB (presented below): (1) A "glycolytic" group (G:D $\geq$ 1.09; n = 23) featured by higher FDG (FDG^{hi}) and lower FDOPA (FDOPA^{lo}) uptake; and (2) a "catecholaminergic" group (G:D < 1.09; n = 19) with lower FDG (FDG^{lo}) and higher FDOPA (FDOPA^{hi}) uptake (**Figure 11C**). Tumors with high-risk features, *i.e.* older age (18/23 *vs*. 6/19; P = 0.004), stage 3/4 disease (23/23 *vs*. 11/19; P = 0.001), and *MYCN* amplification (9/23 *vs*. 0/19; P = 0.002), are enriched in the "glycolytic" group. By contrast, tumors from infants diagnosed at < 18 months of age (13/19 vs. 5/23; P = 0.004), lower stage

patients (8/19 vs. 0/23 with stage 1/2/4S; $P = 0.001$), and *MYCN*-non-amplified patients (19/19 vs. 14/23; $P = 0.002$), were enriched the "catecholaminergic" group.

3.6. Tumor Uptake Distinguishes NB Genomic Types

In the study cohort, 31 of 42 patients had their genomic type of NB determined by array-based comparative genomic hybridization (array-CGH) and/or chromogenic *in situ* hybridization. Twenty-seven (87%) out of the 31 patients with available genomic data showed copy number alterations that fall into one of the three major genomic types in NB [54]: Numerical (whole-chromosomal) alterations (Num$^+$; $n = 11$), segmental chromosomal alterations (Seg$^+$; $n = 7$), or *MYCN*-amplification (MNA$^+$; $n = 9$). In the other four patients with genomic data available, three had no significant copy number alterations (*i.e.* silent or "flat") and one had Beckwith–Wiedemann syndrome with IGF2 microdeletion. (**Figure 11C**)

Comparing tumor uptake of FDG and FDOPA by the three major genomic types, FDG uptake of the primary tumor is highest in MNA$^+$, intermediate in Seg$^+$, and lowest in Num$^+$. By contrast, FDOPA uptake is highest in Num$^+$ and lowest in Seg$^+$ and MNA$^+$ (Fig. 2B and Table 1). ROC analysis identified that FDG^{hi} with SUV$_{max}$ ≥ 3.31, FDOPA^{lo} with SUV$_{max}$ < 4.12, and G:D ratio ≥ 1.09 are the cutoff values that best distinguish the unfavorable Seg$^+$ and MNA$^+$ genomic types from the favorable Num$^+$ and other genomic type of NB (**Figures 12A–12C** and **12E–12J**). Comparing the area under ROC curves (AUC) of FDG uptake, inversion of FDOPA uptake (1/SUV$_{max}$), and G:D ratio in classifying the unfavorable genomic types of NB (Seg$^+$ and MNA$^+$), G:D showed a significantly better performance than FDG or FDOPA ($P = 0.03$; **Figure 12D**) alone with a sensitivity of 87.5% (61.7%–98.4%) and specificity of 86.7% (59.5%–98.3%). Combining the criteria of FDG SUV$_{max}$ ≥ 3.31 and FDOPA SUV$_{max}$ < 4.12 to

define an ultra-high-risk group by PET (PET-UHR; **Figure 11B**) yields a sensitivity of 81.3% (54.4%–96.0%) and specificity of 93.3% (68.1%–99.8%) with an estimated AUC of 0.87 in predicting Seg$^+$ or MNA$^+$ genomic types of NB (**Table 3**).
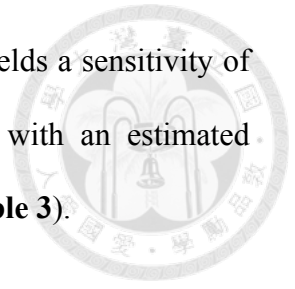
3.7. Tumor uptake predicts surgical outcome

Among 34 evaluable patients, GTR of the primary tumor was achieved at first operation in nine patients (26%) and at subsequent operation(s) in 18 patients (53%), giving a GTR rate of 79%. In the remaining seven patients, only a partial resection could be achieved at the best operation. There was no surgical mortality nor kidney loss. Two patients experienced transient chylous ascites after resection of retroperitoneal tumors and both have spontaneously resolved.

Patients with *MYCN* amplification, unfavorable genomic types, and IDRF(s) have significantly lower rate of GTR (all $P < .05$). Patients' age, stage, gender, and histology are not associated with GTR rates (**Table 4**).

On the scatter plot of FDG and FDOPA uptake by primary NB tumors, IDRF+ and non-GTR cases were enriched in the "glycolytic" group of tumors with G:D ≥ 1.09. The GTR rate of "glycolytic" tumors is significantly lower (56% *vs*. 100%, $P = 0.002$; **Figure 13A**). Among patients with IDRF(s) on diagnostic CT/MR imaging, whose GTR rate is 65% ($P = 0.03$), glycolytic tumors have even lower (46%) probability of GTR ($P = 0.04$). Patients with IDRF(s) and G:D < 1.40 ($P = 0.02$) have 100% GTR rate (**Figure 13B**) . A surgical algorithm is proposed accordingly (**Figure 13C**).

3.8. Prognostic Value of FDG and FDOPA Uptake by the Primary Tumors

At a median follow-up of 39.2 months (range, 8.8–100.3 months), the 42 patients have a 5-year event-free survival (EFS) rate of 41% (25%–57%) and a 5-year overall survival (OS) rate of 50% (28%–68%). Patients with older age, stage 4 disease, *MYCN* amplification, high-risk disease, and unfavorable genomic types (Seg[+] and MNA[+]) had significantly worse EFS and OS rates. By contrast, neither IDRFs nor GTR had an impact on survival (**Figure 14**).

Comparing by the values of tumor uptake, strikingly distinct outcomes were found (**Figure 15**). Specifically, tumors showing higher FDG avidity ($SUV_{max} \geq 3.31$; **Figures 15A** and **15B**), lower FDOPA avidity ($SUV_{max} < 4.12$; **Figures 15C** and **15D**), or higher G:D ratio (ratio ≥ 1.09; **Figures 15E** and **15F**) were associated with significantly worse survival rates (all $P < 0.01$).

Patients of the PET-UHR group ($n = 22$), whose primary tumor showed FDG[hi] ($SUV_{max} \geq 3.31$) and FDOPA[lo] ($SUV_{max} < 4.12$) uptake, had extremely poor 5-year EFS (12% [2%–31%] *vs.* 76% [48%–91%]; $P = 0.0001$) and OS (24% [6%–47%] *vs.* 100% [41%–98%]; $P = 0.0001$) rates (Figs. 3G and 3H). Among the conventionally high-risk patients as defined by age, stage, histology, and *MYCN* status ($n = 30$)[8,21], PET-UHR ($n = 22$) showed a trend of worse 5-year EFS (12% [2%–31%] *vs.* 38% [6%–72%]; $P = 0.16$) and OS (24% [6%–47%] *vs.* 50% [1%–91%]; $P = 0.07$).

Cox proportional hazard modeling showed that, on univariate analysis, age, stage, *MYCN* status, FDG[hi], FDOPA[lo], G:D ≥ 1.09, and PET-UHR were associated with inferior EFS on univariate analysis (**Table 5**). On multivariate analysis, PET-UHR was confirmed as a poor prognostic factor (hazard ratio, 4.9 [1.4–16.9]; $P = 0.012$) that was independent from age, stage, IDRF, and *MYCN* status (**Table 6**). When FDG uptake,

FDOPA uptake, or G:D ratio was analyzed with the traditional risk factors respectively, FDG^{hi} or FDOPA^{lo} each predicted inferior EFS independently, while G:D was not a significant predictor of EFS.
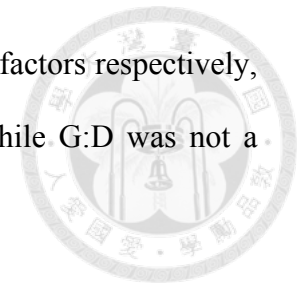
3.9. Tumor uptake of FDG and FDOPA and relevant gene expression

To evaluate the probable mechanisms of tumor uptake, we analyzed the expression of selected PET imaging-related genes in 16 primary tumor samples (**Figure 16**). G:D correlated strongly with hexokinase 2 (*HK2*) expression (Spearman's $\rho = 0.86$, $P < 0.0001$; **Figure 16B**) and negatively with *DDC* expression ($\rho = -0.58$, $P = 0.02$; **Figure 16L**). Although hexokinase 1 (*HK1*) also phosphorylates FDG and is expressed at a much higher levels, there was no correlation between *HK1* expression and tumor uptake. Surprisingly, FDOPA uptake had no significant correlation with *TH* (encoding tyrosine hydroxylase upstream of AADC; $P = 0.09$; **Figure 16H**) or *DDC* ($P = 0.34$; **Figure 16I**) expression levels, but showed positive correlation with the expression of *SLC6A2*, the target of ^{123}I-MIBG scintigraphy ($\rho = 0.68$, $P = 0.004$ **Figure 16J**), supporting our previous finding that ^{123}I-MIBG avidity was associated with higher FDOPA uptake.

3.10. Establishing a preclinical imaging platform for NB

To further extend the use of molecular imaging in experimental models, we established a preclinical imaging platform using genetically-engineered mice that recapitulates human NB with *MYCN* amplification.[60,61,65] After weaning and genotyping, female hemizygous TH-*MYCN* transgenic (*MYCN$^{+/-}$*) mice of 129/SvJ background were evaluated twice a week with Vevo 2100 High-Frequency Ultrasound System using a 40-MHz transducer (VisualSonics, Toronto, ON, Canada). The thorax and abdomen

were scanned ventrally with transverse and sagittal views. (**Figures 17A-17D**)

Screened with ultrasound twice a week since age 34.7±4.3 (mean±SD) days, 46 (87%) out of 53 mice were revealed with a tumor (maximal diameter ≥ 2 mm) at a median age of 56 days (**Figures 17E**). The tumors showed intermediate echogenicity (kidney > tumor > liver) and arose from one of three sites: 1) **Pre-aortic** (n=37; 70%); 2) **juxta-adrenal** (n=6; 11%); and 3) **thoracic** (n=3; 6%). The thoracic tumors were visualized deep in the posterior mediastinum, using the heart or liver as an "acoustic window" (**Figures 17F**). However, thoracic tumors were difficult to be detected until reaching a substantial volume, in contrast to pre-aortic tumors (volume at detection, 98.9±53.5 mm^3 *vs.* 10.9±1.9 mm^3, $P < 0.0001$; **Table 7**).

Upon ultrasound screening ($N = 53$), the probability of developing abdominal or thoracic tumors at age 60, 90, and 120 days were 62%, 80%, and 83%, respectively. In contrast to homozygous Th-MYCN ($MYCN^{+/+}$) mice which uniformly died before age 60 days ($n = 6$; by courtesy of Dr. Shiann-Tarng Jou, NTUH, Taipei, Taiwan; median age of death, 44 days), the hemizygous $MYCN^{+/-}$ mice with tumor onset ($n = 46$) lived a median of 29 days between tumor onset and death (median age of death, 83 days) (**Figure 18A**). Therefore, the longer survival window between tumor onset and death in the hemizygous $MYCN^{+/-}$ mice may enable them as good subjects for testing developmental treatment strategies.

In the screening cohort of $MYCN^{+/-}$ mice, animals with no tumor onset at age 120 days ($n = 7$); with thoracic tumors ($n = 3$; in which delayed tumor detection was common); with uncertain age of onset due to missed follow-up dates ($n = 8$), and those assigned to other experiments ($n = 15$) were excluded from further analysis. The remaining mice ($n = 20$) with abdominal tumors were observed without treatment and used as the control group. During the initial 14 days after tumor detection, their tumor

27

volume had significantly increased for 98 folds (tumor volume at 14 days after onset, 667.6 ± 100.9 mm^3 vs. 7.0 ± 0.7 mm^3; $P < 0.0001$; **Figure 18B**), reflecting rapid progression. Necropsy confirmed that using the ellipsoid volume formula (*i.e.* 1/2 × width × length × thickness) as an estimation of tumor volume, as proposed by Tomayko and Reynold[63] for the study of NB xenografts, showed strong correlation with tumor weight in $MYCN^{+/-}$ mice (n = 13; $R^2 = 0.0097$; $P < 0.0001$; **Figure 18C**). Histopathology showed hypervascularity, frequent mitosis, and occasional ganglionic differentiation of tumor cells, which were morphological features resembling PDNB in human (**Figure 18D**).

3.11. Preclinical PET imaging in Th-*MYCN* mice

Next, we imaged mice bearing abdominal tumors with small animal PET/CT imaging with FDG, FDOPA, and FLT. A total of 10 tumors were evaluated with paired FDG and FDOPA PET, respectively. The range of FDG and FDOPA uptake value were similar (SUV$_{max}$ 2.57 ± 0.29 *vs*. 2.63 ± 0.23). The majority of tumors (n = 6) showed an FDG^{hi}, FDOPA^{lo} uptake pattern (**Figure 19**); others have shown FDG^{lo}, FDOPA^{hi} uptake pattern (*n* = 2; **Figures 20D-20E**) or have shown tumor encapsulation of the kidneys which prevented accurate measurement of SUVmax (**Figures 20A-20C**). The FLT uptake (n=9) was too low to be visualized (**Figure 19H**). The plain CT could not discern the tumors from adjacent organs, although tumors frequently showed calcification spots (**Figure 20F**).

Among the 8 tumors with paired FDG and FDOPA PET imaging data which can be masured for SUVmax, FDG and FDOPA uptake showed a strong and significant inverse correlation (**Figure 20G**), which observation is in consistence with findings in human NB uptake of FDG and FDOPA (**Figures 11B-11C**).
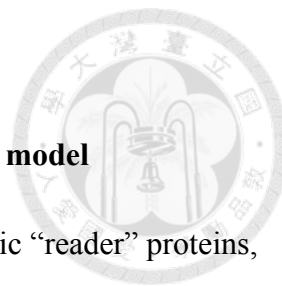
3.12. Efficacy of epigenetic inhibition of *MYCN* in the preclinical model

BRD4, a member of the BET bromodomain family of epigenetic "reader" proteins, has been shown to strongly enhance the transcription of MYC/MYCN and serves as a potential therapeutic target. To test the feasibility of our Th-*MYCN* imaging platform to study developmental therapeutics, we treated the mice with JQ1, a small molecule inhibitor of BRD4 and therefore an indirect, epigenetic inhibitor of MYCN. We also compared the result with 13-cis-retinoic acid (13cRA), a well-established differentiating agent used in maintenance therapy of human NB.

Animals bearing abdominal tumors with diameter ≥ 2 mm were treated with JQ1 (50 mg/kg IP QD for 28 days; $n = 6$) or observation only ($n = 20$). JQ1 treatment induced significant delay of tumor growth (tumor volume index at 28 days, 9.3±6.2 *vs.* 323.9±59.3, $P = 0.0012$; **Figure 21A**) and better survival (median, 18 *vs.* 43 days after treatment, $P = 0.0002$; **Figure 21B**). However, the majority of mice (5/6) had their tumor relapsed after cessation of JQ1, although diminished tumor vascularization has been observed along with the initial tumor volume reduction (**Figure 21C**).

By contrast, no treatment response was observed in mice treated with 13cRA, either given as a therapeutic (5 mg/kg PO QD for 14 days; $n = 6$; **Figure 21C**) or prevention ($n = 10$; 5 mg/kg PO QD continuously since age 5 weeks; **Figure 21D**).

4. Discussion 討論

The background of this study is the lack of commercially available ^{123}I-MIBG in Taiwan during the study period, which has driven us to explore the clinical use of FDG and FDOPA PET in NB. Although we have demonstrated a complementary role of these PET scans in the diagnosis of NB, we must stress that ^{123}I-MIBG scan, in countries with a stable supply, remains the single most important molecular imaging of NB. The more recent application of PET with ^{123}I-MIBG[66] or ^{18}F-labeled MIBG analogs[67,68] may further enhance the diagnostic power of the "MIBG family" of molecular imaging techniques.

To the best of our knowledge, this is the first study showing significant prognostic impact of both FDG and FDOPA PET at initial diagnosis of NB. We showed that the molecular imaging phenotype of FDG^{hi}, FDOPA^{lo} is associated with unfavorable clinico-genomic features and worse treatment outcome in NB. The clinical and biological implications of our findings are four-fold.

4.1. FDG & FDOPA PET imaging reflects the tumor biology of NB

First, FDG^{hi}, FDOPA^{lo} is associated with unfavorable clinical characteristics but also with the poor-risk Seg$^+$ and MNA$^+$ genomic types, indicating a strong relationship between metabolic patterns on PET and underlying tumor biology. Although data on age, stage, histopathology, and *MYCN* amplification can be confidently obtained in most clinical settings[8], the detection of Seg$^+$, that accounts for 37% of NB and confers a dismal outcome[15], requires time- and resource-consuming pangenomic methods or multiple *in situ* hybridizations[54]. The proposed "PET-UHR" criteria yielded a positive predictive value of 92.9% in predicting Seg$^+$ or MNA$^+$, providing a convenient
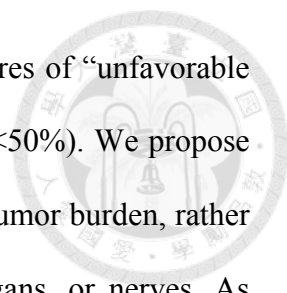
parameter of the underlying tumor biology for patients undergoing diagnostic PET scans. Furthermore, area under the ROC curve of G:D is larger than that of FDG or FDOPA uptake alone in classifying the unfavorable genomic types, indicating that combining the information of FDG and FDOPA uptake may serve as a useful biomarker to predict the underlying tumor biology in NB.

Interestingly, we have also shown the positive correlation among FDOPA uptake, MIBG avidity, and AADC gene expression, indicating the presence of a cluster of "catecholaminergic phenotypes" in NB. We also found that the strongest FDOPA uptake and AADC gene occurs in PDNB and DNB, but not the more differentiated GNB and GN or the least differentiated UNB. These findings probably reflects a recently proposed "cholinergic switch" model in NTs[69,70]: As tumors are differentiating, they undergo a shift from adrenergic to cholinergic enzyme profile, mimicking the process of specification to enteric neurons, and which is at least associated with the activation of sonic hedgehog pathway.[69]

4.2. The impact of molecular imaging on NB surgery

The molecular imaging phenotype of NB tumors at diagnosis also has an impact on NB surgery. We showed that FDG[hi], FDOPA[lo] is associated with the lowest GTR rate and may complement the current concept of diagnostic and preoperative evaluation using IDRF(s) (**Table 4** and **Figure 13**).

We propose that GTR be vigorously attempted for primary tumors with IDRF(s) and "favorable PET" (FDG[lo], FDOPA[hi]), whose NB tumor may be more "catecholaminergic", moderately differentiated, with higher probability of carrying numerical chromosomal alterations, and with higher probability of complete local control through meticulous surgical intervention.

By contrast, in primary tumors with known IDRF(s) and features of "unfavorable PET" (FDG^{hi}, FDOPA^{lo}), their probability of GTR is much lower (<50%). We propose that their major operation be aimed at tumor debulking to decrease tumor burden, rather than at heroic resection which risks sacrificing major vessels, organs, or nerves. As "unfavorable PET" implies unfavorable tumor biology in these patients, high-dose chemotherapy, irradiation, and maintenance therapy after surgery are all important to achieve maximal efficacy. Avoiding surgical complications (e.g. major bleeding or nephrectomy) may help to preserve the patients' organ function and enhance their likelihood of completing multimodality therapy without delay or dose reduction.

We suggest that a new surgical risk stratification system using the information from FDG and FDOPA PET imaging studies may be incorporated into the next generation of NB treatment protocol. Whether this new approach can improve patient survival and decrease surgical complication rates should be prospectively and vigorously evaluated in future clinical trials.

4.3.   Overall genomic pattern predicts the molecular imaging phenotype of NB

Interestingly, while the FDG SUV$_{max}$ was sequentially higher in the three genomic types (Num$^+$ < Seg$^+$ < MNA$^+$), the FDOPA SUV$_{max}$ is equally lower in the two unfavorable types (Num$^+$ > Seg$^+$ = MNA$^+$). Since both the Seg$^+$ and MNA$^+$ genomic types are associated with the FDG^{hi}, FDOPA^{lo} phenotype and a very poor outcome[15], the MYCN oncoprotein *per se* or its downstream signals may further contribute to a metabolic phenotype towards hyper-glycolysis[71], causing significantly higher FDG uptake and more aggressive behavior of MNA$^+$ tumors.

4.4. Diagnostic PET imaging as a predictor of treatment outcome

The prognostic implication of our study is that the signal intensity of tumor uptake, *i.e.* FDG^{hi} and/or FDOPA^{lo}, serves as independent predictors of inferior prognosis. From ^{123}I-MIBG scintigraphy, semi-quantitative scoring systems have been developed to assess the total extent of MIBG-avid lesions and predicted the treatment outcome in NB[30,31]. Adopting these scoring systems of tumor extensity to FDG[37] and FDOPA PET[72] was also prognostic in relapsed/refractory NB. In addition to assessing disease extensiveness, measuring the intensity of tumor uptake may further expand the usefulness of PET scans in NB.

On FDG PET, higher SUV$_{max}$ correlated with higher stage at diagnosis[36,73] and worse survival at relapse[37]. Interestingly, the FDG uptake values in our cohort are similar to results from relevant subgroups in two recent Korean studies (**Table 8**)[36,73]. However, the measurement of SUV$_{max}$ may vary with different instruments and imaging protocols. Through appropriate instrumentation calibration, standardization of protocols for patient preparation and scanning, and stricter uptake-time control with effective correction algorithms [74], In the future, FDG SUV$_{max}$ may become a reproducible imaging biomarker in multi-center and multi-national trials of NB.

On FDOPA PET, Piccardo *et al*. showed that higher "whole-body metabolic burden", defined as the sum of bony metastatic extent plus the product of tumor uptake and tumor volume, correlated with very poor outcome in relapsed/refractory NB; however, the prognostic impact of the mean or maximal uptake of FDOPA by the primary tumor was not reported[72]. More studies are needed to further delineate the impact of FDG and FDOPA uptake across patient populations.

The biological basis of FDG^{hi}, FDOPA^{lo} may largely be explained by the Warburg effect[44]. Both FDG^{hi} and FDOPA^{lo} phenotypes correlated with higher *HK2* expression,

which is required for oncogenic transformation *in vitro* and tumor initiation *in vivo*[75] and is enhanced by MYCN and HIF-1α[76]. In breast cancer, the gene expression profile of tumors with FDG $SUV_{max} > 10$ showed an "FDG signature" that was enriched with glycolysis-related genes and associated with activation of the *MYC* transcription factor (c-Myc), a functional counterpart of *MYCN*[77]. In this study, we demonstrated that higher FDG uptake in NB is associated with *MYCN* amplification and poor prognosis. To validate these findings, we checked the gene expression data from a large cohort published by Kocak *et al.* ($n = 649$ primary NB tumors)[78] and found that higher *HK2* expression is associated with *MYCN* amplification and worse survival (**Figure 22**).

In addition to its prognostic impact, the glycolysis pathway *per se* may serve as a therapeutic target. It has been recently found that treating NB cells and mouse models with 2-deoxyglucose, an analog of FDG and inhibitor of glycolysis, decreased *HK2* expression and induced apoptosis [79]. Preclinical testing has also proved the *in vivo* efficacy of 2-deoxyglucose in NB [80]. Based on these findings, PET imaging may be further studied as a biomarker that identifies patients with NB or other cancers who would most likely to benefit from novel therapies targeting *MYC/MYCN* [71,81] or the glycolytic pathway [79,80,82].

Surprisingly, we found that lower, rather than higher, FDOPA uptake significantly correlated with very poor prognosis, which may be explained by less catecholaminergic differentiation. In the Kocak dataset[78], lower expression of the *DDC* mRNA, which would be translated into the AADC enzyme, the main target of FDOPA, was also associated with MYCN amplification and worse prognosis (**Figure 23**). Although FDOPA uptake did not correlate with the degree of differentiation on histopathology, its negative correlation with *HK2* and positive correlation with *SLC6A2* expression levels suggests that FDOPA^{lo} tumors may confer a hyper-glycolytic and catecholaminergically

34

dedifferentiated phenotype at the molecular level. Characterization of an "FDOPA signature" of gene expression is warranted.
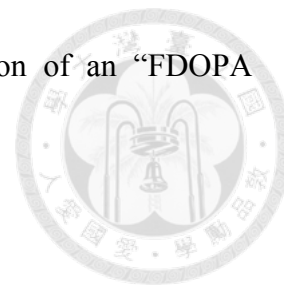
4.5. The utility of a preclinical molecular imaging platform of NB

We also showed that FDG and FDOPA PET scans are feasible in characterizing the molecular nature of NBs in Th-*MYCN* hemizygous mice. We found the majority of NB tumor in this model showed the FDG[hi], FDOPA[lo] uptake pattern. However, there was no distant metastasis detected in this mouse model based on a multitude of PET scans. Although it is a promising new imaging modality, FLT PET may not be sensitive enough to detect the proliferation activity of primary NB tumors in mice.

Furthermore, we confirmed the feasibility of this imaging platform and the therapeutic efficacy of epigenetic inhibition of *MYCN* transcription. Genomic instability and mutations is a hallmark of cancer[83]. In the recent decade, epigenetic mechanisms such as DNA methylation, histone modification, nucleosome remodeling, and RNA-mediated targeting are being found to be involved in the tumorigenesis in many cancer types.[84] Therefore, small molecules that inhibit the "reader", "writer", or "eraser" proteins/enzymes involved in epigenetic pathways have been tested in the pipelines of new cancer drug development.[84]

Bromodomain-containing epigenetic "reader" proteins are of substantial biological interest as components of transcription factor complexes and determinants of epigenetic memory. In 2010, a group at Harvard/Dana Farber Cancer Institute reported a cell-permeable small molecule that binds competitively to acetyl-lysine recognition motifs, or bromodomains, showing high potency and specificity[85]. The name of the drug is JQ1, named after Dr. Jun Qi (祁軍博士), the chemist who first synthesized it. The original idea of JQ1 was to target NUT (nuclear protein in testis) midline carcinoma

with t(15;19) (NMC), a aggressive adult carcinoma. Due to the extreme rarity of NMC, the group that developed JQ1 had "open-sourced" JQ1 to the world by publishing its formula and properties without patenting[85]. Subsequently, MYC was identified as the most significantly down-regulated signaling pathway[86], and the biological activity of JQ1 in NB was also proven *in vitro* and *in vivo*[81].

In our experiment, BRD4 inhibition showed therapeutic efficacy in transgenic mice with ultrasound-confirmed abdominal NB tumors and may serve as a novel therapeutic strategy for ultra-high-risk neuroblastoma. Further translational efforts are warranted to incorporate novel BET bromodomain inhibitors into phase 1/2 clinical trials.

4.6. Limitations of this study

Our study has some limitations. As the tumor uptake values are continuous variables, they may have continuous impact on prognosis, similar to the age effect in NB.[14] Our sample size precluded extensive statistical analyses to search for the best cutoffs that predict the highest risk of incomplete resection or poor prognosis. Instead, we utilized the ROC analysis to determine the cutoffs of FDG uptake, FDOPA uptake, and combined as PET-UHR, which were associated with significantly inferior outcome, independent from age, stage, IDRF, and *MYCN* amplification. We postulate that PET scans may add value to anatomical imaging and conventional risk stratification systems by identifying a subgroup of patients with excellent prognosis, who can truly benefit from modern multimodal therapy, from the ultra-high-risk patients who should be enrolled in novel therapeutic trials. However, this observation cannot yet be made with assurance. Our data support that the utility of diagnostic FDG and/or FDOPA PET should be further evaluated in a larger cohort of high-risk NB, ideally through multi-center or international collaborations.
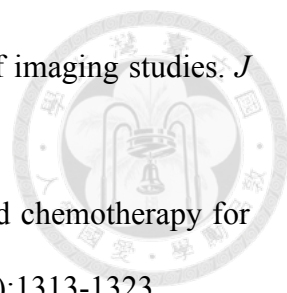
4.7. Conclusion

In conclusion, we showed that FDG and FDOPA PET scans are not only sensitive in imaging primary NB tumors, but may also be useful in characterization of NB tumor behavior. The tumor uptake intensity of FDG and FDOPA on PET scans at diagnosis distinguish the tumor biology and treatment outcome in NB. The unfavorable PET imaging phenotype with FDG^{hi}, FDOPA^{lo} uptake patterns were associated with poor-risk clinico-genomic features, less likelihood of gross total resection, and much worse prognosis. The prognostic value of PET-UHR, using FDG $SUV_{max} \geq 3.31$ and FDOPA $SUV_{max} < 4.12$ as criteria, may be incorporated in future risk stratification systems and be validated in prospective trials. Furthermore, we established a small-animal imaging platform of NB using both ultrasound and PET imaging, which is useful to carry out preclinical new drug investigations in the future.

5. References 參考文獻

1. Yang CP, Hung IJ, Jaing TH, Chang WH. Cancers in infancy: percent distribution and incidence rates. *Acta Paediatr Taiwan.* 2006;47(6):273-277.

2. Maris JM. Recent advances in neuroblastoma. *N Engl J Med.* 2010;362(23):2202-2211.

3. Shimada H, Ambros IM, Dehner LP, et al. The International Neuroblastoma Pathology Classification (the Shimada system). *Cancer.* 1999;86(2):364-372.

4. Hoehner JC, Gestblom C, Hedborg F, Sandstedt B, Olsen L, Pahlman S. A developmental model of neuroblastoma: differentiating stroma-poor tumors' progress along an extra-adrenal chromaffin lineage. *Lab. Invest.* 1996;75(5):659-675.

5. Hiyama E, Iehara T, Sugimoto T, et al. Effectiveness of screening for neuroblastoma at 6 months of age: a retrospective population-based cohort study. *Lancet.* 2008;371(9619):1173-1180.

6. Woods WG, Tuchman M, Robison LL, et al. A population-based study of the usefulness of screening for neuroblastoma. *Lancet.* 1996;348(9043):1682-1687.

7. Segi M. *Cancer Mortality for Selected Sites in 24 Countries (1950-57).* Sendai, Japan: Department of Public Health, Tohoku University of Medicine; 1960.

8. Henderson TO, Bhatia S, Pinto N, et al. Racial and ethnic disparities in risk and survival in children with neuroblastoma: a Children's Oncology Group study. *J. Clin. Oncol.* 2011;29(1):76-82.

9. Liu YL, Lo WC, Chiang CJ, et al. Incidence of cancer in children aged 0-14 years in Taiwan, 1996-2010. *Cancer Epidemiol.* 2015;39(1):21-28.

10. Caiulo VA, Caiulo S, Gargasole C, et al. Ultrasound mass screening for congenital anomalies of the kidney and urinary tract. *Pediatr. Nephrol.* 2012.
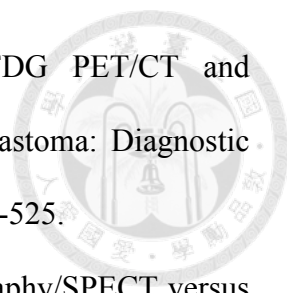
11. Kushner BH. Neuroblastoma: a disease requiring a multitude of imaging studies. *J Nucl Med.* 2004;45(7):1172-1188.

12. Baker DL, Schmidt ML, Cohn SL, et al. Outcome after reduced chemotherapy for intermediate-risk neuroblastoma. *New Engl J Med.* 2010;363(14):1313-1323.

13. Cohn SL, Pearson AD, London WB, et al. The International Neuroblastoma Risk Group (INRG) classification system: an INRG Task Force report. *J. Clin. Oncol.* 2009;27(2):289-297.

14. London WB, Castleberry RP, Matthay KK, et al. Evidence for an age cutoff greater than 365 days for neuroblastoma risk group stratification in the Children's Oncology Group. *J Clin Oncol.* 2005;23(27):6459-6465.

15. Janoueix-Lerosey I, Schleiermacher G, Michels E, et al. Overall genomic pattern is a predictor of outcome in neuroblastoma. *J Clin Oncol.* 2009;27(7):1026-1033.

16. Tomioka N, Oba S, Ohira M, et al. Novel risk stratification of patients with neuroblastoma by genomic signature, which is independent of molecular signature. *Oncogene.* 2008;27(4):441-449.

17. Monclair T, Brodeur GM, Ambros PF, et al. The International Neuroblastoma Risk Group (INRG) staging system: an INRG Task Force report. *J Clin Oncol.* 2009;27(2):298-303.

18. Simon T, Haberle B, Hero B, von Schweinitz D, Berthold F. Role of Surgery in the Treatment of Patients With Stage 4 Neuroblastoma Age 18 Months or Older at Diagnosis. *J. Clin. Oncol.* 2013;31(6):752-758.

19. Simon T, Hero B, Benz-Bohm G, von Schweinitz D, Berthold F. Review of image defined risk factors in localized neuroblastoma patients: Results of the GPOH NB97 trial. *Pediatr Blood Cancer.* 2008;50(5):965-969.

20. Cecchetto G, Mosseri V, De Bernardi B, et al. Surgical risk factors in primary
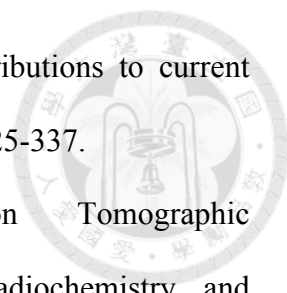
surgery for localized neuroblastoma: the LNESG1 study of the European International Society of Pediatric Oncology Neuroblastoma Group. *J. Clin. Oncol.* 2005;23(33):8483-8489.
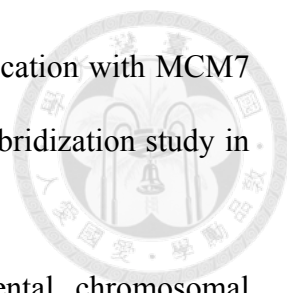
21. Liu YL, Miser JS, Hsu WM. Risk-directed therapy and research in neuroblastoma. *J Formos Med Assoc.* 2014;113(12):887-889.

22. Kreissman SG, Seeger RC, Matthay KK, et al. Purged versus non-purged peripheral blood stem-cell transplantation for high-risk neuroblastoma (COG A3973): a randomised phase 3 trial. *Lancet Oncol.* 2013;14(10):999-1008.

23. Yu AL, Gilman AL, Ozkaynak MF, et al. Anti-GD2 antibody with GM-CSF, interleukin-2, and isotretinoin for neuroblastoma. *N Engl J Med.* 2010;363(14):1324-1334.

24. Pugh TJ, Morozova O, Attiyeh EF, et al. The genetic landscape of high-risk neuroblastoma. *Nat. Genet.* 2013;45(3):279-284.

25. La Quaglia MP, Kushner BH, Su W, et al. The impact of gross total resection on local control and survival in high-risk neuroblastoma. *J Pediatr Surg.* 2004;39(3):412-417; discussion 412-417.

26. Hsu WM, Jen YM, Lee H, et al. The influence of biologic factors on the surgical decision in advanced neuroblastoma. *Ann Surg Oncol.* 2006;13(2):238-244.

27. Brisse HJ, McCarville MB, Granata C, et al. Guidelines for imaging and staging of neuroblastic tumors: consensus report from the International Neuroblastoma Risk Group Project. *Radiology.* 2011;261(1):243-257.

28. Kushner BH, Kramer K, Modak S, Cheung NK. Sensitivity of surveillance studies for detecting asymptomatic and unsuspected relapse of high-risk neuroblastoma. *J Clin Oncol.* 2009;27(7):1041-1046.

29. Dubois SG, Geier E, Batra V, et al. Evaluation of Norepinephrine Transporter
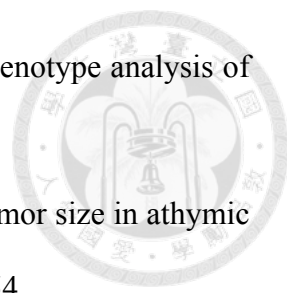
Expression and Metaiodobenzylguanidine Avidity in Neuroblastoma: A Report from the Children's Oncology Group. *Int. J. Mol. Imag.* 2012;2012:250834.
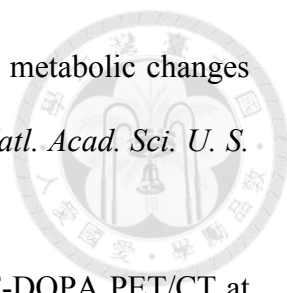
30. Yanik GA, Parisi MT, Shulkin BL, et al. Semiquantitative mIBG Scoring as a Prognostic Indicator in Patients with Stage 4 Neuroblastoma: A Report from the Children's Oncology Group. *J. Nucl. Med.* 2013;54(4):541-548.

31. Decarolis B, Schneider C, Hero B, et al. Iodine-123 metaiodobenzylguanidine scintigraphy scoring allows prediction of outcome in patients with stage 4 neuroblastoma: results of the cologne interscore comparison study. *J. Clin. Oncol.* 2013;31(7):944-951.

32. Matthay KK, Shulkin B, Ladenstein R, et al. Criteria for evaluation of disease extent by (123)I-metaiodobenzylguanidine scans in neuroblastoma: a report for the International Neuroblastoma Risk Group (INRG) Task Force. *Br J Cancer.* 2010;102(9):1319-1326.

33. Wilson JS, Gains JE, Moroz V, Wheatley K, Gaze MN. A systematic review of 131I-meta iodobenzylguanidine molecular radiotherapy for neuroblastoma. *Eur J Cancer.* 2014;50(4):801-815.

34. French S, DuBois SG, Horn B, et al. 131I-MIBG followed by consolidation with busulfan, melphalan and autologous stem cell transplantation for refractory neuroblastoma. *Pediatr. Blood Cancer.* 2013;60(5):879-884.

35. Matthay KK, Yanik G, Messina J, et al. Phase II study on the effect of disease sites, age, and prior therapy on response to iodine-131-metaiodobenzylguanidine therapy in refractory neuroblastoma. *J Clin Oncol.* 2007;25(9):1054-1060.

36. Choi YJ, Hwang HS, Kim HJ, et al. (18)F-FDG PET as a single imaging modality in pediatric neuroblastoma: comparison with abdomen CT and bone scintigraphy. *Ann Nucl Med.* 2014;28(4):304-313.
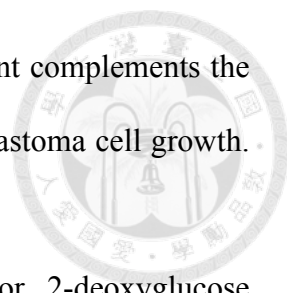
37. Papathanasiou ND, Gaze MN, Sullivan K, et al. 18F-FDG PET/CT and 123I-Metaiodobenzylguanidine Imaging in High-Risk Neuroblastoma: Diagnostic Comparison and Survival Analysis. *J Nucl Med.* 2011;52(4):519-525.

38. Melzer HI, Coppenrath E, Schmid I, et al. 123I-MIBG scintigraphy/SPECT versus 18F-FDG PET in paediatric neuroblastoma. *Eur. J. Nucl. Med. Mol. Imaging.* 2011;38(9):1648-1658.

39. Chawla M, Kumar R, Agarwala S, Bakhshi S, Gupta DK, Malhotra A. Role of positron emission tomography-computed tomography in staging and early chemotherapy response evaluation in children with neuroblastoma. *Indian J Nucl Med.* 2010;25(4):147-155.

40. Taggart DR, Han MM, Quach A, et al. Comparison of iodine-123 metaiodobenzylguanidine (MIBG) scan and [18F]fluorodeoxyglucose positron emission tomography to evaluate response after iodine-131 MIBG therapy for relapsed neuroblastoma. *J Clin Oncol.* 2009;27(32):5343-5349.

41. Sharp SE, Shulkin BL, Gelfand MJ, Salisbury S, Furman WL. 123I-MIBG scintigraphy and 18F-FDG PET in neuroblastoma. *J Nucl Med.* 2009;50(8):1237-1243.

42. Kushner BH, Yeung HW, Larson SM, Kramer K, Cheung NK. Extending positron emission tomography scan utility to high-risk neuroblastoma: fluorine-18 fluorodeoxyglucose positron emission tomography as sole imaging modality in follow-up of patients. *J Clin Oncol.* 2001;19(14):3397-3405.

43. Shulkin BL, Hutchinson RJ, Castle VP, Yanik GA, Shapiro B, Sisson JC. Neuroblastoma: positron emission tomography with 2-[fluorine-18]-fluoro-2-deoxy-D-glucose compared with metaiodobenzylguanidine scintigraphy. *Radiology.* 1996;199(3):743-750.

44. Koppenol WH, Bounds PL, Dang CV. Otto Warburg's contributions to current concepts of cancer metabolism. *Nat. Rev. Cancer.* 2011;11(5):325-337.

45. Vallabhajosula S. 18F-Labeled Positron Emission Tomographic Radiopharmaceuticals in Oncology: An Overview of Radiochemistry and Mechanisms of Tumor Localization. *Seminars in Nuclear Medicine.* 2007;37(6):400-419.

46. Kumakura Y, Cumming P. PET studies of cerebral levodopa metabolism: a review of clinical findings and modeling approaches. *Neuroscientist.* 2009;15(6):635-650.

47. Minn H, Kauhanen S, Seppanen M, Nuutila P. 18F-FDOPA: a multiple-target molecule. *J Nucl Med.* 2009;50(12):1915-1918.

48. Gilbert J, Haber M, Bordow SB, Marshall GM, Norris MD. Use of tumor-specific gene expression for the differential diagnosis of neuroblastoma from other pediatric small round-cell malignancies. *Am J Pathol.* 1999;155(1):17-21.

49. Bozzi F, Luksch R, Collini P, et al. Molecular detection of dopamine decarboxylase expression by means of reverse transcriptase and polymerase chain reaction in bone marrow and peripheral blood: utility as a tumor marker for neuroblastoma. *Diagn Mol Pathol.* 2004;13(3):135-143.

50. Geerts D, Koster J, Albert D, et al. The polyamine metabolism genes ornithine decarboxylase and antizyme 2 predict aggressive behavior in neuroblastomas with and without MYCN amplification. *International journal of cancer. Journal international du cancer.* 2010;126(9):2012-2024.

51. Koster J. R2: microarray analysis and visualization platform. http://r2.amc.nl.

52. Brodeur GM, Pritchard J, Berthold F, et al. Revisions of the international criteria for neuroblastoma diagnosis, staging, and response to treatment. *J Clin Oncol.* 1993;11(8):1466-1477.

53. Tsai HY, Hsi BL, Hung IJ, et al. Correlation of MYCN amplification with MCM7 protein expression in neuroblastomas: a chromogenic in situ hybridization study in paraffin sections. *Hum Pathol.* 2004;35(11):1397-1403.

54. Schleiermacher G, Mosseri V, London WB, et al. Segmental chromosomal alterations have prognostic impact in neuroblastoma: a report from the INRG project. *Br. J. Cancer.* 2012;107(8):1418-1422.

55. Chang HH, Lee H, Hu MK, et al. Notch1 expression predicts an unfavorable prognosis and serves as a therapeutic target of patients with neuroblastoma. *Clin Cancer Res.* 2010;16(17):4411-4420.

56. Yang AS, Chiang TC, Shen LH. Acute intravenous injection toxicity study of MIBG in mice. *Drug Chem Toxicol.* 2010;33(1):17-19.

57. de Vries EFJ, Luurtsema G, Brussermann M, Elsinga PH, Vaalburg W. Fully automated synthesis module for the high yield one-pot preparation of 6-[18F]fluoro-l-DOPA. *Appl Radiat Isot.* 1999;51(4):389-394.

58. Hsu WM, Hsieh FJ, Jeng YM, et al. Calreticulin expression in neuroblastoma--a novel independent prognostic factor. *Ann Oncol.* 2005;16(2):314-321.

59. Fischer M, Skowron M, Berthold F. Reliable transcript quantification by real-time reverse transcriptase-polymerase chain reaction in primary neuroblastoma using normalization to averaged expression levels of the control genes HPRT1 and SDHA. *J Mol Diagn.* 2005;7(1):89-96.

60. Teitz T, Stanke JJ, Federico S, et al. Preclinical models for neuroblastoma: establishing a baseline for treatment. *PLoS One.* 2011;6(4):e19133.

61. Weiss WA, Aldape K, Mohapatra G, Feuerstein BG, Bishop JM. Targeted expression of MYCN causes neuroblastoma in transgenic mice. *The EMBO journal.* 1997;16(11):2985-2995.

62. Haraguchi S, Nakagawara A. A simple PCR method for rapid genotype analysis of the TH-MYCN transgenic mouse. *PLoS One.* 2009;4(9):e6902.

63. Tomayko MM, Reynolds CP. Determination of subcutaneous tumor size in athymic (nude) mice. *Cancer Chemother. Pharmacol.* 1989;24(3):148-154.

64. Hsu WC, Tzen KY, Huy PT, Duet M, Yeh TH. An animal model of central auditory pathway imaging in the rat brain by high resolution small animal positron emission tomography. *Acta Otolaryngol.* 2009;129(4):423-428.

65. Rasmuson A, Segerstrom L, Nethander M, et al. Tumor Development, Growth Characteristics and Spectrum of Genetic Aberrations in the TH-MYCN Mouse Model of Neuroblastoma. *PLoS One.* 2012;7(12):e51297.

66. Cistaro A, Quartuccio N, Caobelli F, et al. 124I-MIBG: a new promising positron-emitting radiopharmaceutical for the evaluation of neuroblastoma. *Nucl Med Rev Cent East Eur.* 2015;18(2):102-106.

67. Zhang H, Huang R, Cheung NK, et al. Imaging the norepinephrine transporter in neuroblastoma: a comparison of [18F]-MFBG and 123I-MIBG. *Clin Cancer Res.* 2014;20(8):2182-2191.

68. Vaidyanathan G, Affleck DJ, Zalutsky MR. (4-[18F]fluoro-3-iodobenzyl)guanidine, a potential MIBG analogue for positron emission tomography. *J. Med. Chem.* 1994;37(21):3655-3662.

69. Gershon TR, Shirazi A, Qin LX, Gerald WL, Kenney AM, Cheung NK. Enteric neural crest differentiation in ganglioneuromas implicates Hedgehog signaling in peripheral neuroblastic tumor pathogenesis. *PLoS One.* 2009;4(10):e7491.

70. Bourdeaut F, Janoueix-Lerosey I, Lucchesi C, et al. Cholinergic switch associated with morphological differentiation in neuroblastoma. *J Pathol.* 2009;219(4):463-472.

71. Zirath H, Frenzel A, Oliynyk G, et al. MYC inhibition induces metabolic changes leading to accumulation of lipid droplets in tumor cells. *Proc. Natl. Acad. Sci. U. S. A.* 2013;110(25):10258-10263.

72. Piccardo A, Puntoni M, Lopci E, et al. Prognostic value of 18F-DOPA PET/CT at the time of recurrence in patients affected by neuroblastoma. *Eur. J. Nucl. Med. Mol. Imaging.* 2014;41(6):1046-1056.

73. Lee JW, Cho A, Yun M, Lee JD, Lyu CJ, Kang WJ. Prognostic value of pretreatment FDG PET in pediatric neuroblastoma. *Eur J Radiol.* 2015;84(12):2633-2639.

74. Kurland BF, Muzi M, Peterson LM, et al. Multicenter Clinical Trials Using 18F-FDG PET to Measure Early Response to Oncologic Therapy: Effects of Injection-to-Acquisition Time Variability on Required Sample Size. *J Nucl Med.* 2016;57(2):226-230.

75. Patra KC, Wang Q, Bhaskar PT, et al. Hexokinase 2 is required for tumor initiation and maintenance and its systemic deletion is therapeutic in mouse models of cancer. *Cancer Cell.* 2013;24(2):213-228.

76. Qing G, Skuli N, Mayes PA, et al. Combinatorial regulation of neuroblastoma tumor progression by N-Myc and hypoxia inducible factor HIF-1alpha. *Cancer Res.* 2010;70(24):10351-10361.

77. Palaskas N, Larson SM, Schultz N, et al. 18F-fluorodeoxy-glucose positron emission tomography marks MYC-overexpressing human basal-like breast cancers. *Cancer Res.* 2011;71(15):5164-5174.

78. Kocak H, Ackermann S, Hero B, et al. Hox-C9 activates the intrinsic pathway of apoptosis and is associated with spontaneous regression in neuroblastoma. *Cell Death Dis.* 2013;4:e586.

79. Chuang JH, Chou MH, Tai MH, et al. 2-Deoxyglucose treatment complements the cisplatin- or BH3-only mimetic-induced suppression of neuroblastoma cell growth. *Int. J. Biochem. Cell. Biol.* 2013;45(5):944-951.

80. Huang CC, Wang SY, Lin LL, et al. Glycolytic inhibitor 2-deoxyglucose simultaneously targets cancer and endothelial cells to suppress neuroblastoma growth in mice. *Dis Model Mech.* 2015;8(10):1247-1254.

81. Puissant A, Frumm SM, Alexe G, et al. Targeting MYCN in neuroblastoma by BET bromodomain inhibition. *Cancer Discov.* 2013;3(3):308-323.

82. Bean JF, Qiu YY, Yu S, Clark S, Chu F, Madonna MB. Glycolysis inhibition and its effect in doxorubicin resistance in neuroblastoma. *J Pediatr Surg.* 2014;49(6):981-984; discussion 984.

83. Hanahan D, Weinberg RA. Hallmarks of cancer: the next generation. *Cell.* 2011;144(5):646-674.

84. Dawson MA, Kouzarides T. Cancer epigenetics: from mechanism to therapy. *Cell.* 2012;150(1):12-27.

85. Filippakopoulos P, Qi J, Picaud S, et al. Selective inhibition of BET bromodomains. *Nature.* 2010;468(7327):1067-1073.

86. Mertz JA, Conery AR, Bryant BM, et al. Targeting MYC dependence in cancer by inhibiting BET bromodomains. *Proc. Natl. Acad. Sci. U. S. A.* 2011;108(40):16669-16674.

6. Tables 附表

Table 1. The sensitivity and specificity of ^{18}F-FDOPA PET in comparison to ^{123}I-MIBG Scan or ^{18}F-FDG PET.

Modality	Sensitivity; % (95%CI)	Specificity; % (95%CI)	Accuracy (%)	AUC (95%CI)*
All tissue-proven tumors (n=50; 42 had viable tumor cells)				
^{18}F-FDOPA PET	41/42; 97.6% (87.4%–99.9%)	7/8; 87.5% (47.3%–99.7%)	48/50 (96.0%)	0.9680 (0.9193–1.0000)†
Tumors with concomitant ^{123}I-MIBG scan (n=18; 16 had viable tumor cells)				
^{18}F-FDOPA PET	16/16; 100% (79.4%–100.0%)	1/2; 50.0% (1.26%–98.7%)	17/18 (94.4%)	0.9062 (0.6976–1.0000)
^{123}I-MIBG scan	12/16; 75% (47.6%–92.7%)	2/2; 100.0% (15.8%–100.0%)	14/18 (77.8%)	Non-applicable
P value	0.0455	0.3173		Non-applicable
Tumors with concomitant ^{18}F-FDG PET scans (n=46; 38 had viable tumor cells)				
^{18}F-FDOPA PET	37/38; 97.4% (86.2%–99.9%)	7/8; 87.5% (47.3–99.7)	44/46 (95.6%)	0.9645 (0.9101–1.000)†
^{18}F-FDG PET	33/38; 86.8% (71.9%–95.6%)	5/8; 62.5% (24.5–91.5)	38/46 (82.6%)	0.8801 (0.7861–0.9740)†
P value	0.0455	0.1573		0.0682

* Area under the ROC curve, calculated from the tumor-to-liver standard uptake value ratio in the PET studies.

† Excluding one infant patient with diffuse hepatic uptake at diagnosis, which precluded the calculation of T/L.

Table 2. Patient characteristics and tumor uptake of FDG and FDOPA at diagnosis.

Characteristics	No.	FDG Uptake[*]	P[†]	FDOPA Uptake[*]	P[†]	G:D Ratio[*]	P[†]
All patients	42	4.07 (2.76–6.36)	–	3.54 (2.79–5.03)	–	1.40 (0.75–1.89)	–
Gender			0.35		0.46		0.73
Female	14	3.25 (2.49–5.64)		3.53 (2.32–4.72)		1.29 (0.75–1.75)	
Male	28	4.53 (2.84–6.99)		3.54 (2.94–6.09)		1.40 (0.66–2.25)	
Age group			**0.0095**		**0.01**		**0.0018**
< 18 months	18	2.83 (2.24–5.09)		5.06 (2.96–6.65)		0.79 (0.35–1.59)	
≥ 18 months	24	5.09 (3.56–7.60)		3.28 (2.59–3.70)		1.64 (1.09–2.61)	
Stage			**0.0069**		**0.0013**		**0.0005**
1/2/3/4S	6/1/9/1	2.77 (1.94–4.29)		5.00 (3.46–6.67)		0.61 (0.32–1.26)	
4	25	5.16 (3.40–7.31)		3.09 (2.43–3.61)		1.67 (1.04–2.56)	
MYCN			**0.0067**		0.11		**0.0023**
Non-amplified	33	3.79 (2.64–5.11)		3.59 (2.95–5.30)		0.99 (0.57–1.63)	
Amplified	9	6.85 (5.64–8.17)		3.24 (2.04–3.66)		1.86 (1.69–2.90)	
Genomic type			**0.0003**		**0.0074**		**0.0001**
Numerical	11	2.68 (2.08–3.03)		5.49 (4.12–7.34)		0.43 (0.27–0.78)	
Segmental	7	5.01 (3.48–5.76)		3.58 (3.33–3.70)		1.35 (0.99–1.61)	
MYCN-amplified	9	6.85 (5.64–8.17)		3.24 (2.04–3.66)		1.86 (1.69–2.90)	
Flat/IGF2[‡]	3/1	6.38 (1.73–12.45)		3.95 (2.14–6.19)		1.29 (0.51–3.63)	
Histology			0.70		0.95		0.67
UNB/PDNB	9/26	4.10 (3.03–6.19)		3.58 (2.85–5.00)		1.44 (0.78–1.86)	
DNB/GNBi	3/2	2.72 (1.75–11.38)		3.48 (2.39–5.76)		0.92 (0.58–2.84)	
NB, others[‡]	2	–		–		–	
Risk group			**0.0037**		**0.0057**		**0.0008**
Low	7	2.30 (1.62–2.77)		5.49 (4.12–6.72)		0.43 (0.27–0.98)	
Intermediate	5	3.03 (2.04–7.72)		6.62 (4.06–9.10)		0.61 (0.26–1.33)	
High	30	5.11 (3.44–7.17)		3.28 (2.55–3.69)		1.64 (1.06–2.43)	
Site			0.97		0.69		0.78
Adrenal	29	4.05 (2.70–6.94)		3.48 (2.43–5.24)		1.49 (0.64–2.34)	
RP/Med	11/2	4.10 (3.11–5.47)		3.59 (2.91–4.61)		1.35 (0.89–1.74)	
IDRF			**0.03**		0.24		**0.03**
0	15	2.77 (1.80–5.60)		4.12 (2.45–6.47)		0.98 (0.22–0.97)	
≥ 1	27	4.59 (3.32–7.03)		3.41 (2.85–4.09)		1.61 (0.80–2.33)	

* Presented as median (interquartile range).

† By two-tailed Kruskal-Wallis test; *P* values in bold font indicate significance.

‡ These categories were not included in statistical analyses.

Abbreviations: CR = complete response after induction chemotherapy; DNB = differentiating neuroblastoma; GNBi, ganglioneuroblastoma, intermixed; G:D = the ratio between the SUV$_{max}$ of FDG and FDOPA; GTR = gross total resection; IDRF, image-defined risk factor; IGF2 = Beckwith-Wiedemann syndrome with *IGF2* microdeletion; IQR = interquartile range; Med = mediastinal; NA = second operation was not attempted due to ongoing chemotherapy or disease progression; NB = neuroblastoma; PDNB = poorly-differentiated neuroblastoma; RP = retroperitoneal; UNB = undifferentiated neuroblastoma.

Table 3. Diagnostic power of tumor uptake parameters in predicting the unfavorable genomic types[*] of neuroblastoma.

Statistics (95%CI)	FDG Uptake (SUV$_{max}$ ≥ 3.31)	FDOPA Uptake (SUV$_{max}$ < 4.12)	G:D Ratio (≥ 1.09)	PET-UHR*
TP / FN	15 / 1	14 / 2	14 / 2	13 / 3
FP / TN	4 / 11	4 / 11	2 / 13	1 / 14
Sensitivity	93.8% (69.8%–99.8%)	87.5% (61.7%–98.4%)	87.5% (61.7%–98.4%)	81.3% (54.4%–96.0%)
Specificity	73.3% (44.9%–92.2%)	73.3% (44.9%–92.2%)	86.7% (59.5%–98.3%)	93.3% (68.1%–99.8%)
ROC area	0.83[‡] (0.65–1.00)	0.78[‡] (0.60–0.95)	0.89[‡] (0.75–1.00)	0.87[§] (0.76–0.99)
Positive Predictive Value	78.9% (54.4%–93.9%)	77.8% (52.4%–93.6)	87.5% (61.7%–98.4%)	92.9% (66.1%–99.8%)
Negative Predictive Value	91.7% (61.5%–99.8%)	84.6% (54.6%–98.1%)	86.7% (59.5%–98.3%)	82.4% (56.6%–96.2%)

* Including segmental chromosomal alterations ($n = 7$) and *MYCN* amplification ($n = 9$) among 31 patients with genomic data.

† Defined by FDG SUV$_{max}$ ≥ 3.31 and FDOPA SUV$_{max}$ < 4.12.

‡ The areas under ROC curves of FDG, FDOPA, and G:D are significantly different ($\chi^2 = 6.78$; $P = 0.03$).

§ Estimated by (Sensitivity + Specificity) / 2.

Abbreviations: TP = true positive; TN = true negative; FP = false positive; FN = false negative; ROC = receiver operating characteristic.
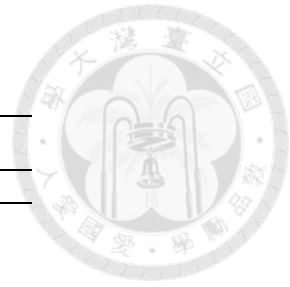
Table 4. Predictors of GTR among 34 evaluable patients.

Characteristics	n	GTR (rate)	P^*
Evaluable patients	34	27 (79%)	–
Gender			1.00
Female	10	8 (80%)	
Male	24	19 (79%)	
Age group			0.10
< 18 mo	15	14 (93%)	
≥ 18 mo	19	13 (68%)	
Stage			0.40
1/2/3/4S	17	15 (88%)	
4	17	12 (71%)	
MYCN			**0.05**
Non-amplified	29	25 (86%)	
Amplified	5	2 (40%)	
Genomic type			**0.02**
Numerical	11	11 (100%)	
Segmental	5	4 (80%)	
MYCN-amplified	5	2 (40%)	
Flat/IGF2 [†]	2/1	2 (100%)	
Histology			1.00
UNB/PDNB	6/21	21 (78%)	
DNB/GNB	3/2	4 (80%)	
NB, unspecified [†]	2	2 (100%)	
Risk group			**0.04**
Low/Intermediate	7/5	12 (100%)	
High	22	15 (68%)	
Site			1.00
Adrenal	29	17 (81%)	
RP/Med	11/2	10 (77%)	
IDRF			**0.03**
0	14	14 (100%)	
≥ 1	20	13 (65%)	
FDG uptake[‡]			**0.03**
≥ 3.31	21	14 (67%)	
< 3.31	13	13 (100%)	
FDOPA uptake[‡]			.07
≥ 4.12	11	11 (100%)	
< 4.12	23	16 (70%)	
G:D ratio			**0.002**
≥ 1.09	17	10 (59%)	
< 1.09	17	17 (100%)	
PET-UHR			**0.011**
Yes	19	12 (79%)	
No	15	15 (100%)	

NOTES. *P* values in bold font indicate significance.

* By Fisher exact text.

† These categories were not included in statistical analyses.

‡ SUVmax.

Abbreviations: GTR = gross total resection; IGF2 = Beckwith-Wiedemann syndrome with *IGF2* microdeletion; Med = mediastinal; NA, second operation was not attempted due to ongoing chemotherapy or disease progression; PET-UHR = ultra-high-risk PET; RP = retroperitoneal.

Table 5. Cox proportional hazard modeling of event-free survival.

Variable	Univariate			Multivariate		
	HR	95%CI	P	HR	95%CI	P
Age ≥ 18 months	4.6	1.5–13.7	0.006	0.8	0.2–2.8	0.741
Stage 4	10.1	2.4–45.6	0.002	7.4	1.5–35.4	0.012
MYCN amplification	4.0	1.6–10.1	0.004	4.2	1.5–11.9	0.006
IDRF[+]	2.1	0.8–5.7	0.145	0.6	0.2–1.8	0.382
PET-UHR	6.9	2.3–20.8	0.001	4.9	1.4–16.9	0.012
FDG[hi] (SUV$_{max}$ ≥ 3.31)	8.1	1.9–35.0	0.005			
FDOPA[lo] (SUV$_{max}$ < 4.12)	7.5	1.8–32.4	0.007			
Higher G:D ratio (≥ 1.09)	6.3	2.1–19.2	0.001			

Abbreviations: 95%CI = 95% confindence interval; HR = hazard ratio; IDRF[+] = presence of image-defined risk factor(s); PET-UHR = ultra-high-risk tumor uptake pattern on FDG and FDOPA PET, defined as FDG SUV$_{max}$ ≥ 3.31 and FDOPA SUV$_{max}$ < 4.12.

Table 6. Cox proportional hazard modeling on event-free survival using individual PET imaging parameters.

Variable	Multivariate		
	HR	95%CI	*P*
Model 1: Age, Stage, *MYCN*, IDRF, and FDG uptake			
Age ≥ 18 months	0.9	0.2–3.3	0.876
Stage 4	9.3	1.7–51.4	0.011
MYCN amplification	2.5	1.0–6.5	0.058
IDRF$^+$	0.6	0.2–1.6	0.245
FDG^{hi} (SUV$_{max}$ ≥ 3.31)	5.0	1.0–23.9	0.045
Model 2: Age, Stage, *MYCN*, IDRF, and FDOPA uptake			
Age ≥ 18 months	1.6	0.5–4.9	0.416
Stage 4	6.3	1.4–29.4	0.018
MYCN amplification	4.5	1.6–12.6	0.004
IDRF$^+$	0.7	0.3–2.0	0.534
FDOPA^{lo} (SUV$_{max}$ < 4.12)	4.8	1.0–22.4	0.047
Model 3: Age, Stage, *MYCN*, IDRF, and G:D ratio			
Age ≥ 18 months	1.3	0.4–4.6	0.673
Stage 4	74	1.3–42.7	0.026
MYCN amplification	2.5	0.9–6.7	0.073
IDRF$^+$	0.6	0.2–1.7	0.311
G:D (ratio ≥ 1.09)	2.0	0.5–7.7	0.290

Abbreviations: 95%CI = 95% confidence interval; HR = hazard ratio; IDRF$^+$ = presence of image-defined risk factor(s); PET-UHR = ultra-high-risk tumor uptake pattern on FDG and FDOPA PET, defined as FDG SUV$_{max}$ ≥ 3.31 and FDOPA SUV$_{max}$ < 4.12.

Table 7. Comparison of tumor latency and volume in $MYCN^{+/-}$ mice by site.

Site	n (%)	Excluded (n)*	Age of onset (d)	Tumor volume (mm^3)
Thoracic	3 (6%)	0	68.7±23.3	98.9±92.6
Juxta-Adrenal	6 (11%)	3	50.3±11.9	3.8±1.5
Pre-Aortic	37 (70%)	5	52.6±15.9	6.7±4.1
P	–	–	0.51 (log-rank)	< 0.0001 (ANOVA)

* 8 mice were excluded from this analysis due to uncertain age of onset because of missed follow-up dates during the screening period.

Table 8. Comparison of FDG uptake by primary neuroblastoma across studies.

Study[36,77]	Subgroup	n	SUV$_{max}$*	Equipment	FDG Dose	Uptake Time†
Choi *et al.*	Stage 3/4	23	5.45 (1.23–13.72)	GE Advance (GE)	5-10 MBq/kg or	60 min
	Stage 1/2	7	3.03 (0.94–7.49)	or Allegro (Philips)	5.18 MBq/kg	
This study	Stage 3/4	34	5.48 (1.41–12.94)	Discovery ST-16	5 MBq/kg	45 min
	Stage 1/2	7	2.61 (1.44–4.05)	(GE)		
Lee *et al.*	Stage 4	31	5.2±2.8	GE Advance (GE)	5 MBq/kg or	60 min
	St. 1/2/3/4S	19	2.5±1.3	or Allegro (Philips)	5.18 MBq/kg	
This study	Stage 4	25	5.7±2.8	Discovery ST-16	5 MBq/kg	45 min
	St. 1/2/3/4S	17	3.8±2.7	(GE)		

* Mean (range) or mean ± standard deviation.

† Injection-to-acquisition time.
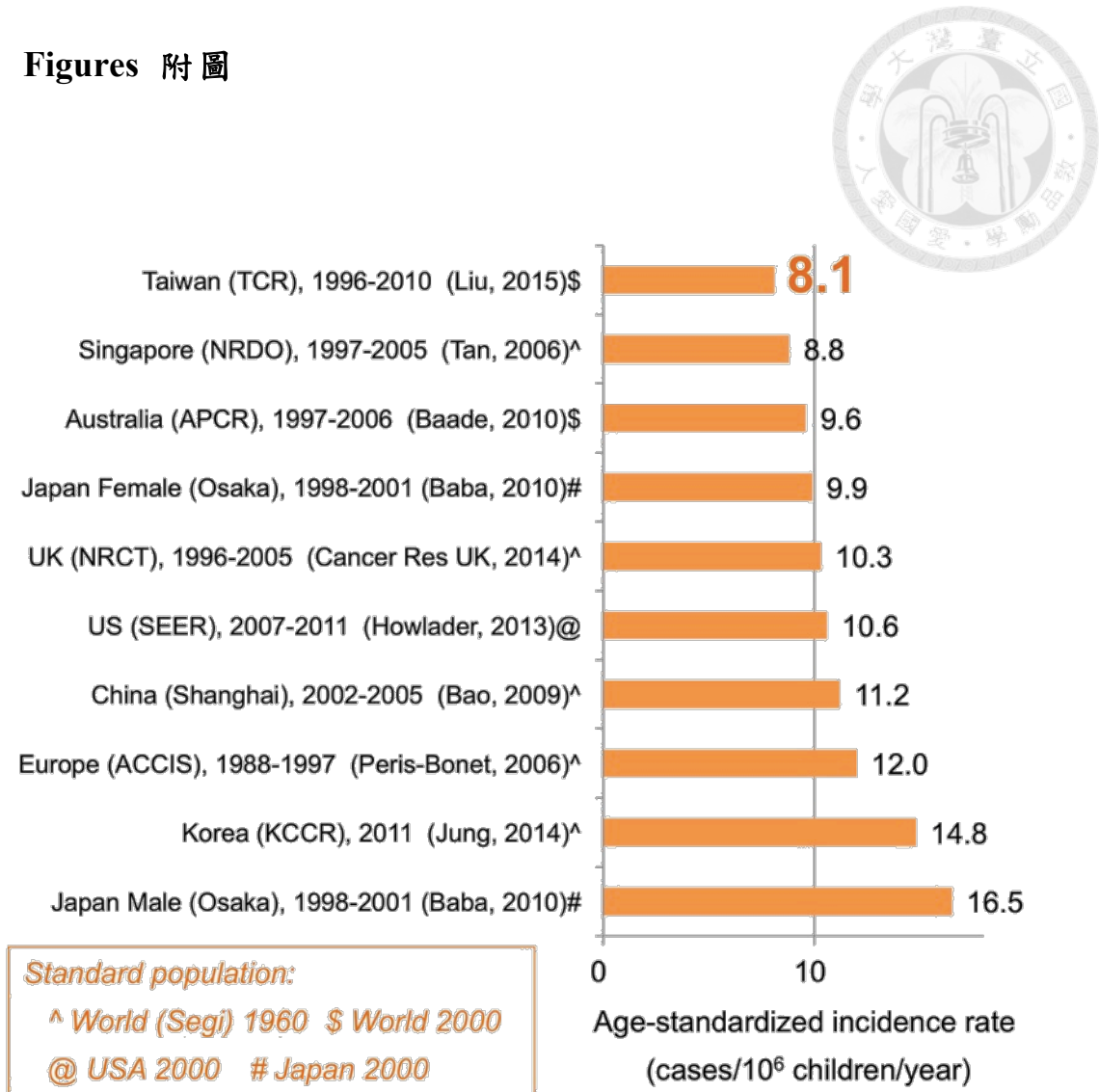
7. Figures 附圖

Figure 1. NB incidence rate among children aged 0–14 years across the world.

Abbreviations: ACCIS = The Automated Childhood Cancer Information System; APCR = Australian Paediatric Cancer Registry; KCCR = Korea Central Cancer Registry; NRCT = National Registry of Childhood Tumours; NRDO = National Registry Of Diseases Office; SEER = Surveillance, Epidemiology, and End Results Program; TCR = Taiwan Cancer Registry; UK = United Kindom; USA = United States of America.
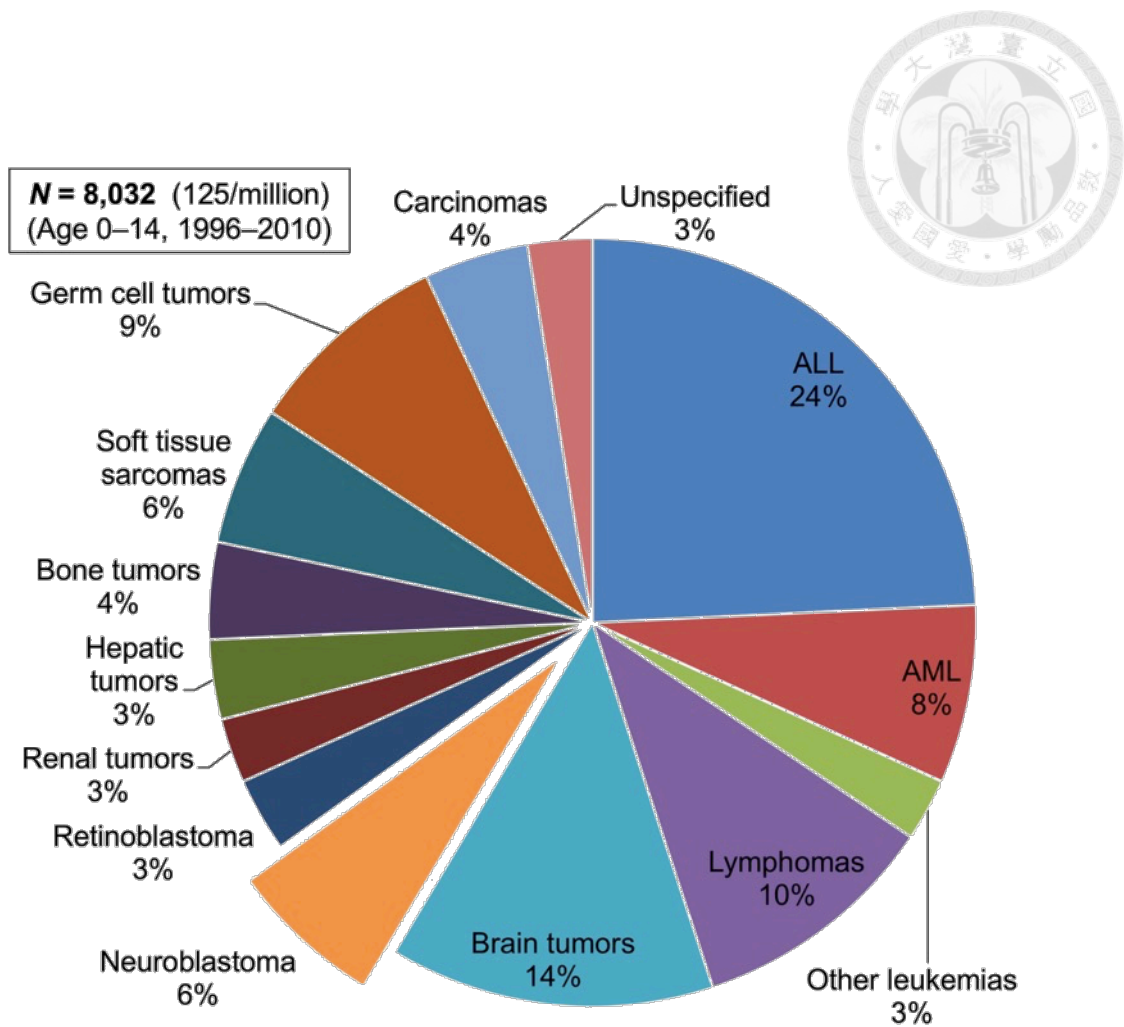
Figure 2. Relative distribution of childhood cancer categories in Taiwan.

Data are extracted from a recent study with the Taiwan Cancer Registry.[9] The ASIR of

all cancer categories combined is 125 cases/1,000,000 children/year.

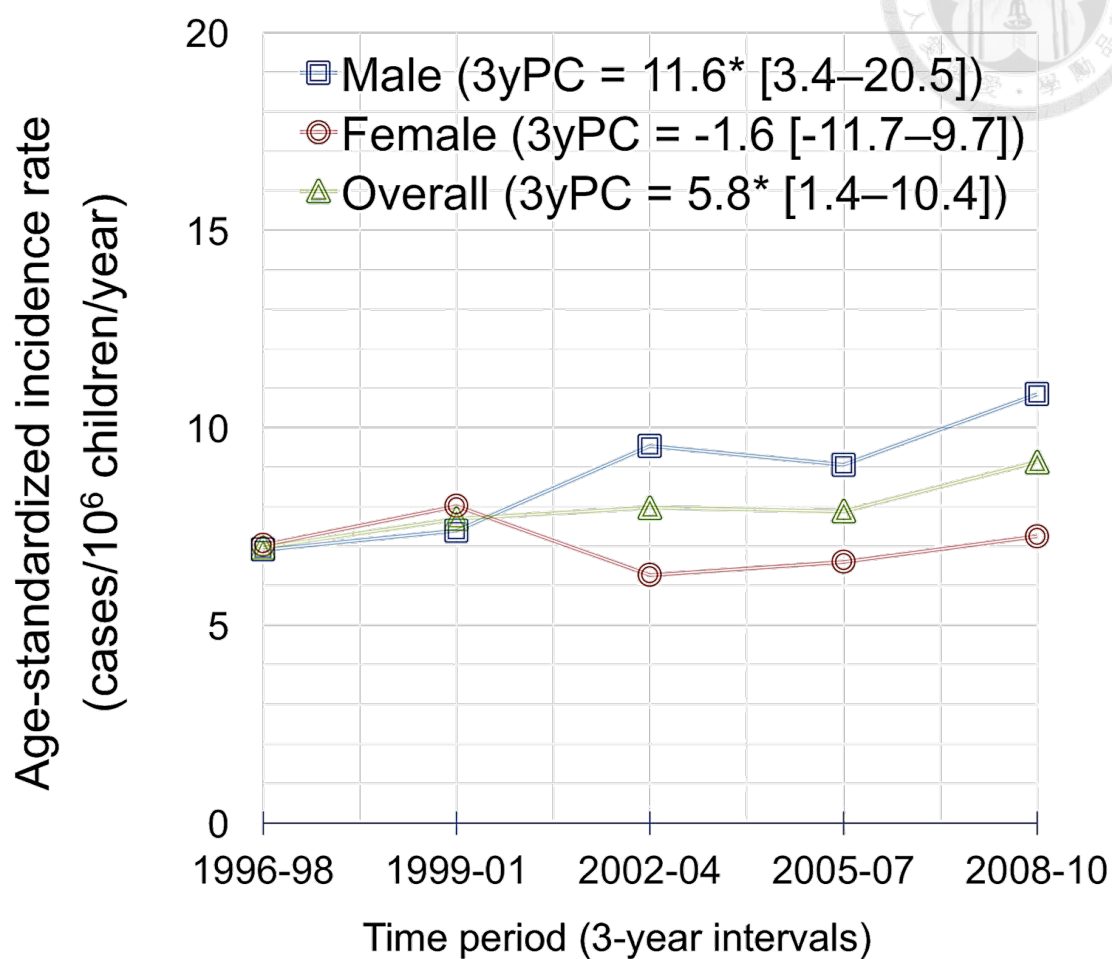Abbreviations: ALL = acute lymphoblastia leukemia; AML = acute myeloid leukemia.

Figure 3. Trends of NB incidence in Taiwan.

Data are from Taiwan Cancer Registry.
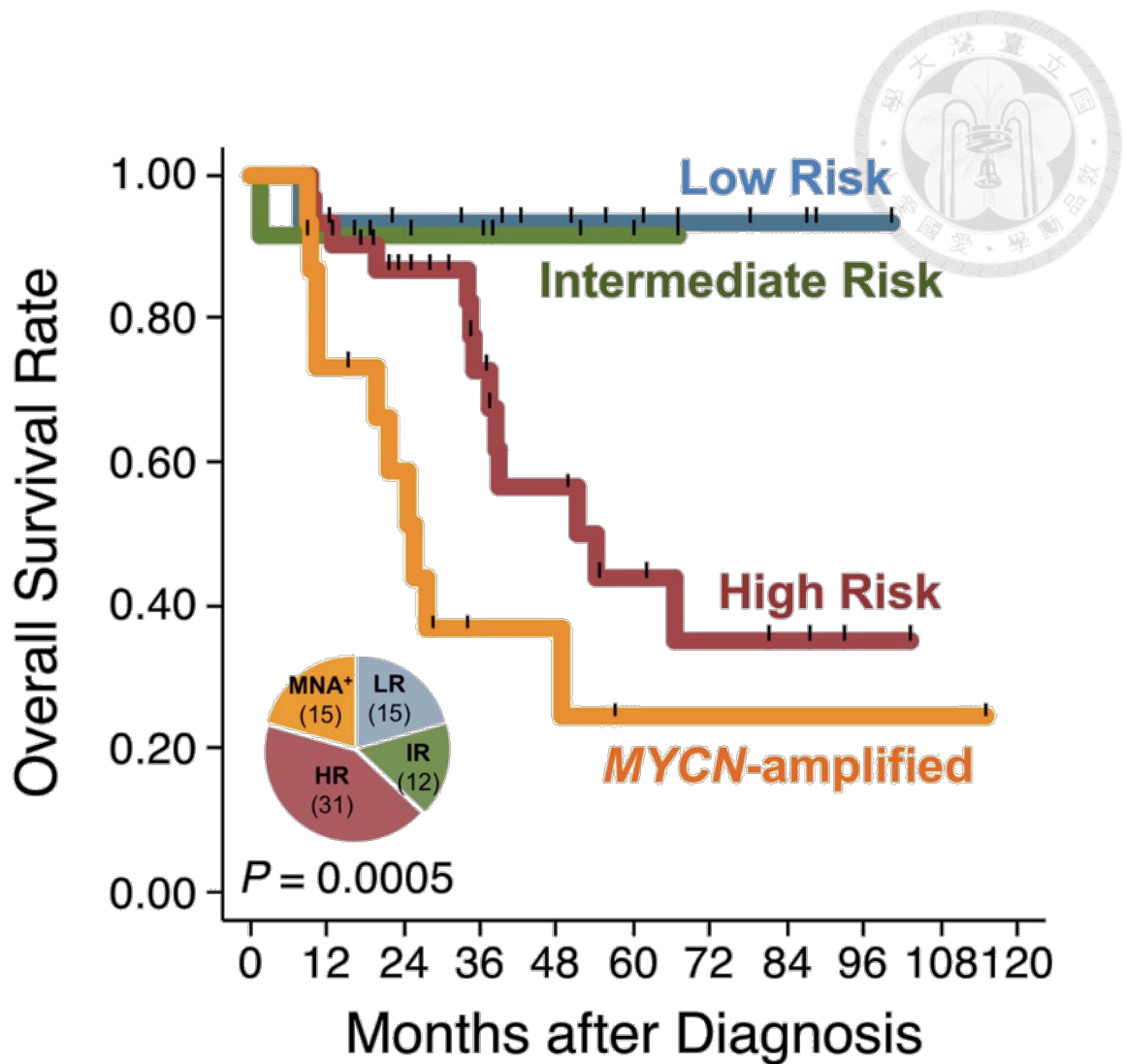
Abbreviation: 3yPC = 3-year percentage change.

Figure 4. Risk-stratified survival outcome of NB in a major center in Taiwan.

Survival curves of 73 NB patients treated at National Taiwan University Hospital during 2006–2014 are stratified by risk group. Data are updates after a previous report.[21]

Abbreviation: MNA+, amplification of the *MYCN* oncogene.
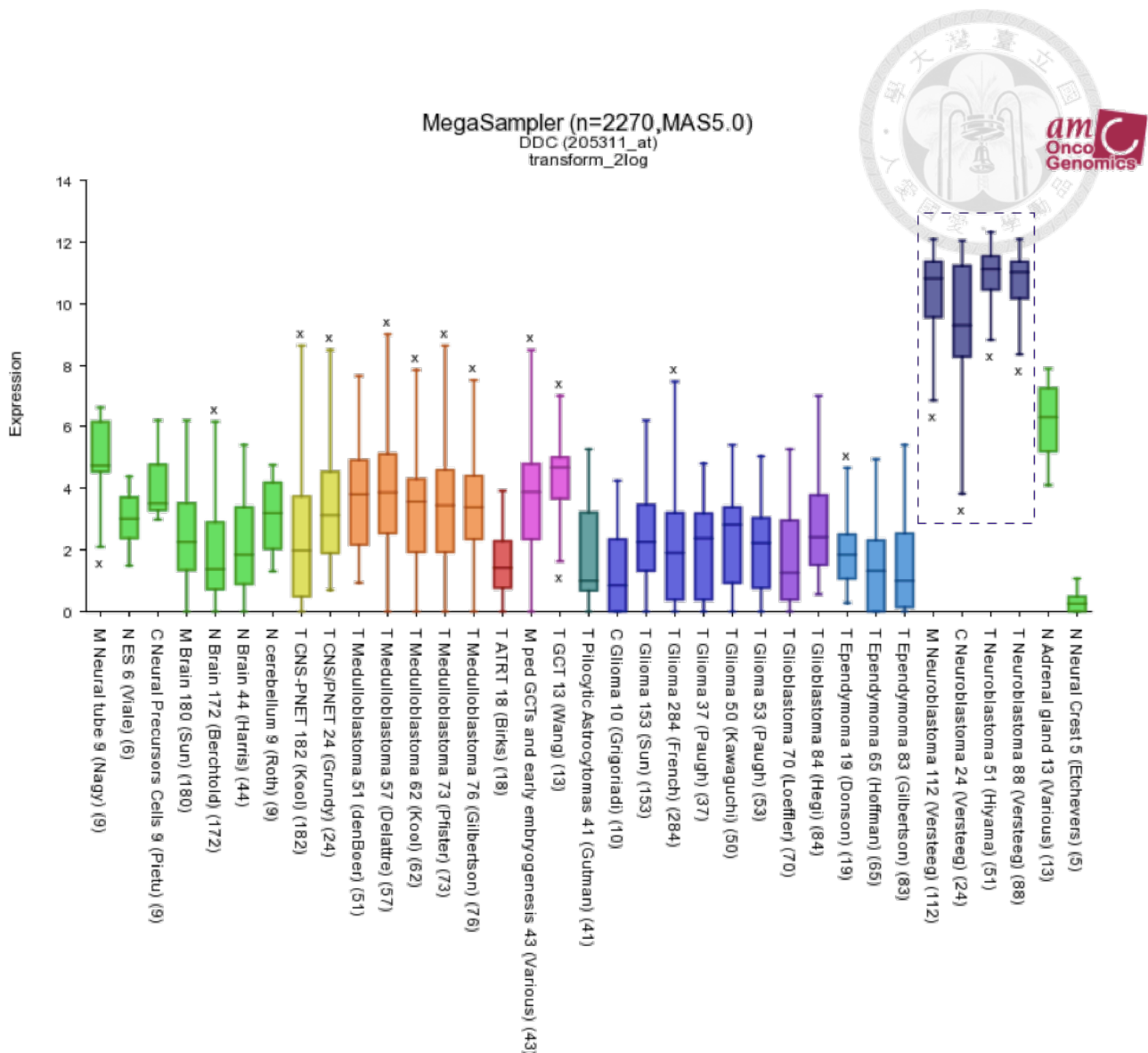
Figure 5. Expression of *DDC* mRNA in NB and other neural tumors.

Meta-analysis of microarray gene expression datasets revealed uniformly high levels of DDC gene expression in NB tumor datasets (box). Using R2, an on-line microarray platform ([r2.amc.nl](r2.amc.nl))[50,51], public gene expression datasets of Affymetrix Human Genome U133 Plus 2.0 platform were retrieved and compared for *DDC* gene expression. Different colors represent normal neural tissues (lime green) or various types of tumors. Abbreviations: C = cell lines; GCTs = germ cell tumors; M = mixed; N = normal tissue; T = tumor.

Figure 6. Abnormal ^{18}F-FDOPA uptake by NB tumors.

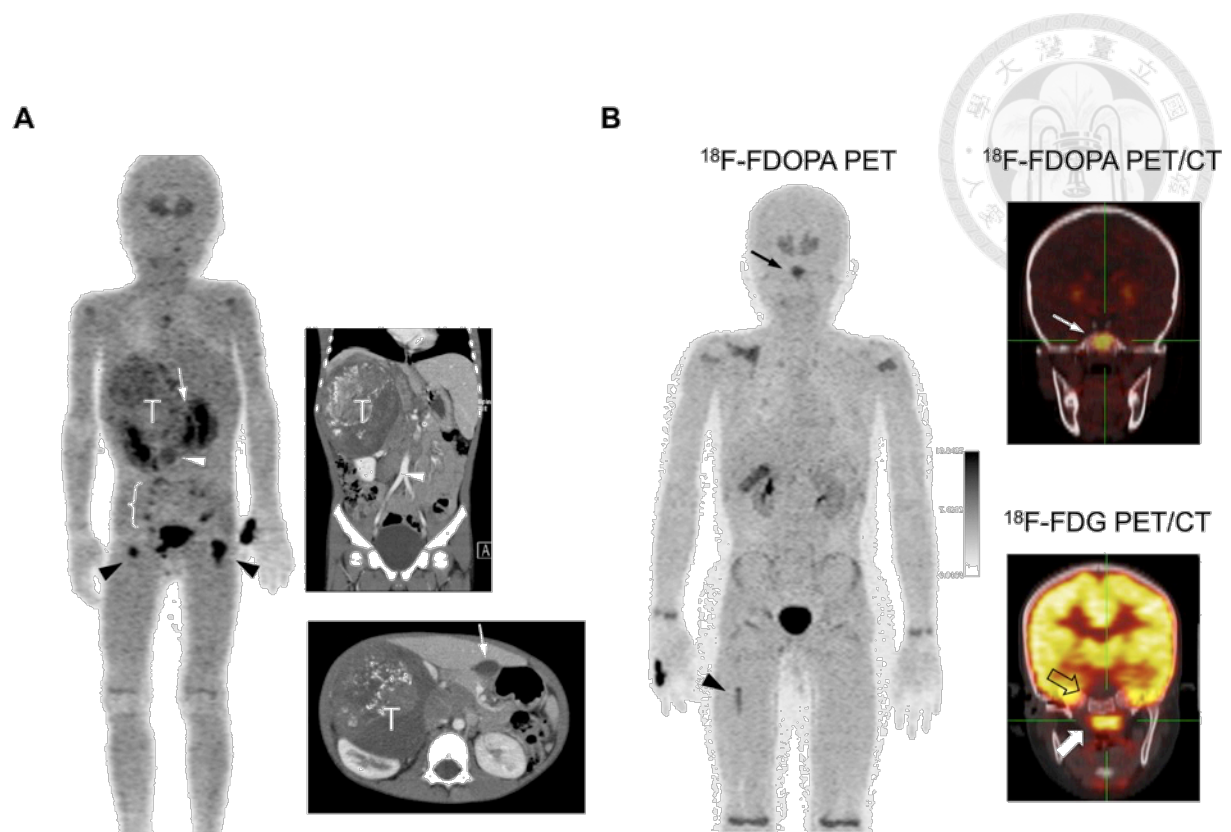(**A**) A five-year-old boy with stage 4 NB presented with a huge suprarenal tumor (T) with heterogeneous ^{18}F-FDOPA uptake pattern, which displaced the gall bladder (white arrow) and kidneys. ^{18}F-FDOPA PET also revealed metastases to paraspinal lymph nodes (brace), paraaortic lymph nodes (white arrow head), and bilateral proximal femurs (black arrow heads). Histology of the main tumor showed poorly differentiated neuroblastoma. (**B**) A nine-year-old boy with stage 4 NB after multimodality therapy for 3 years was revealed with a metastatic lesion at the sphenoid bone on ^{18}F-FDOPA PET (arrow). The lesion was negative on ^{18}F-FDG PET (open arrow), while there was strong uptake by the brain and nearby pharyngeal lymphoid tissue (thick arrow). The concurrently abnormal ^{18}F-FDOPA uptake at right femoral shaft (arrow head) was proven to be a metastatic neuroblastoma on curettage.
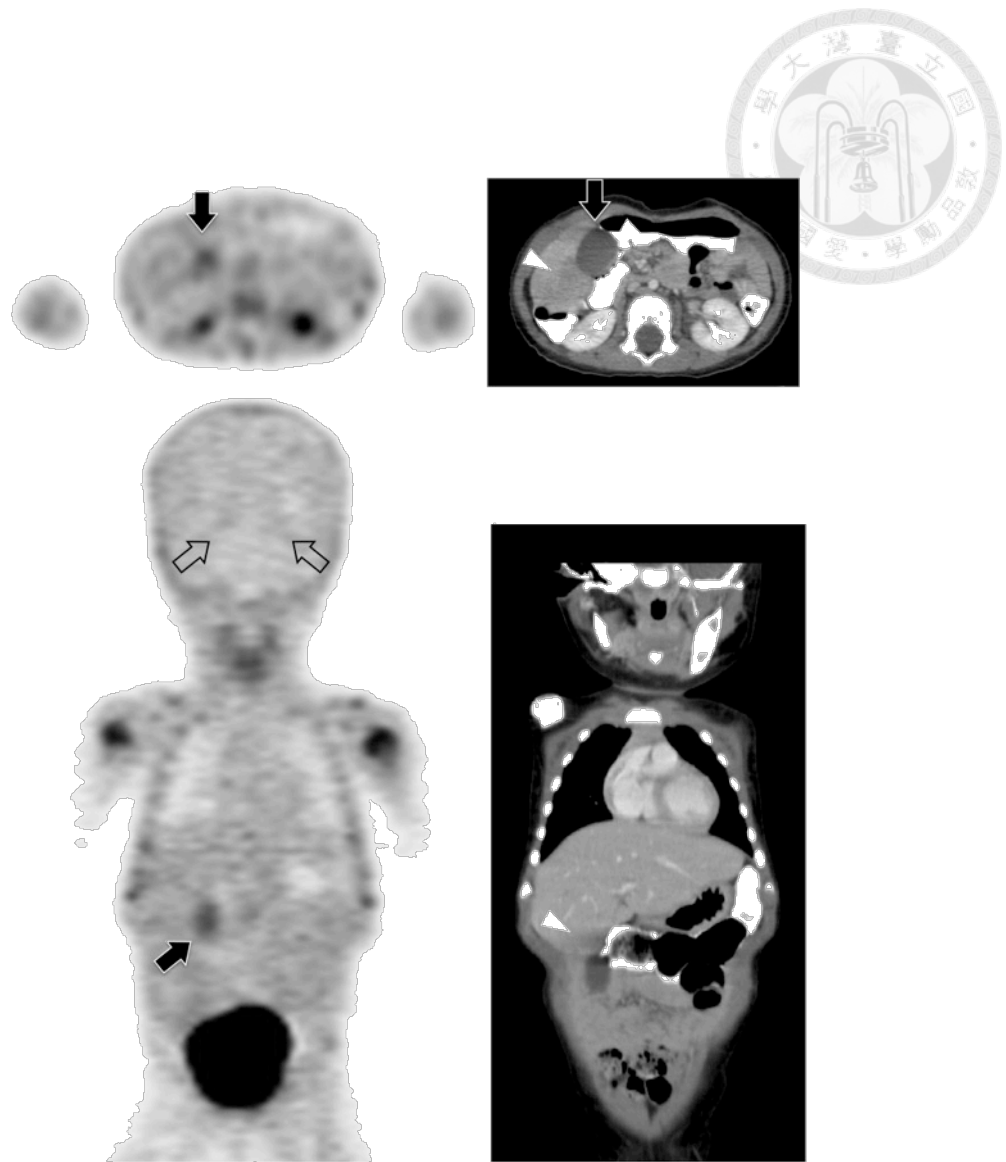
Figure 7. Normal FDOPA uptake pattern.

Representative transverse and coronal PET images (left panel) from a 19-month-old girl with stage 4S, *MYCN*-amplified disease after completion of therapy showed normal uptake over the basal ganglia (open arrows), gallbladder (thick black arrows), urinary tract, and epiphyseal plates of the long bones. Due to a hypodense lesion over the right inferior segment of liver on a concomitant CT scan with contrast enhancement (arrow heads, right panel), the mass was resected surgically and proven to be fibrosis only.

61
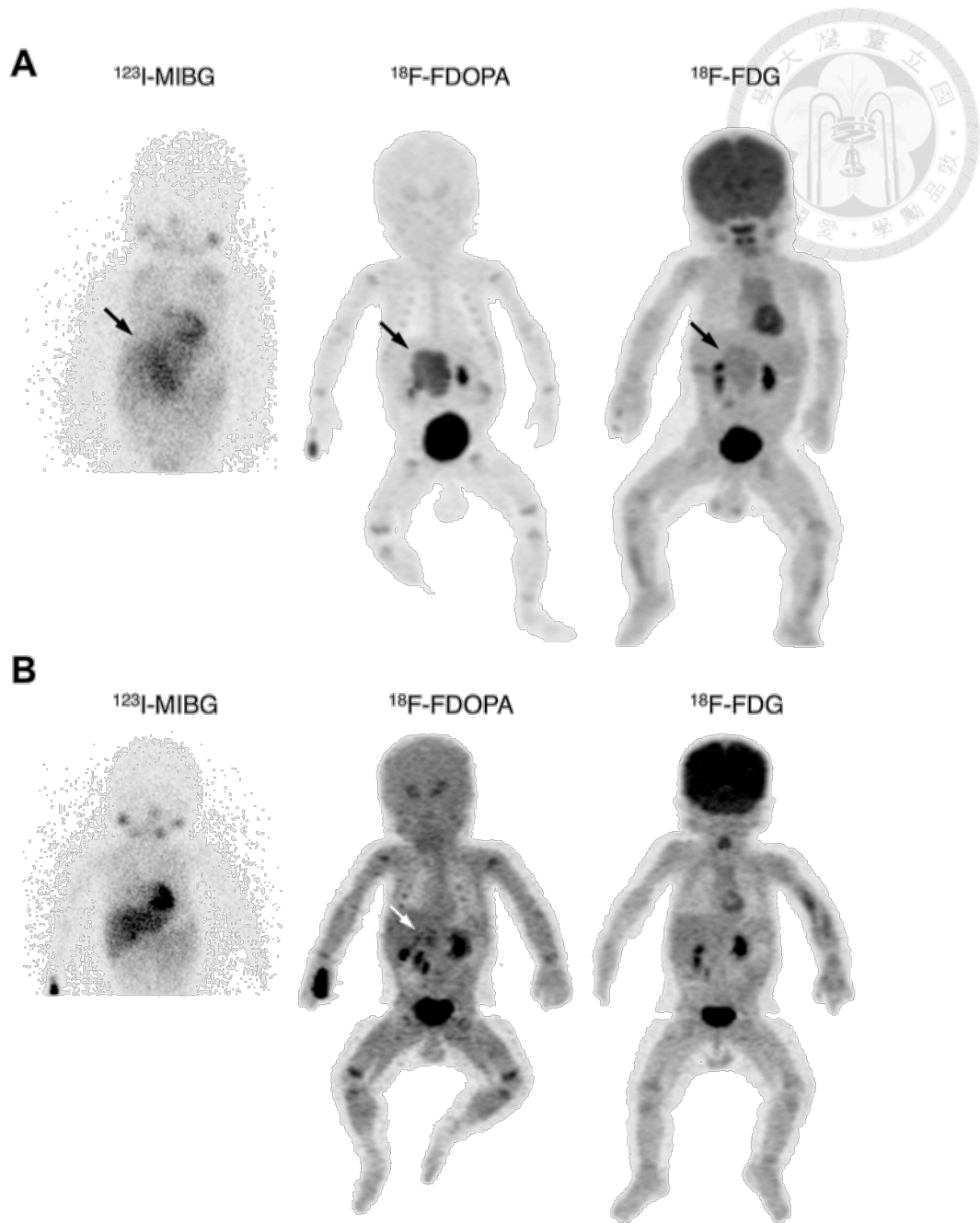
Figure 8. Comparison among ^{123}I-MIBG scan, ^{18}F-FDOPA PET, and ^{18}F-FDG PET.

(**A**) A three-month-old boy with stage 3, MYCN-non-amplified disease at diagnosis

showed MIBG$^+$ / FDOPA$^+$ / FDG$^+$. Histology of the right adrenal tumor showed poorly

differentiated neuroblastoma. (**B**) After three courses of chemotherapy, the imaging

results became MIBG$^-$ / FDOPA$^+$ / FDG$^-$ before total resection of the tumor. Histology

confirmed the presence of neuroblastic cells.
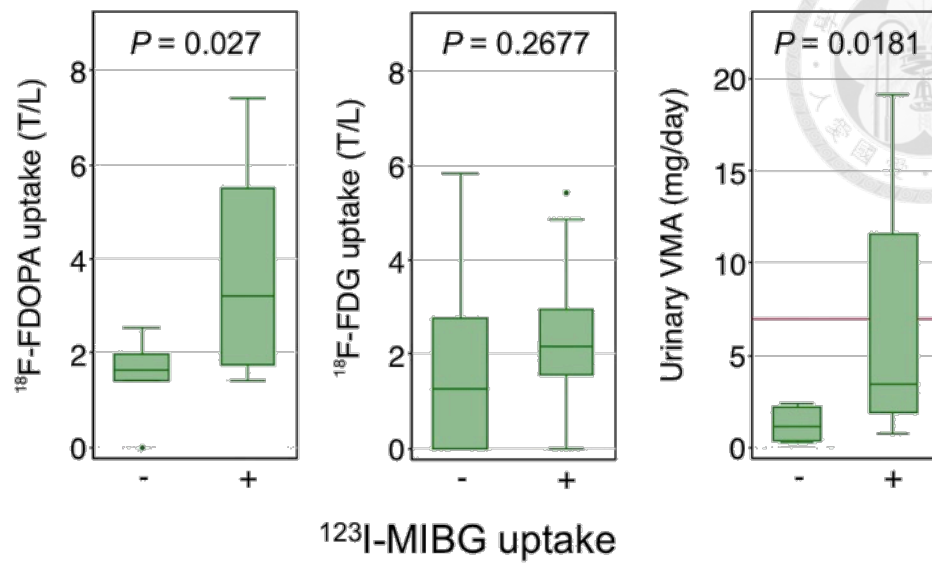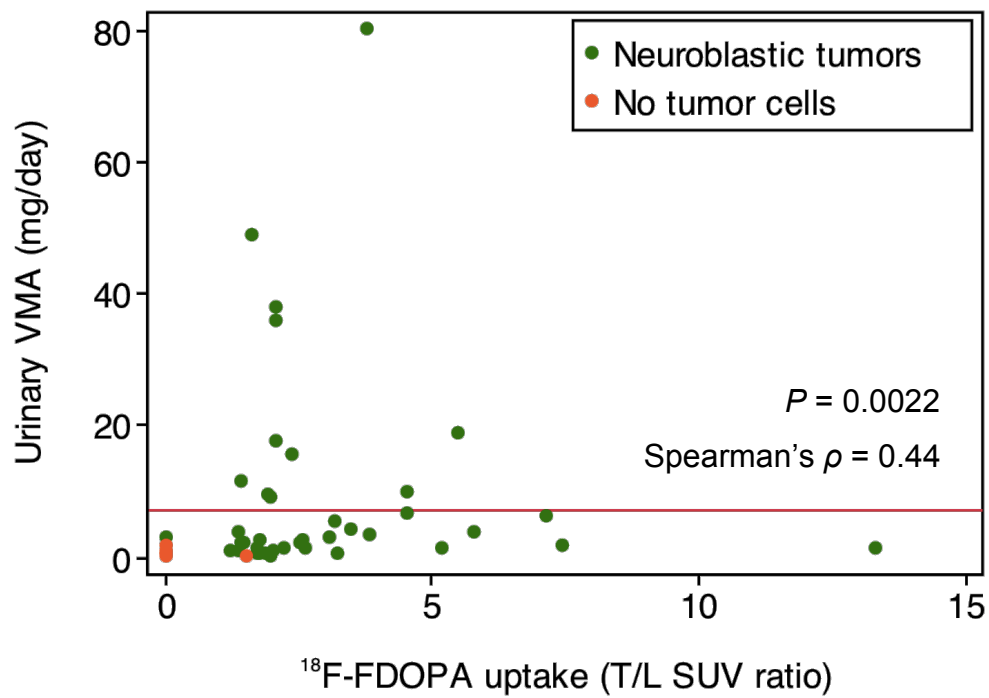
Figure 9. Tumor uptake, catecholamine metabolism, and histologic differentiation.

doi:10.6342/NTU201600303

C

D
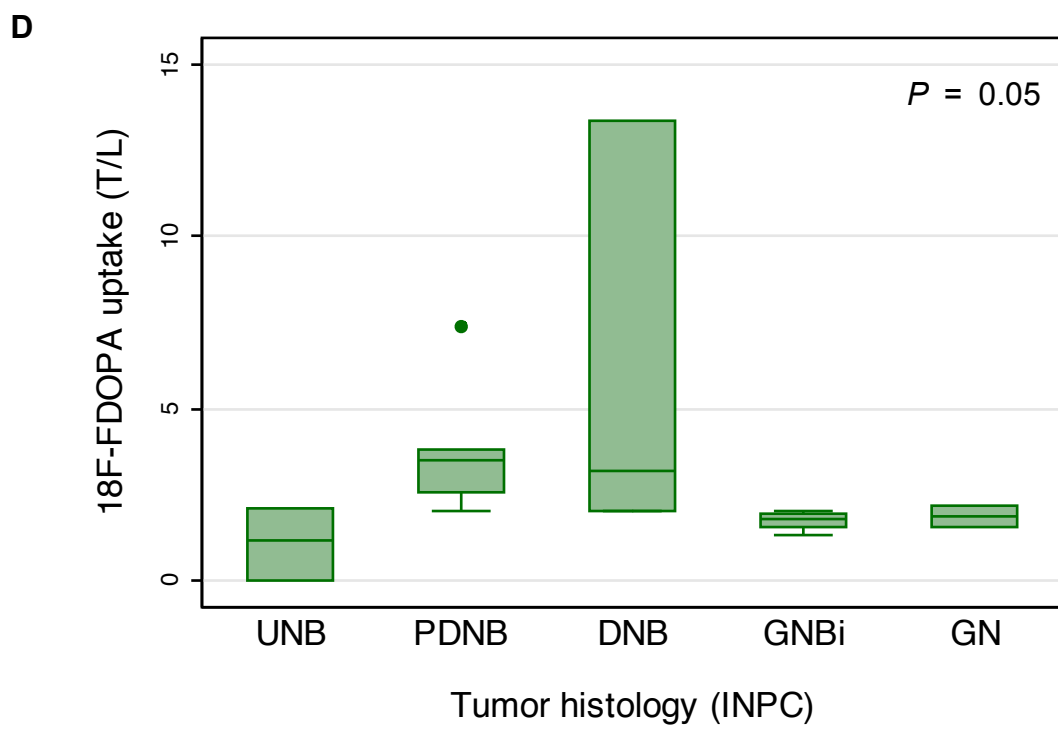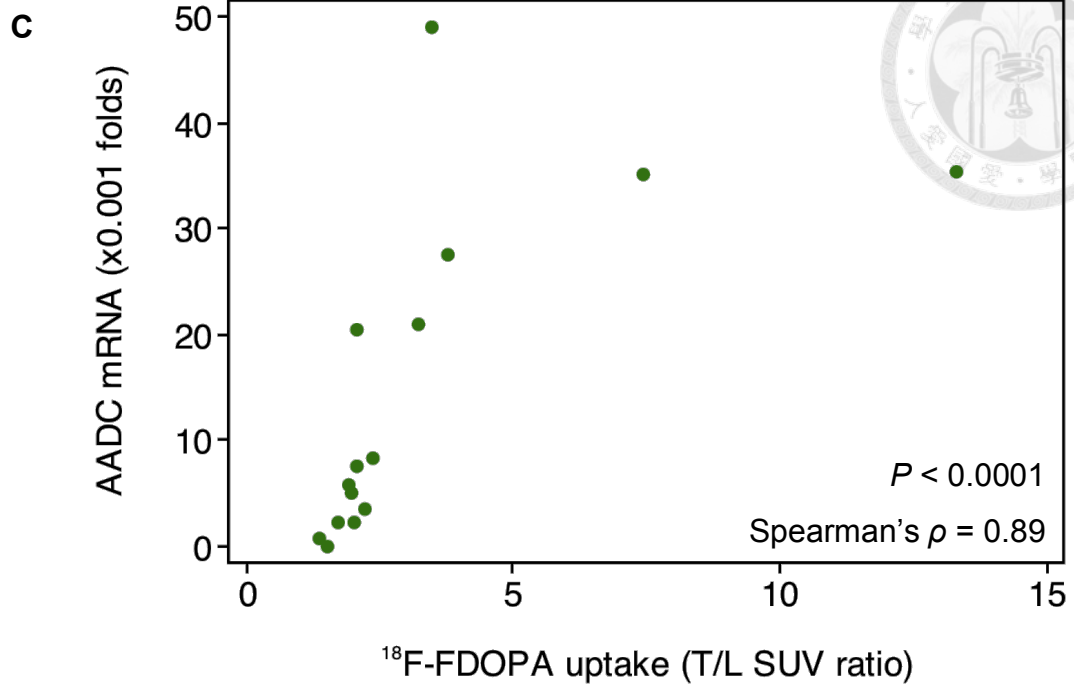
E
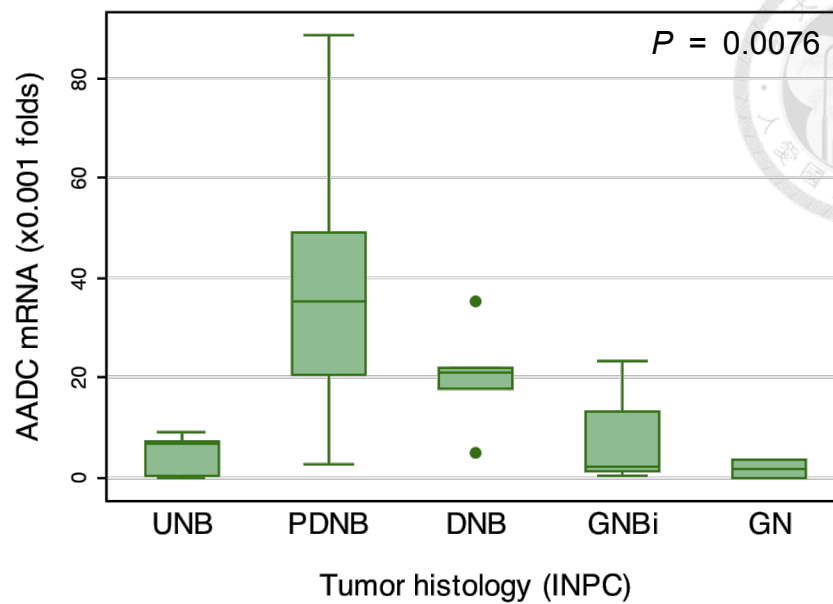
F
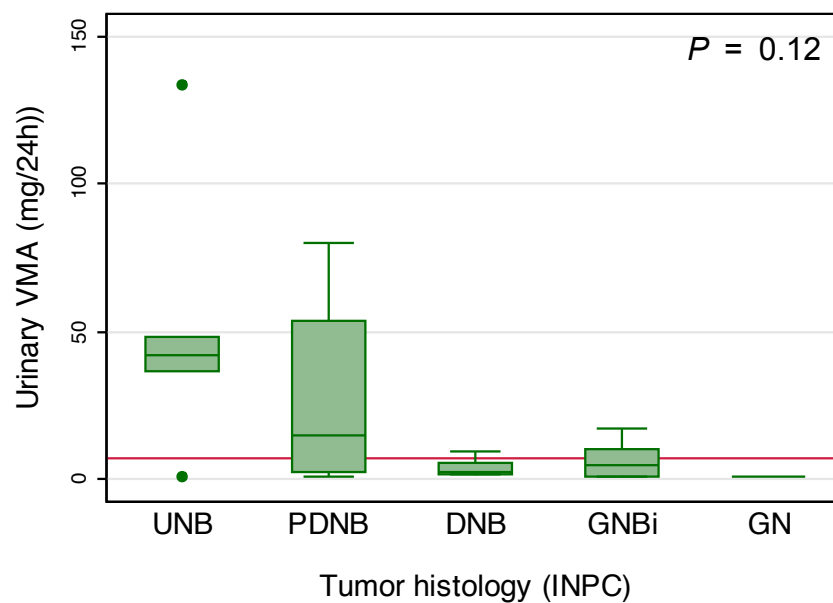
 (A) Tumors with concomitant FDG, FDOPA, and MIBG images were compared by MIBG avidity (n = 17). (B) Correlation between tumor uptake of FDOPA and patients' VMA excretion (*n* = 47). (C) Relationship between tumor uptake of 18F-FDOPA and AADC expression (*n* = 15 nonhepatic tumors). Next, NTs of different degree of histologic differentiation were compared for their FDOPA uptake (n = 17; **D**), AADC gene expression (n = 33; **E**), and urinary VMA levels (**F**).

Abbreviations: UNB = undifferentiated neuroblastoma; PDNB = poorly-differentiated neuroblastoma; DNB = differentiating neuroblastoma; GNBi = ganglioneuroblastoma, intermixed; GN, ganglioneuroma. Reference line in panels (**B**) and (**F**) = upper limit.
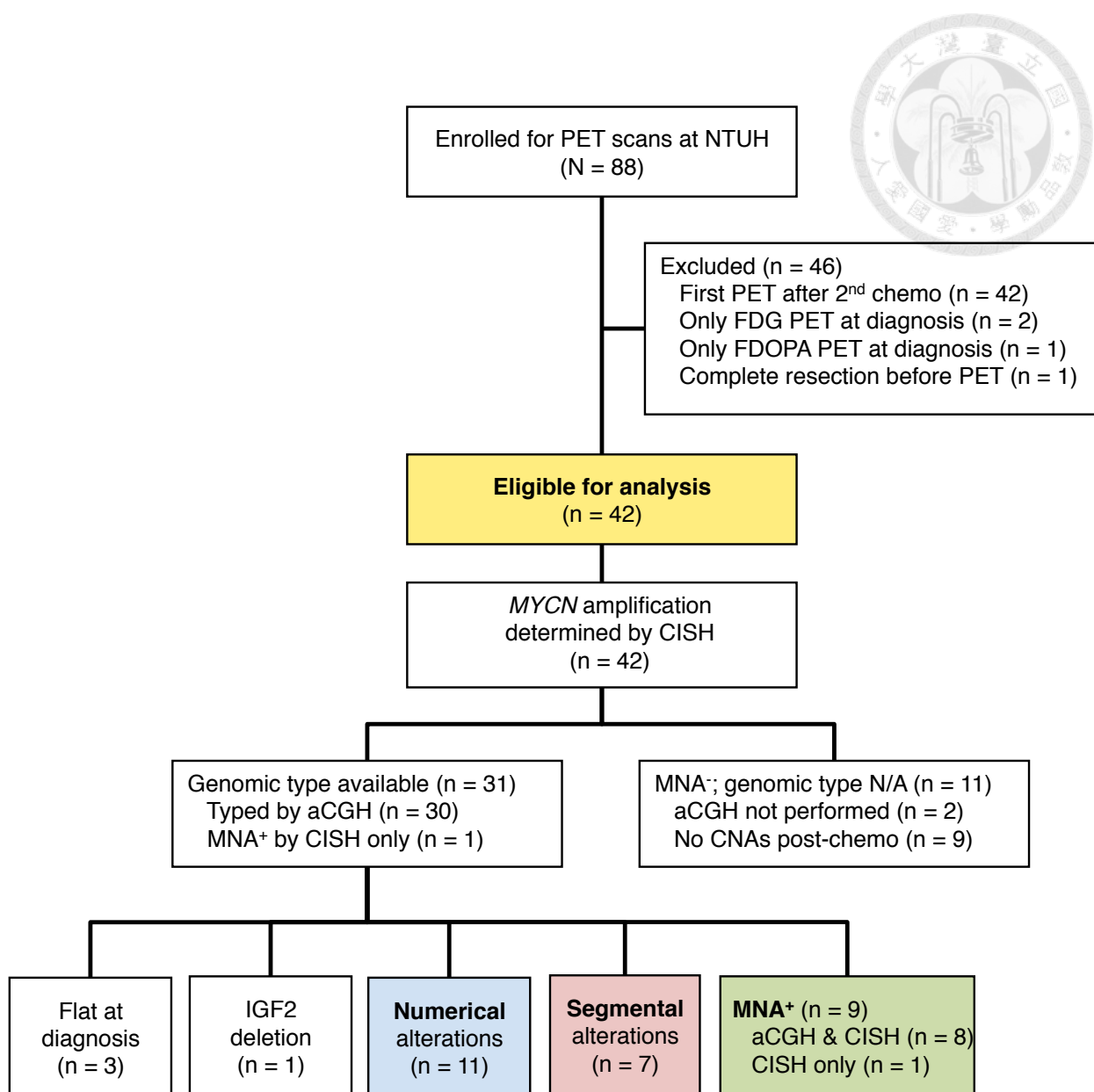
Figure 10. Patient flow diagram.

Abbreviations: aCGH = array-based comparative genomic hybridization; chemo = chemotherapy; CISH = chromogenic *in situ* hybridization; CR = complete response; MNA = *MYCN* amplification; N/A = not available; NTUH = National Taiwan University Hospital, Taipei, Taiwan.
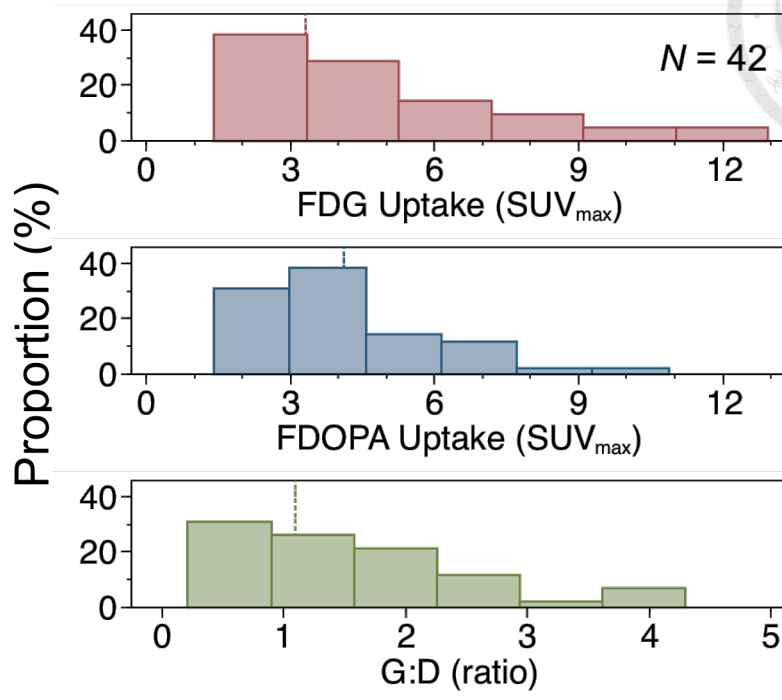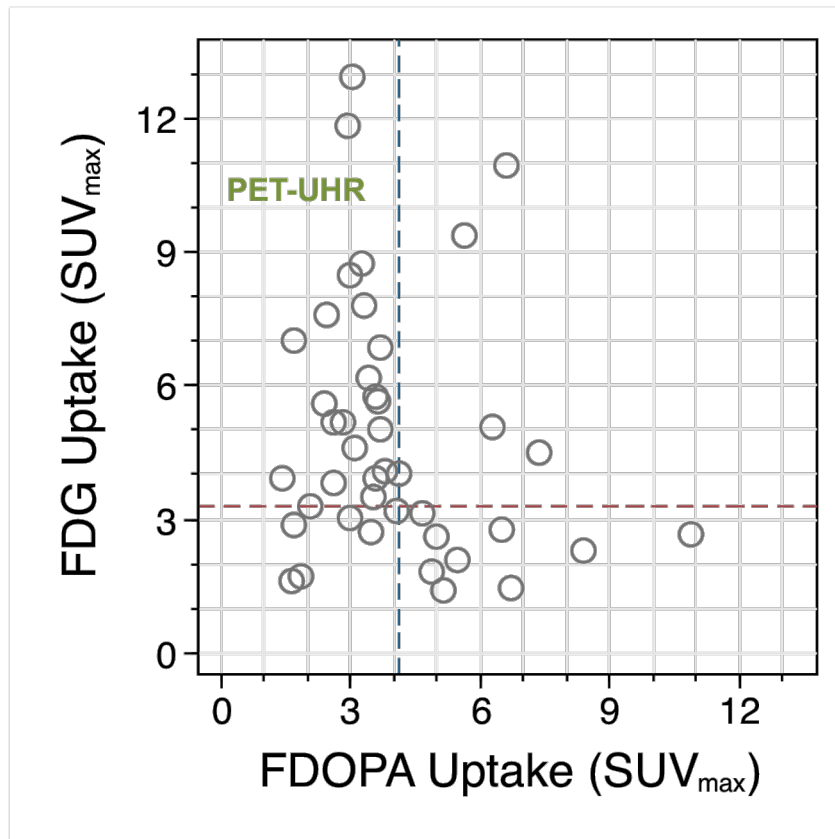
Figure 11. FDG and FDOPA uptake by primary NB tumors and their genomic types.

C

D

FDG (SUV$_{max}$)	FDOPA (SUV$_{max}$)	G:D (ratio)
$P = 0.0003$	$P = 0.0074$	$P = 0.0001$

Genomic Type (n)
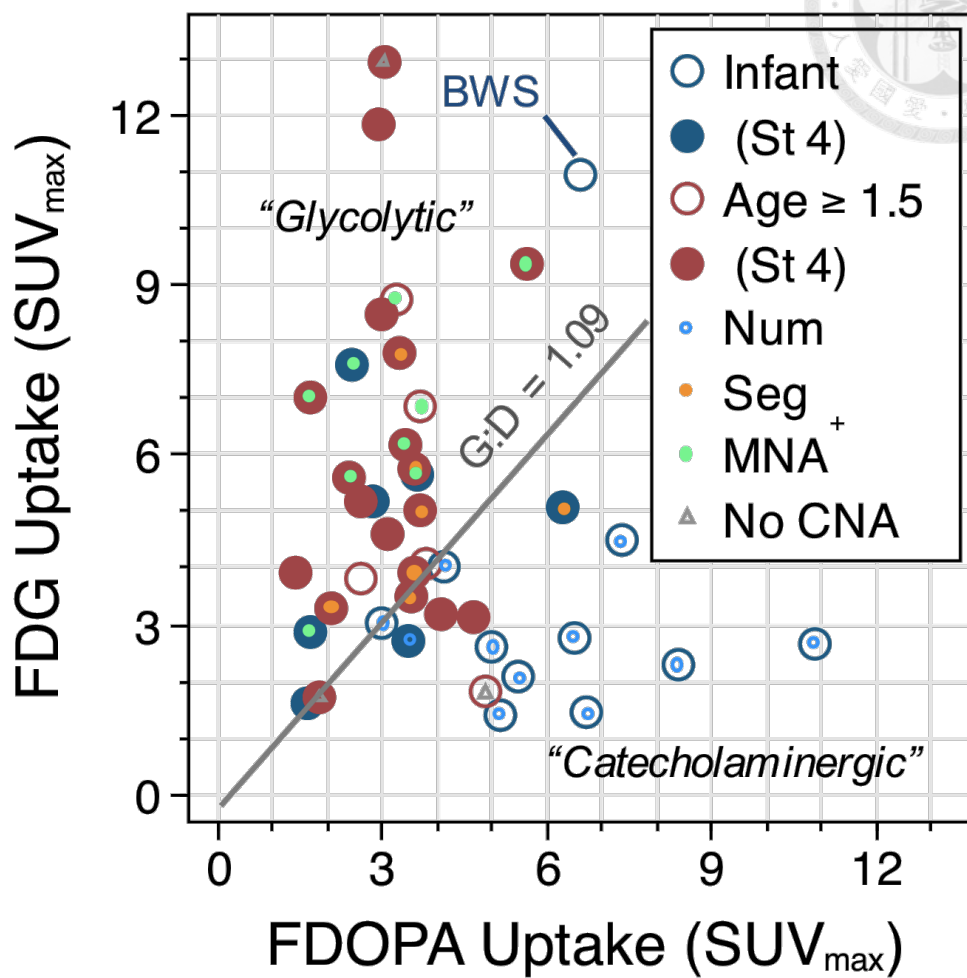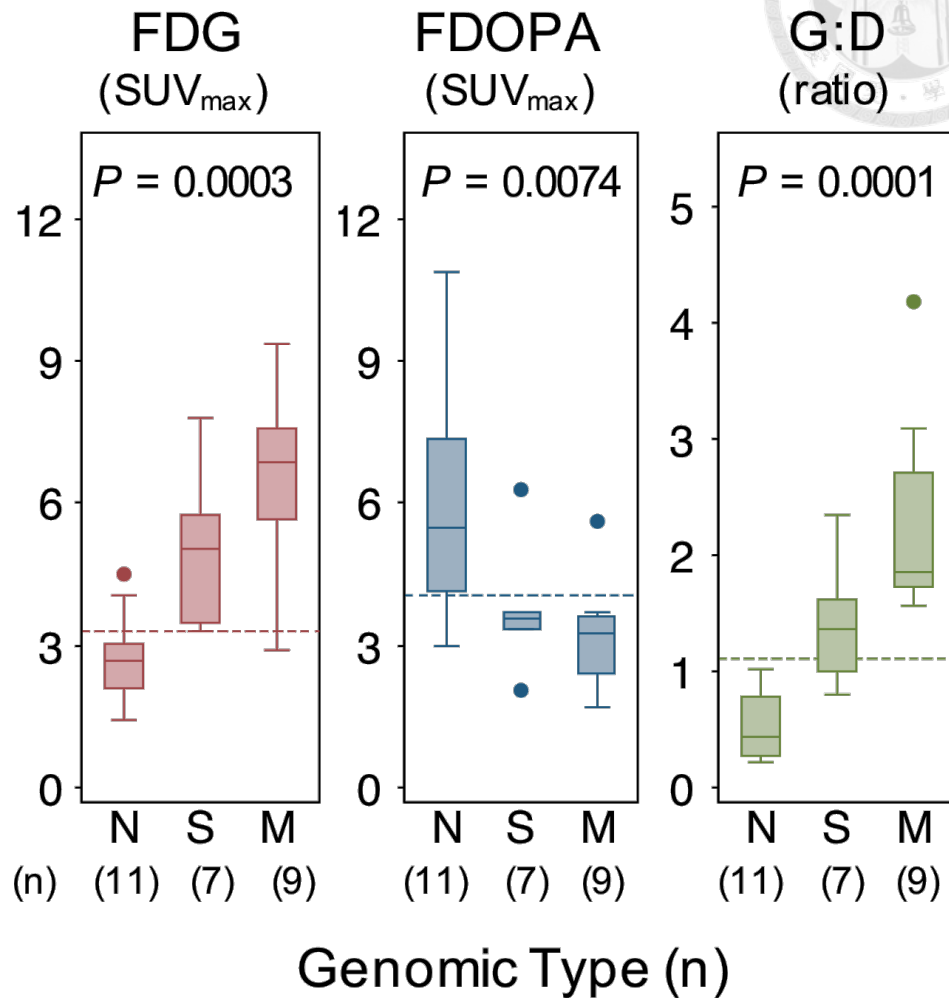
Histograms (**A**) and scatter plot (**B**) showing the Distribution of FDG uptake, FDOPA uptake, and G:D ratio. Dashed lines indicate the FDG SUVmax $\geq$ 3.31 and FDOPA SUVmax < 4.12 cutoff identified by ROC analysis. The left upper quadrant indicated PET-UHR cases. (**C**) Scatter plot of FDG and FDOPA uptake by primary NB tumors (*n* = 42) with clinical characteristics annotated. (**D**) The three major genomic types of NB showed distinctive FDG and FDOPA uptake patterns. Dashed lines indicate the cutoff value identified by ROC analysis.

Abbreviations: BWS, Beckwith–Wiedemann syndrome with *IGF2* microdeletion; CNA = copy number alterations; G:D = ratio between the SUV$_{max}$ of primary tumors on FDG and FDOPA PET scans; MNA[+] = M = MYCN amplification; Num[+] = N = numerical chromosomal alterations; ROC, receiver operating characteristics; Seg[+] = S = segmental chromosomal alterations; St 4 = stage 4. SUV$_{max}$ = maximum standard uptake value.

A FDG (SUV$_{max}$)

AUC = 0.83
(0.65–1.00)

SUV$_{max}$ ≥ 3.31

B FDOPA (SUV$_{max}$)

AUC = 0.78
(0.60–0.95)

SUV$_{max}$ ≥ 4.12

C G:D ratio

AUC = 0.89
(0.75–1.00)

G:D ≥ 1.09

D Comparison

$\chi^2 = 6.78$
$P = 0.03$

E

fdg_tumor	segmna 0	1	Total
1.412	1	0	1
1.437	1	0	1
1.706	1	0	1
1.798	1	0	1
2.078	1	0	1
2.295	1	0	1
2.606	1	0	1
2.676	1	0	1
2.722	1	0	1
2.774	1	0	1
2.877	0	1	1
3.03	1	0	1
3.316	0	1	1
3.483	0	1	1
3.919	0	1	1
4.049	1	0	1
4.481	1	0	1
5.014	0	1	1
5.057	0	1	1
5.603	0	1	1
5.67	0	1	1
5.756	0	1	1
6.191	0	1	1
6.853	0	1	1
7.03	0	1	1
7.595	0	1	1
7.79	0	1	1
8.751	0	1	1
9.367	0	1	1
10.954	1	0	1
12.942	1	0	1
Total	15	16	31

F Detailed report of Sensitivity and Specificity

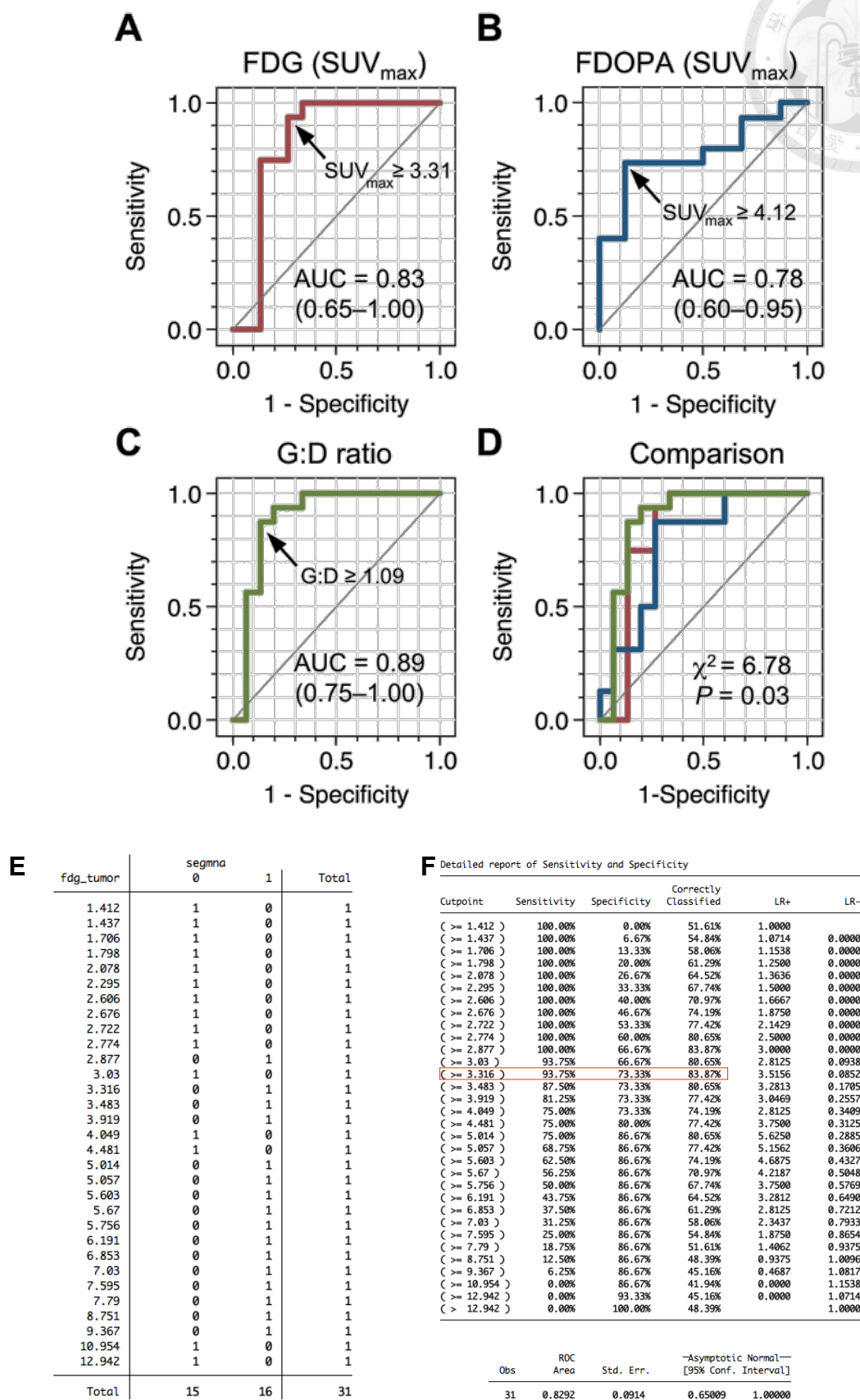| Cutpoint	Sensitivity	Specificity	Correctly Classified	LR+	LR−
(>= 1.412)	100.00%	0.00%	51.61%	1.0000	
(>= 1.437)	100.00%	6.67%	54.84%	1.0714	0.0000
(>= 1.706)	100.00%	13.33%	58.06%	1.1538	0.0000
(>= 1.798)	100.00%	20.00%	61.29%	1.2500	0.0000
(>= 2.078)	100.00%	26.67%	64.52%	1.3636	0.0000
(>= 2.295)	100.00%	33.33%	67.74%	1.5000	0.0000
(>= 2.606)	100.00%	40.00%	70.97%	1.6667	0.0000
(>= 2.676)	100.00%	46.67%	74.19%	1.8750	0.0000
(>= 2.722)	100.00%	53.33%	77.42%	2.1429	0.0000
(>= 2.774)	100.00%	60.00%	80.65%	2.5000	0.0000
(>= 2.877)	100.00%	66.67%	83.87%	3.0000	0.0000
(>= 3.03)	93.75%	66.67%	80.65%	2.8125	0.0938
(>= 3.316)	93.75%	73.33%	83.87%	3.5156	0.0852
(>= 3.483)	87.50%	73.33%	80.65%	3.2813	0.1705
(>= 3.919)	81.25%	73.33%	77.42%	3.0469	0.2557
(>= 4.049)	75.00%	73.33%	74.19%	2.8125	0.3409
(>= 4.481)	75.00%	80.00%	77.42%	3.7500	0.3125
(>= 5.014)	75.00%	86.67%	80.65%	5.6250	0.2885
(>= 5.057)	68.75%	86.67%	77.42%	5.1562	0.3606
(>= 5.603)	62.50%	86.67%	74.19%	4.6875	0.4327
(>= 5.67)	56.25%	86.67%	70.97%	4.2187	0.5048
(>= 5.756)	50.00%	86.67%	67.74%	3.7500	0.5769
(>= 6.191)	43.75%	86.67%	64.52%	3.2812	0.6490
(>= 6.853)	37.50%	86.67%	61.29%	2.8125	0.7212
(>= 7.03)	31.25%	86.67%	58.06%	2.3437	0.7933
(>= 7.595)	25.00%	86.67%	54.84%	1.8750	0.8654
(>= 7.79)	18.75%	86.67%	51.61%	1.4062	0.9375
(>= 8.751)	12.50%	86.67%	48.39%	0.9375	1.0096
(>= 9.367)	6.25%	86.67%	45.16%	0.4687	1.0817
(>= 10.954)	0.00%	86.67%	41.94%	0.0000	1.1538
(>= 12.942)	0.00%	93.33%	45.16%	0.0000	1.0714
(> 12.942)	0.00%	100.00%	48.39%		1.0000

Obs	ROC Area	Std. Err.	—Asymptotic Normal— [95% Conf. Interval]	
31	0.8292	0.0914	0.65009	1.00000

Figure 12. ROC analysis of tumor uptake values and the poor-risk genomic types.

G

fdopa_tumor	segmnafav 0	1	Total
1.672	1	0	1
1.682	1	0	1
1.855	0	1	1
2.061	1	0	1
2.401	1	0	1
2.455	1	0	1
2.999	0	1	1
3.013	0	1	1
3.238	1	0	1
3.33	1	0	1
3.407	1	0	1
3.477	0	1	1
3.504	1	0	1
3.579	1	0	1
3.585	1	0	1
3.627	1	0	1
3.691	1	0	1
3.703	1	0	1
4.123	0	1	1
4.892	0	1	1
4.996	0	1	1
5.122	0	1	1
5.487	0	1	1
5.613	1	0	1
6.289	1	0	1
6.475	0	1	1
6.622	0	1	1
6.721	0	1	1
7.343	0	1	1
8.365	0	1	1
10.865	0	1	1
Total	16	15	31

H Detailed report of Sensitivity and Specificity

Cutpoint	Sensitivity	Specificity	Correctly Classified	LR+	LR-
(>= 1.672)	100.00%	0.00%	48.39%	1.0000	
(>= 1.682)	100.00%	6.25%	51.61%	1.0667	0.0000
(>= 1.855)	100.00%	12.50%	54.84%	1.1429	0.0000
(>= 2.061)	93.33%	12.50%	51.61%	1.0667	0.5333
(>= 2.401)	93.33%	18.75%	54.84%	1.1487	0.3556
(>= 2.455)	93.33%	25.00%	58.06%	1.2444	0.2667
(>= 2.999)	93.33%	31.25%	61.29%	1.3576	0.2133
(>= 3.013)	86.67%	31.25%	58.06%	1.2606	0.4267
(>= 3.238)	80.00%	31.25%	54.84%	1.1636	0.6400
(>= 3.33)	80.00%	37.50%	58.06%	1.2800	0.5333
(>= 3.407)	80.00%	43.75%	61.29%	1.4222	0.4571
(>= 3.477)	80.00%	50.00%	64.52%	1.6000	0.4000
(>= 3.504)	73.33%	50.00%	61.29%	1.4667	0.5333
(>= 3.579)	73.33%	56.25%	64.52%	1.6762	0.4741
(>= 3.585)	73.33%	62.50%	67.74%	1.9556	0.4267
(>= 3.627)	73.33%	68.75%	70.97%	2.3467	0.3879
(>= 3.691)	73.33%	75.00%	74.19%	2.9333	0.3556
(>= 3.703)	73.33%	81.25%	77.42%	3.9111	0.3282
(>= 4.123)	73.33%	87.50%	80.65%	5.8667	0.3048
(>= 4.892)	66.67%	87.50%	77.42%	5.3333	0.3810
(>= 4.996)	60.00%	87.50%	74.19%	4.8000	0.4571
(>= 5.122)	53.33%	87.50%	70.97%	4.2667	0.5333
(>= 5.487)	46.67%	87.50%	67.74%	3.7333	0.6095
(>= 5.613)	40.00%	87.50%	64.52%	3.2000	0.6857
(>= 6.289)	40.00%	93.75%	67.74%	6.4000	0.6400
(>= 6.475)	40.00%	100.00%	70.97%		0.6000
(>= 6.622)	33.33%	100.00%	67.74%		0.6667
(>= 6.721)	26.67%	100.00%	64.52%		0.7333
(>= 7.343)	20.00%	100.00%	61.29%		0.8000
(>= 8.365)	13.33%	100.00%	58.06%		0.8667
(>= 10.865)	6.67%	100.00%	54.84%		0.9333
(> 10.865)	0.00%	100.00%	51.61%		1.0000

	Obs	ROC Area	Std. Err.	—Asymptotic Normal— [95% Conf. Interval]	
	31	0.7750	0.0897	0.59913	0.95087

I

gdr_suv	segmna 0	1	Total
.214	1	0	1
.246	1	0	1
.274	1	0	1
.276	1	0	1
.368	1	0	1
.379	1	0	1
.428	1	0	1
.522	1	0	1
.61	1	0	1
.783	1	0	1
.804	0	1	1
.92	1	0	1
.982	1	0	1
.994	0	1	1
1.01	1	0	1
1.095	0	1	1
1.354	0	1	1
1.563	0	1	1
1.606	0	1	1
1.609	0	1	1
1.654	1	0	1
1.669	0	1	1
1.721	0	1	1
1.817	0	1	1
1.857	0	1	1
2.334	0	1	1
2.339	0	1	1
2.703	0	1	1
3.094	0	1	1
4.18	0	1	1
4.295	1	0	1
Total	15	16	31

J Detailed report of Sensitivity and Specificity

Cutpoint	Sensitivity	Specificity	Correctly Classified	LR+	LR-
(>= .214)	100.00%	0.00%	51.61%	1.0000	
(>= .246)	100.00%	6.67%	54.84%	1.0714	0.0000
(>= .274)	100.00%	13.33%	58.06%	1.1538	0.0000
(>= .276)	100.00%	20.00%	61.29%	1.2500	0.0000
(>= .368)	100.00%	26.67%	64.52%	1.3636	0.0000
(>= .379)	100.00%	33.33%	67.74%	1.5000	0.0000
(>= .428)	100.00%	40.00%	70.97%	1.6667	0.0000
(>= .522)	100.00%	46.67%	74.19%	1.8750	0.0000
(>= .61)	100.00%	53.33%	77.42%	2.1429	0.0000
(>= .783)	100.00%	60.00%	80.65%	2.5000	0.0000
(>= .804)	100.00%	66.67%	83.87%	3.0000	0.0000
(>= .92)	93.75%	66.67%	80.65%	2.8125	0.0938
(>= .982)	93.75%	73.33%	83.87%	3.5156	0.0852
(>= .994)	93.75%	80.00%	87.10%	4.6875	0.0781
(>= 1.01)	87.50%	80.00%	83.87%	4.3750	0.1562
(>= 1.095)	87.50%	86.67%	87.10%	6.5625	0.1442
(>= 1.354)	81.25%	86.67%	83.87%	6.0937	0.2163
(>= 1.563)	75.00%	86.67%	80.65%	5.6250	0.2885
(>= 1.606)	68.75%	86.67%	77.42%	5.1562	0.3606
(>= 1.609)	62.50%	86.67%	74.19%	4.6875	0.4327
(>= 1.654)	56.25%	86.67%	70.97%	4.2187	0.5048
(>= 1.669)	56.25%	93.33%	74.19%	8.4375	0.4687
(>= 1.721)	50.00%	93.33%	70.97%	7.5000	0.5357
(>= 1.817)	43.75%	93.33%	67.74%	6.5625	0.6027
(>= 1.857)	37.50%	93.33%	64.52%	5.6250	0.6696
(>= 2.334)	31.25%	93.33%	61.29%	4.6875	0.7366
(>= 2.339)	25.00%	93.33%	58.06%	3.7500	0.8036
(>= 2.703)	18.75%	93.33%	54.84%	2.8125	0.8705
(>= 3.094)	12.50%	93.33%	51.61%	1.8750	0.9375
(>= 4.18)	6.25%	93.33%	48.39%	0.9375	1.0045
(>= 4.295)	0.00%	93.33%	45.16%	0.0000	1.0714
(> 4.295)	0.00%	100.00%	48.39%		1.0000

	Obs	ROC Area	Std. Err.	—Asymptotic Normal— [95% Conf. Interval]	
	31	0.8875	0.0721	0.74611	1.00000

ROC curves of FDG (**A**), FDOPA (**B**), and G:D (**C**) are compared (**D**) and raw data of FDG (**E**, **F**), FDOPA (**G**, **H**), and G:D (**I**, **J**) are shown. Red boxes indicate cutoff values of the highest accuracy.
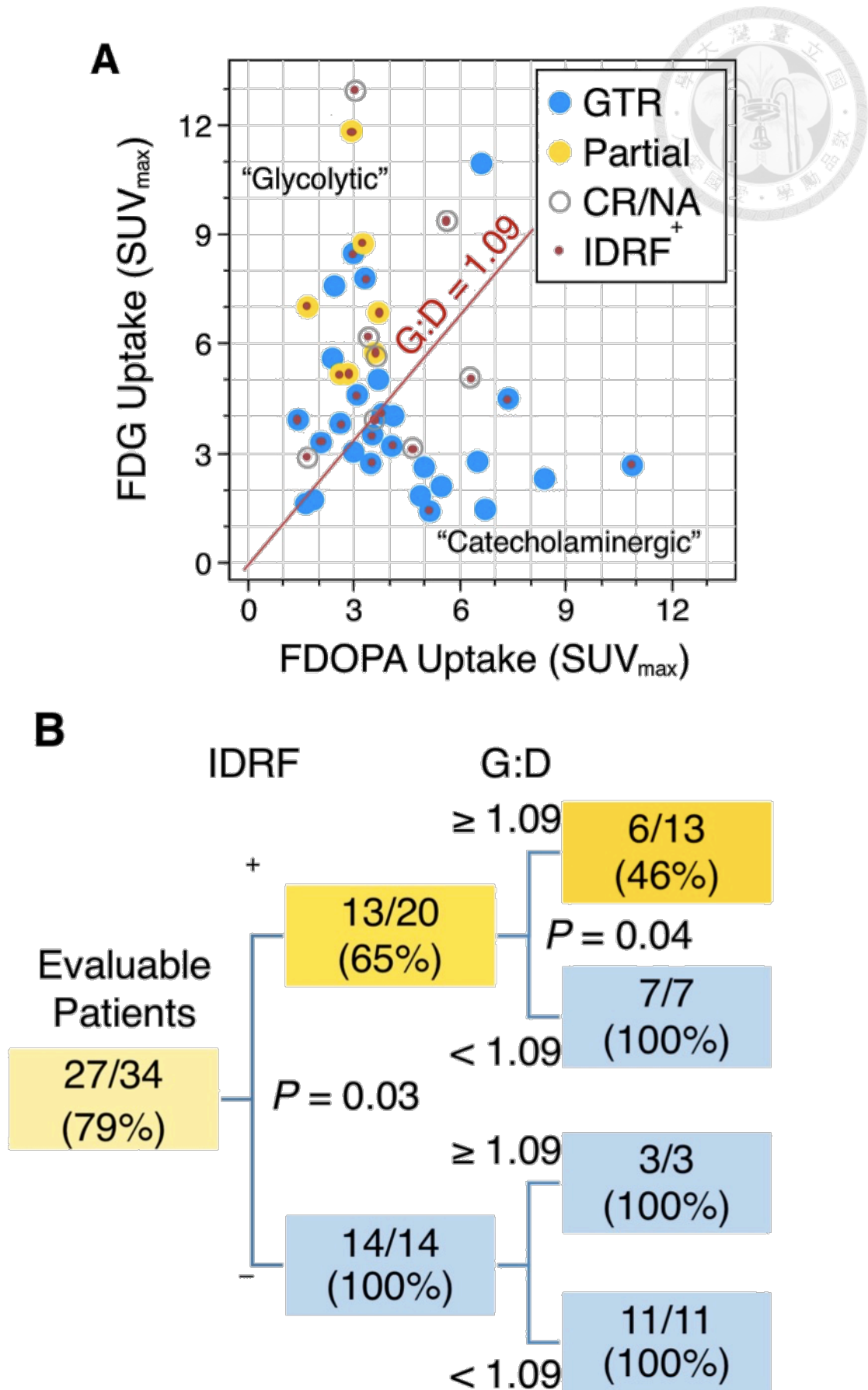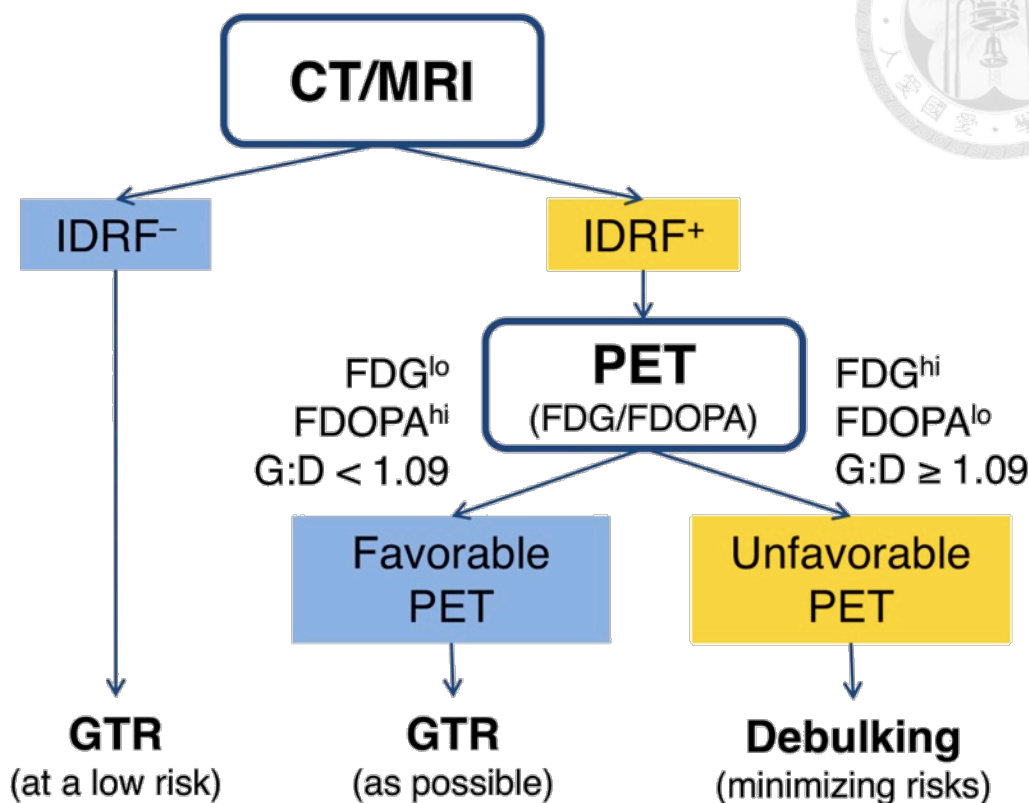
Abbreviations: AUC = area under curve; LR = likelihood ratio.

Figure 13. FDG and FDOPA uptake and surgical resection.

(**A**) Distribution of tumor uptake with IDRF and surgical outcome annotated. (**B**) GTR rate (%) among 34 evaluable patients. IDRF and G:D identified a subgroup of patients with lower probability of GTR. (**C**) Proposed principles of incorporating diagnostic PET imaging into the surgical planning for the resection of NB tumors at their primary site. Unfavorable PET is defined by G:D ratio ≥ 1.09.

Abbreviations: CR/NA, complete response of the primary tumor after induction chemotherapy or resection of the primary tumor has not yet been attempted; G:D, ratio between the uptake (SUV_{max}) of primary tumor on FDG and FDOPA PET scans; GTR, gross total resection was achieved at first or best surgery; IDRF, image-defined risk factors on diagnostic CT or MRI; SUV_{max}, maximal standardized uptake value.
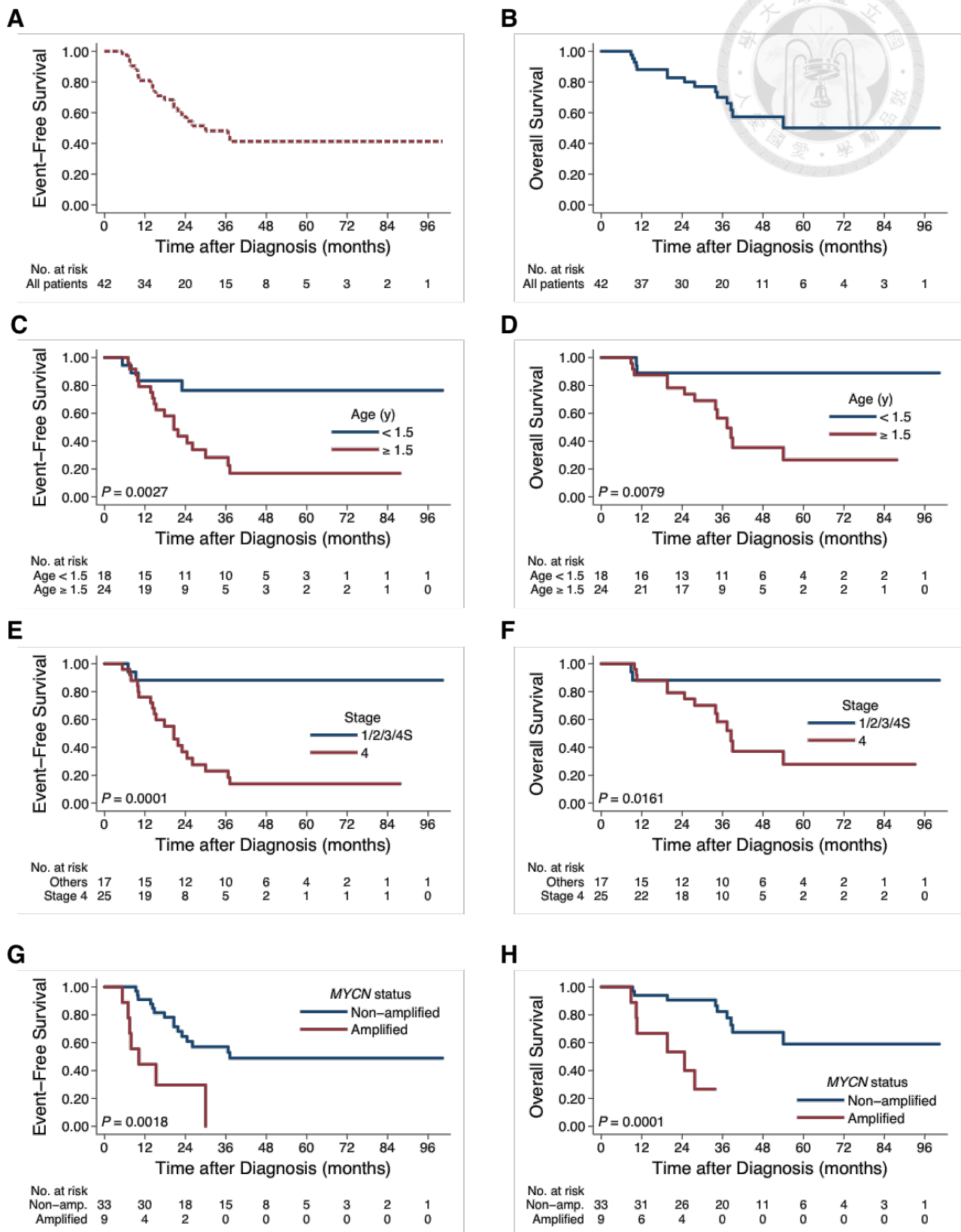
Figure 14. Treatment outcome compared by traditional risk factors.

Survival curves of Cohort 2 combined (EFS, **A**. and OS, **B**.) and compared by age (EFS, **C**. and OS, **D**.), stage (EFS, **E**. and OS, **F**.), *MYCN* amplification (EFS, **G**. and OS, **H**.),

74
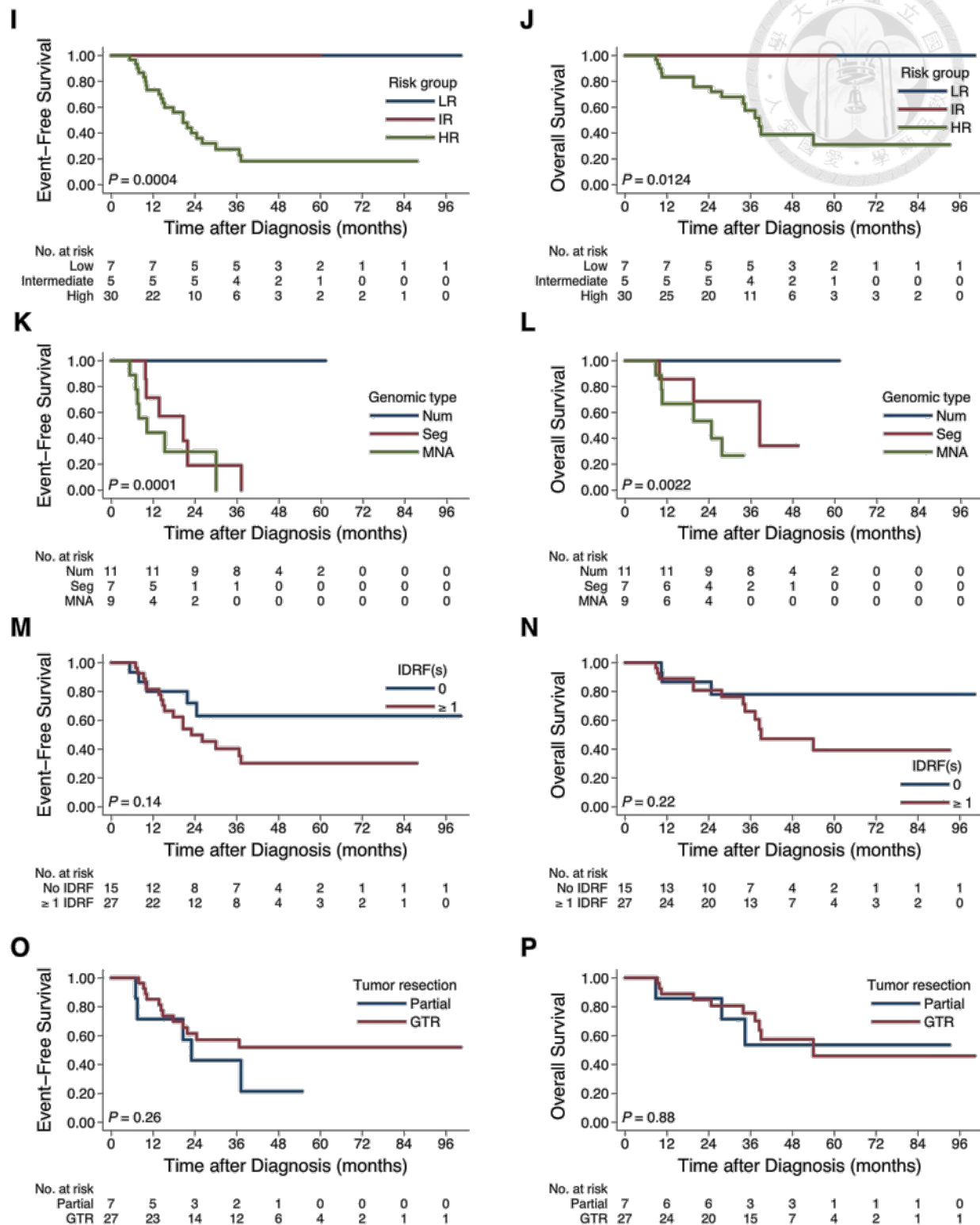
risk group (EFS, **I.** and OS, **J.**), major genomic type (EFS, **K.** and OS, **L.**), IDRF (EFS, **M.** and OS, **N.**), and extent of surgery (EFS, **O.** and OS, **P.**).

Abbreviations: GTR = gross total resection; MNA = *MYCN* amplification; Num = numerical chromosomal alterations; Seg = segmemtal chromosomal alterations.
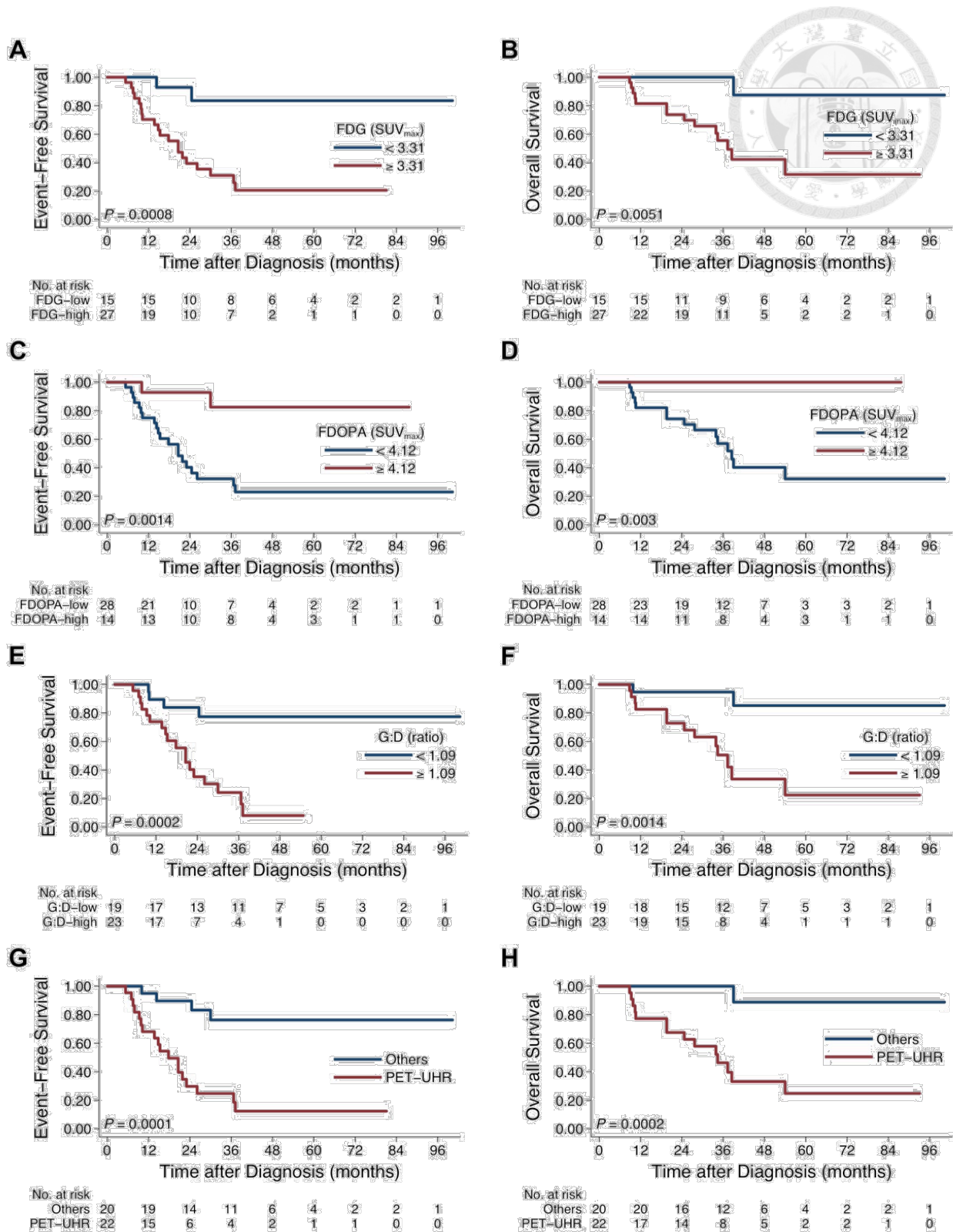
Figure 15. Treatment outcome compared by FDG and FDOPA uptake.

Survival curves were compared by FDG uptake (EFS, **A.** and OS, **B.**), FDOPA uptake (EFS, **C.** and OS, **D.**), G:D ratio (EFS, **E.** and OS, **F.**), and PET-defined ultra-high-risk (PET-UHR, FDG $SUV_{max} \geq 3.31$ and FDOPA $SUV_{max} < 4.12$; EFS, **G.** and OS, **H.**)
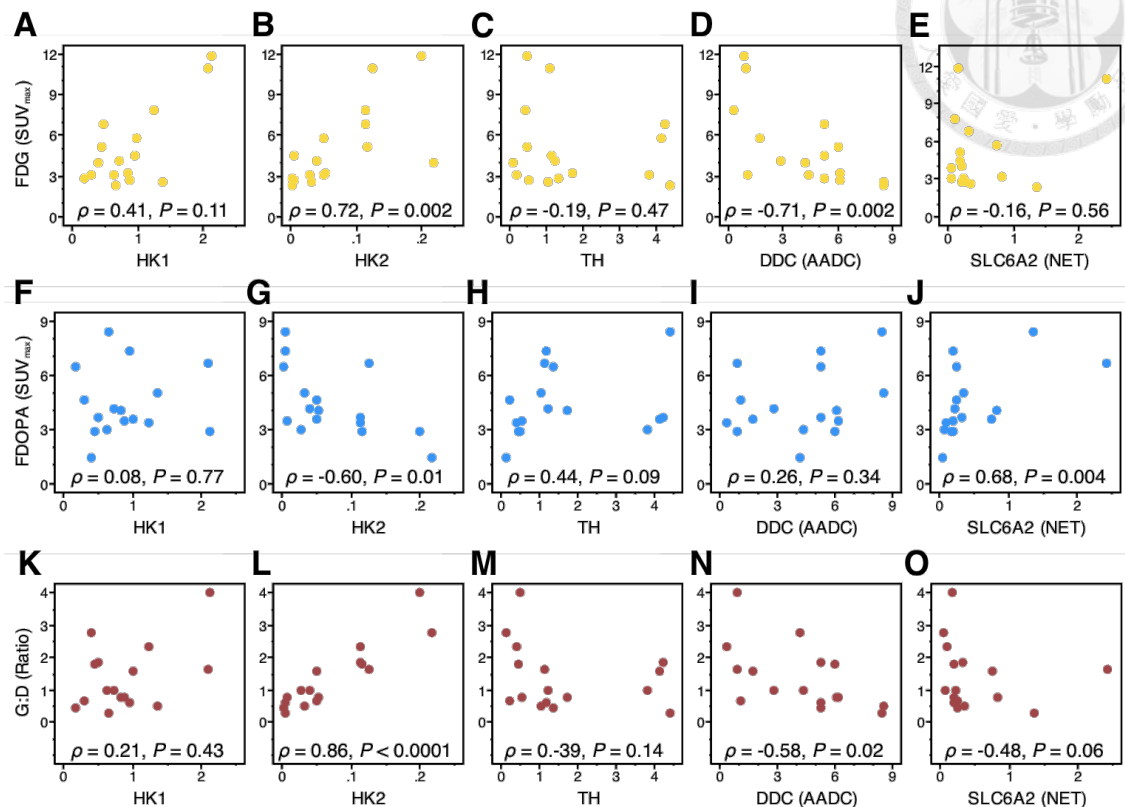
Figure 16. Gene expression and tumor uptake of FDG and FDOPA uptake.

Correlation between tumor uptake of FDG (**A-E**), FDOPA (**F-J**), or G:D ratio (**K-O**) and selected gene expression related with glycolysis (*HK1*, *HK2*) and catecholamine metabolism (*TH*, *DDC*) and transport (*SLC6A2*). The Spearman's nonparametric correlation coefficient (ρ) and its *P* value in each correlation test are shown. The *x* axis represents the relative folds of target gene expression normalized to the geometric mean of *HPRT1* and *SDHA* transcript levels serving as controls.

Abbreviations: G:D = ratio between the SUV_{max} of FDG and FDOPA by the primary tumor; AADC = aromatic l-amino acid decarboxylase; NET = norepinephrine transporter.

Figure 17. Tumor latency and disease progression in Th-*MYCN* transgenic mice.

(**A,B**) Experiment setting of the ultrasound evaluation of hemizygous Th-*MYCN* transgenic mice.
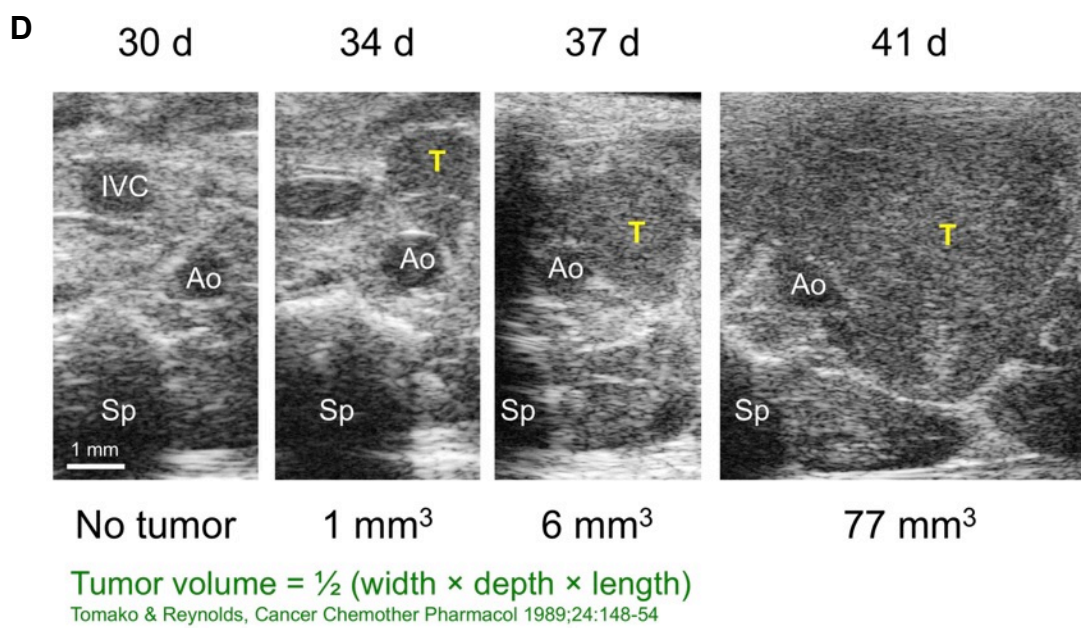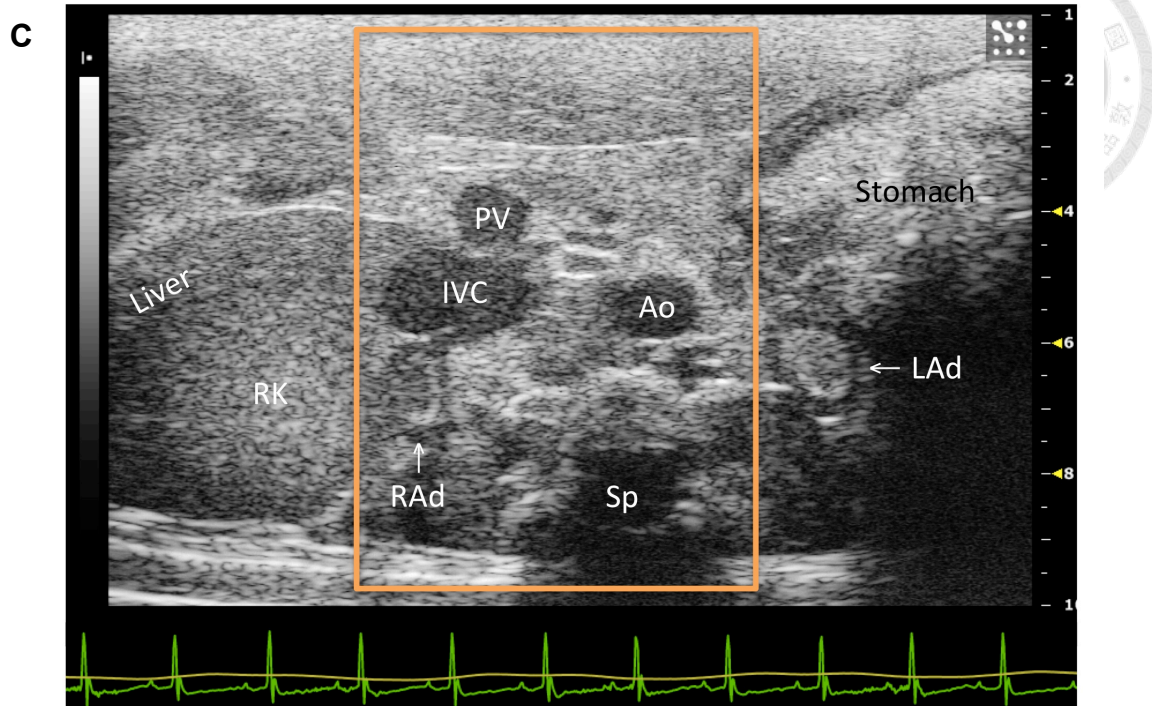
(**C**) Normal abdominal imaging in a wild-type (WT) mouse. The pre-aortic region (box) and adrenal glands were carefully examined for tumors. (**D**) Tumor onset and progression in a hemizygous Tg mouse.

E

F

Ultrasound imaging (42 days)	Necropsy findings (50 days)

Sagittal view from chest
Tumor size = 4.8 × 5.4 × 6.9 mm
Estimated volume = 89.7 mm³
(½ × width × depth × height)

Sacrificed due to suffering
Tumor weight = 0.44 gram
(H, heart; T, tumor; L, lung; K, kidney)
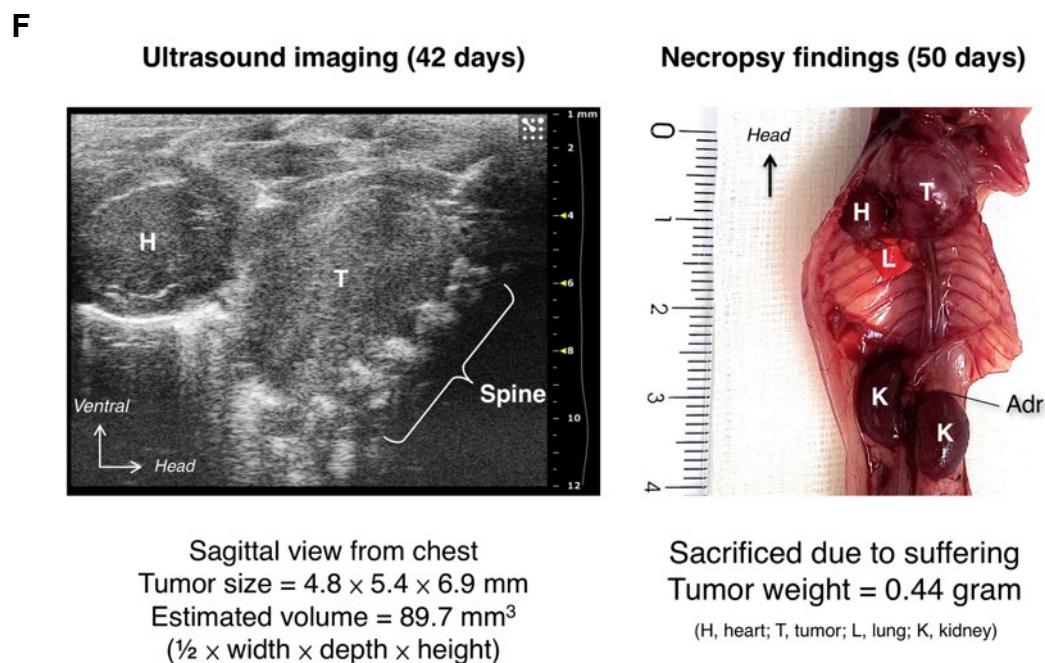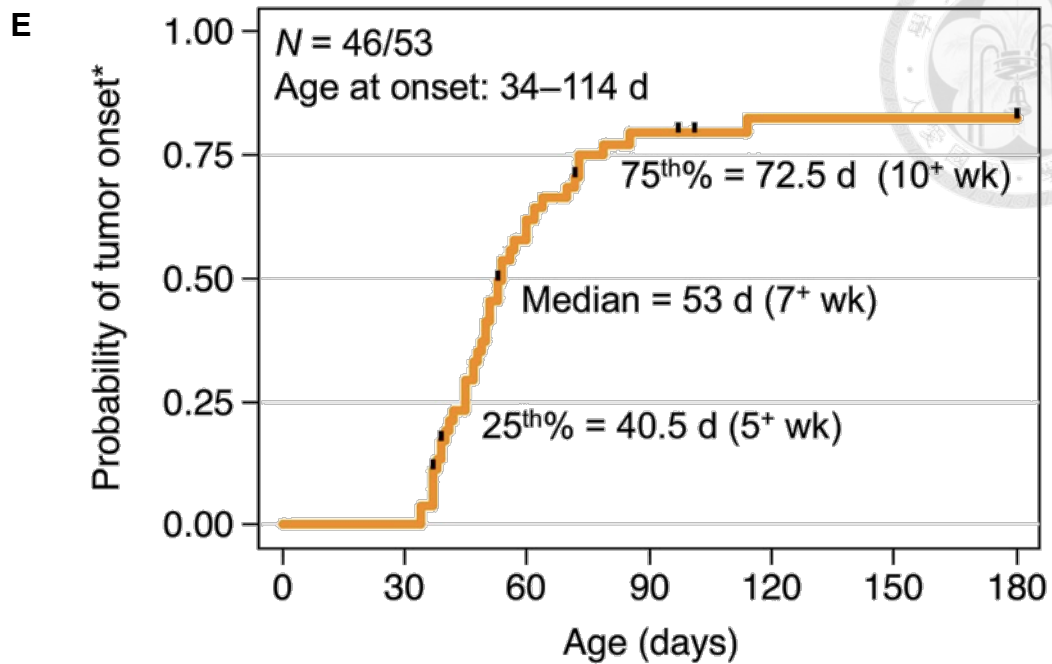
(**E**) Age of tumor detection with maximal diameter ≥ 2 mm by ultrasound. (**F**) Detection of a thoracic tumor.

Abbreviations: Ao = aorta; IVC = inferior vena cava; LAd, left adrenal gland; PV = portal vein; RAd, right adrenal gland; RK = right kidney; Sp = spine; T = tumor.

A
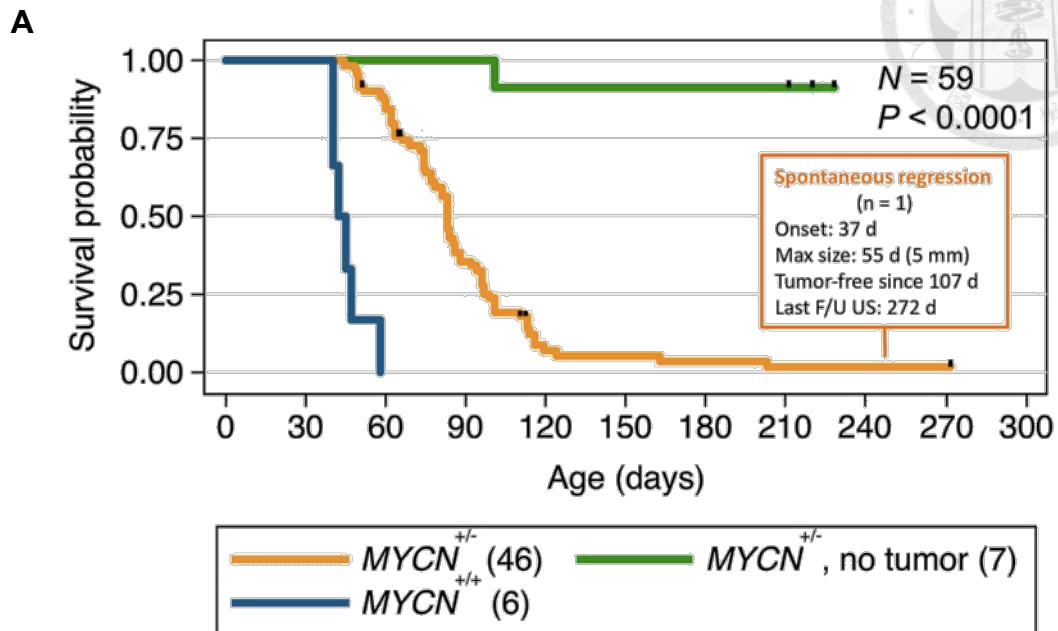
MYCN$^{+/+}$: By courtesy of Dr. Shiann-Tarng Jou, NTUH, Taipei, Taiwan

B
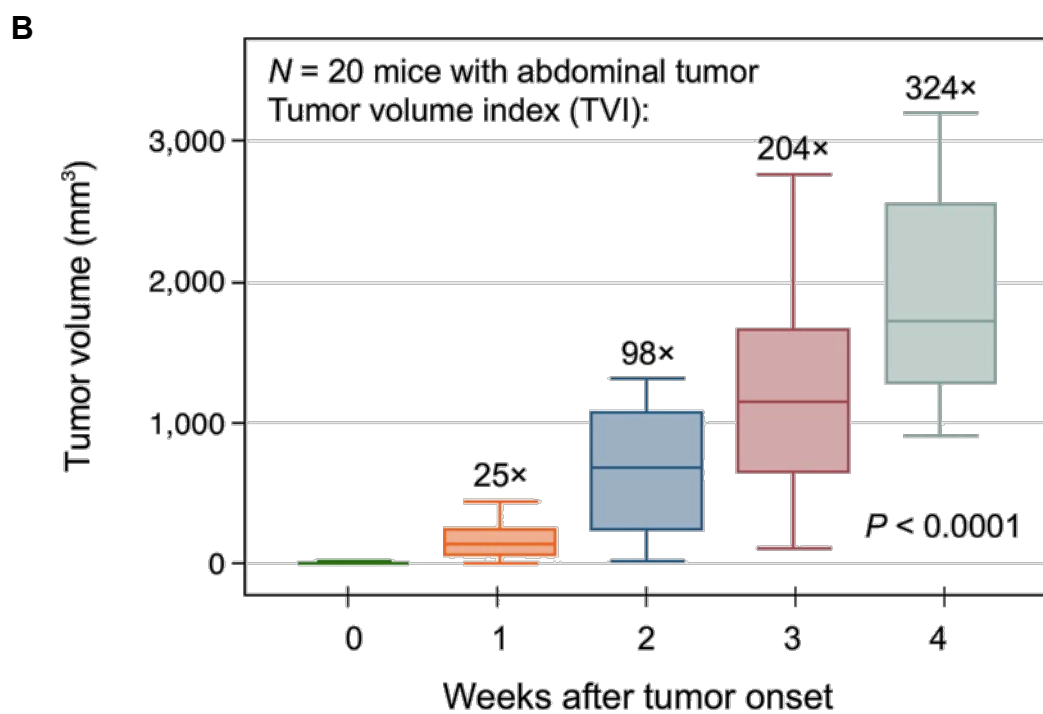
Figure 18. Animal survival and tumor progression.

doi:10.6342/NTU201600303

C

D

H&E, 100×　　　　　　　　H&E, 400×
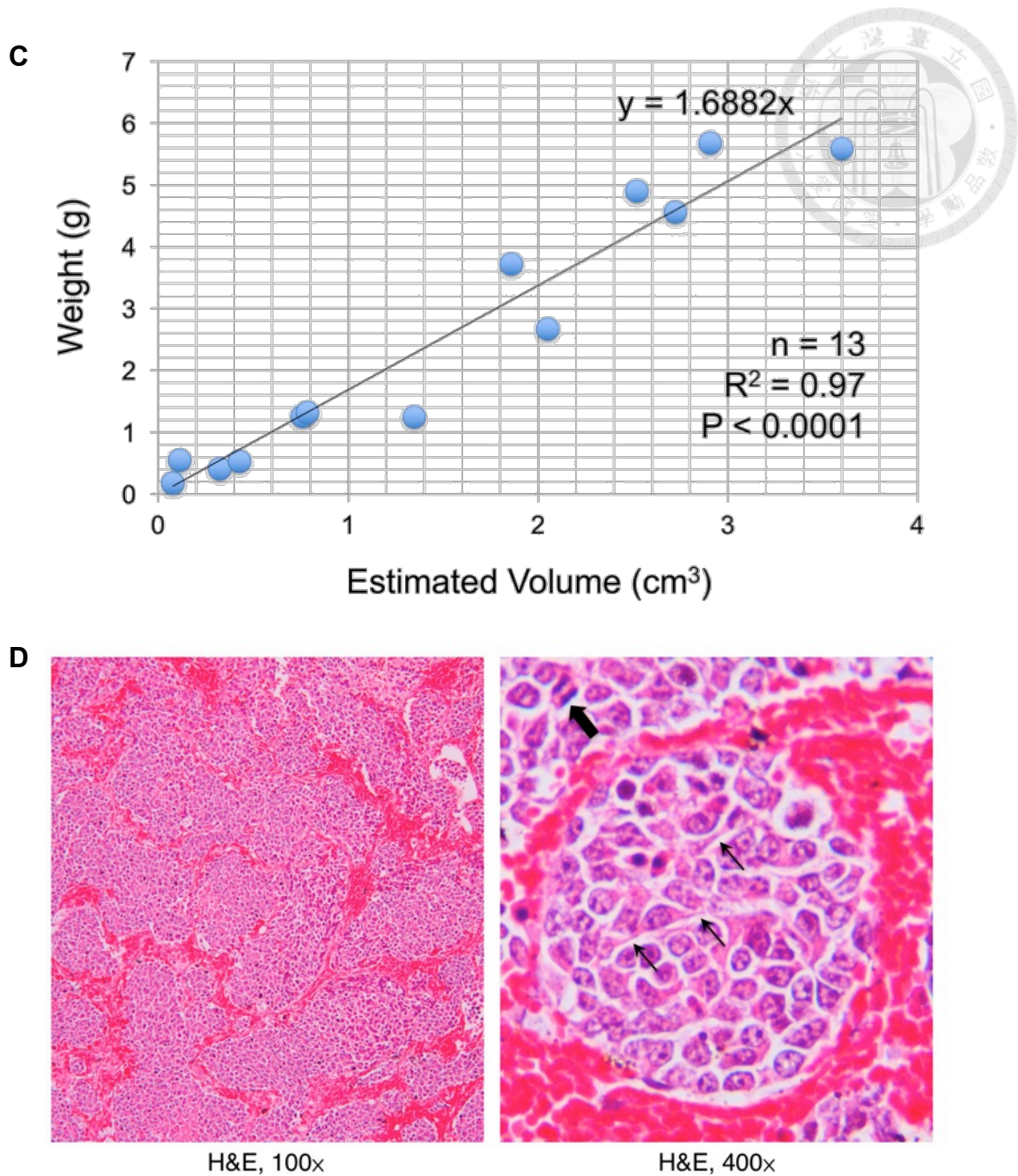
(**A**) Kaplan-Meier survival curves of *MYCN*$^{+/-}$ mice with or without tumor onset and of *MYCN*$^{+/+}$ mice. (**B**) Progression of tumor volume after tumor onset. (**C**) Correlation between ultrasound-estimation of tumor volume and tumor weight measured upon necropsy. (**D**) Histopathology of the tumor arose from the preaortic region of a 62-day-old female *MYCN*$^{+/-}$ mouse. Thick arrow, mitotic figure. Thin arrow, ganglionic differentiation of tumor cells.
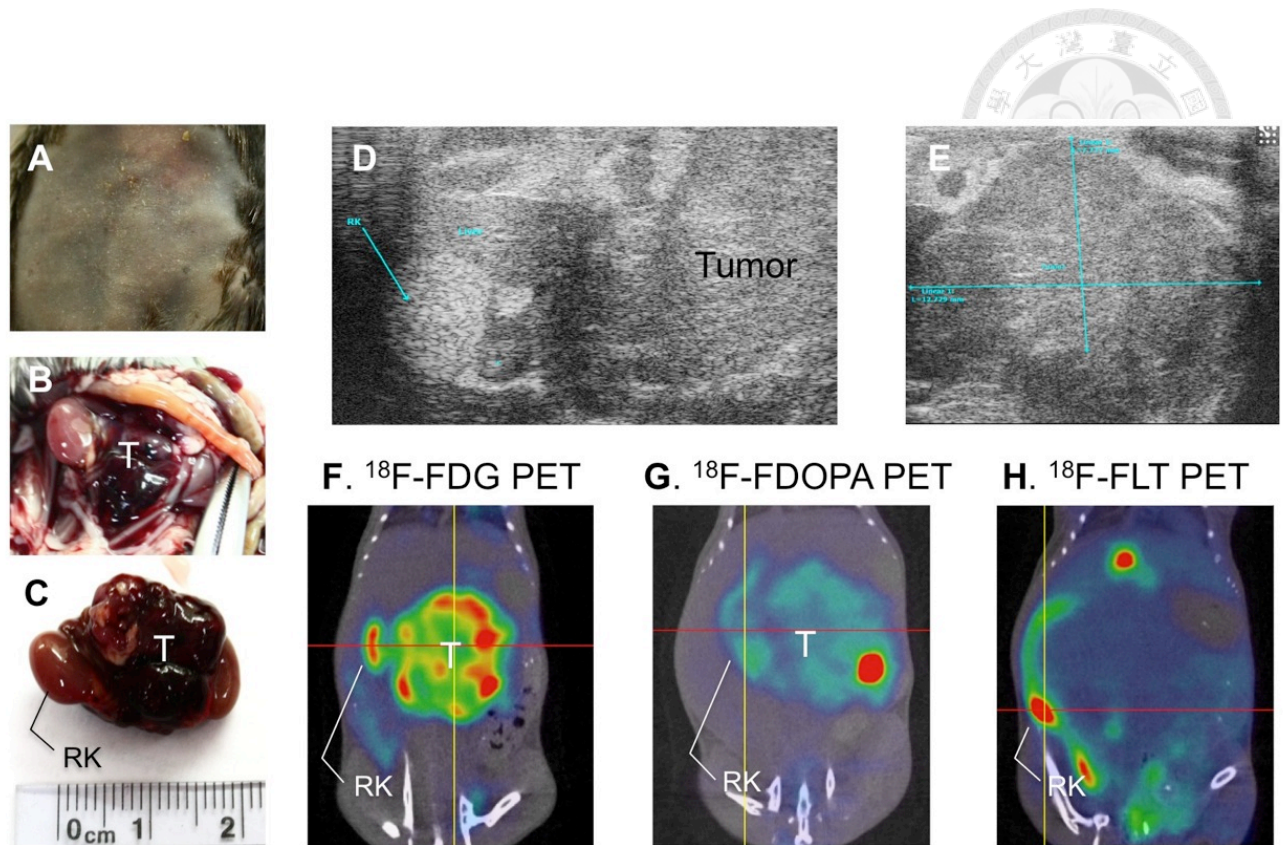
Figure 19. Comparison of ultrasound and PET images in Th-MYCN mouse.

(**A,B,C**) Necropsy at age 97 days showed abdominal distention, ecchymosis, and a dark reddish tumor (T) encapsulating bilateral kidneys. (**D,E**) Ultrasound screening at age 87 days showed a mass with heterogeneous echogenicity adjacent to the right kidney (RK). (**F,G,H**) PET scans using three PET probes showed an FDG-high, FDOPA-low, FLT-negative phenotype (FDG/FDOPA/FLT at age 89/95/94 days, T/L ratios 6.621/3.169/0.794 respectively).
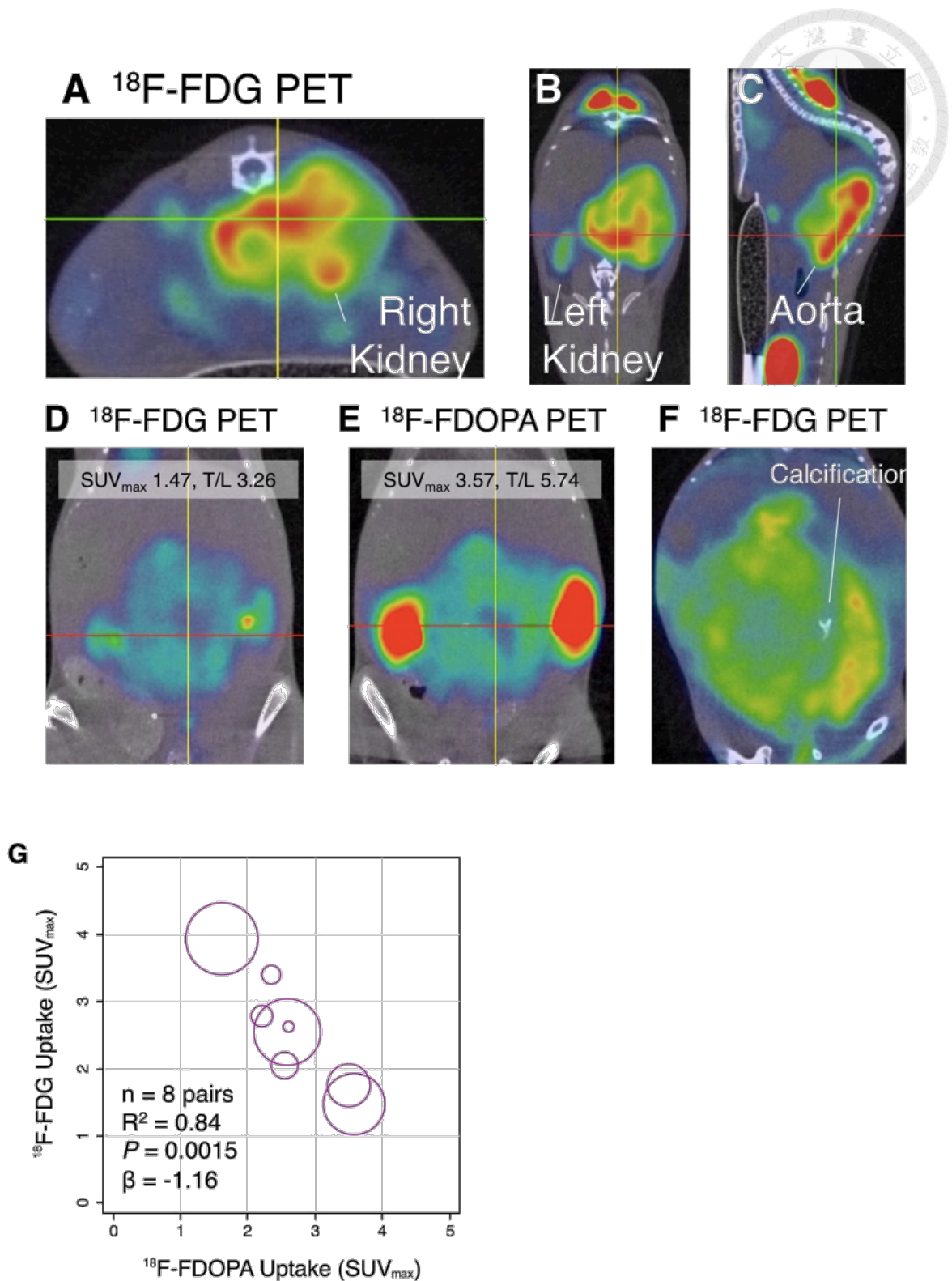
Figure 20. FDG and FDOPA PET imaging patterns in Th-*MYCN* mice.

Tumors with encapsulation of kidneys & aorta (**A-C**); lower FDG & higher FDOPA

uptake (**D-E**); and calcification (**F**). (**G**) Correlation between FDG and FDOPA uptake.

Circles represent relative tumor volume.
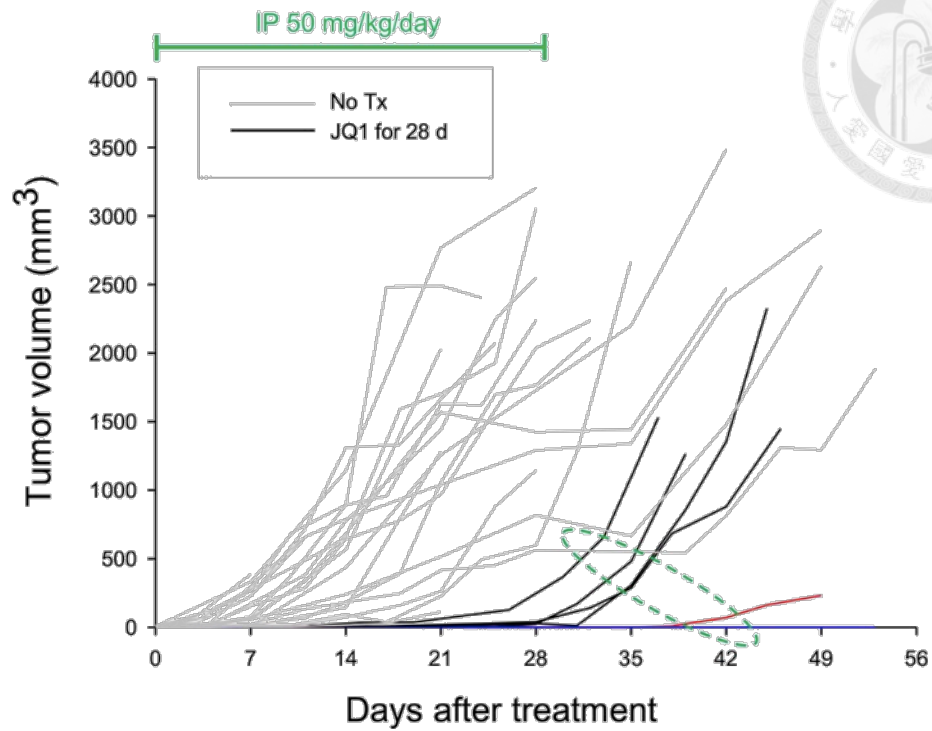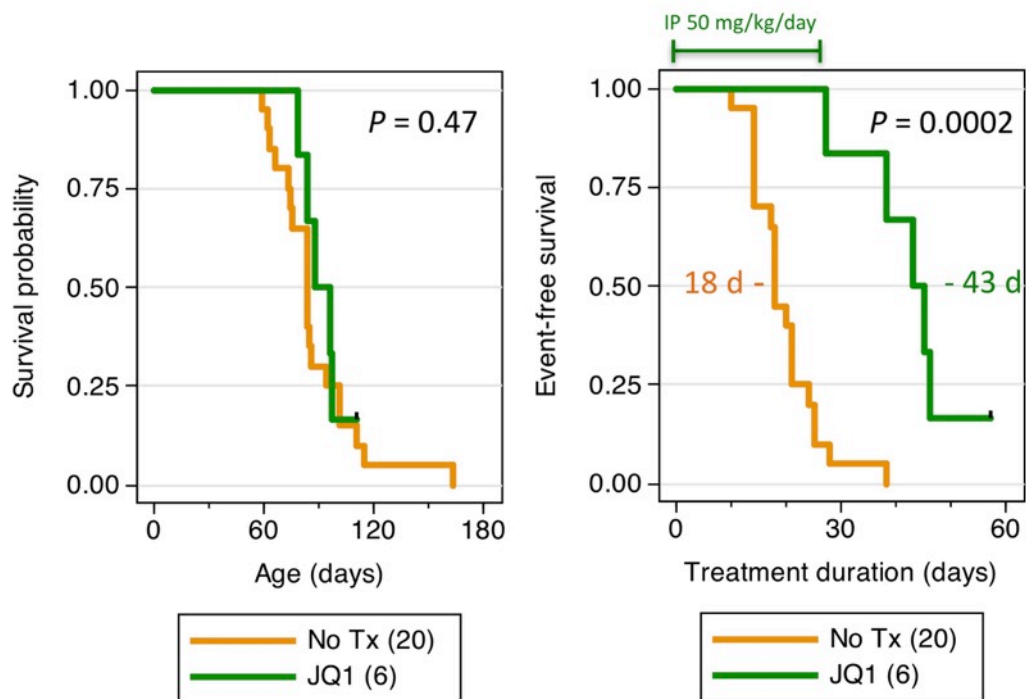
Figure 21. Comparison of BRD4 inhibition and retinoic acid effects.
(**A**) Tumor growth curves of JQ1 (*n* = 6) *vs*. no treatment (*n* = 20). (**B**) Survival curves
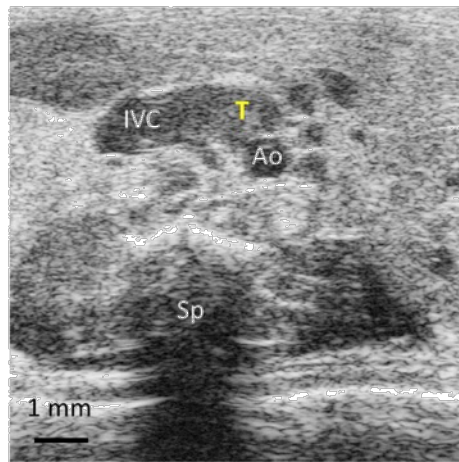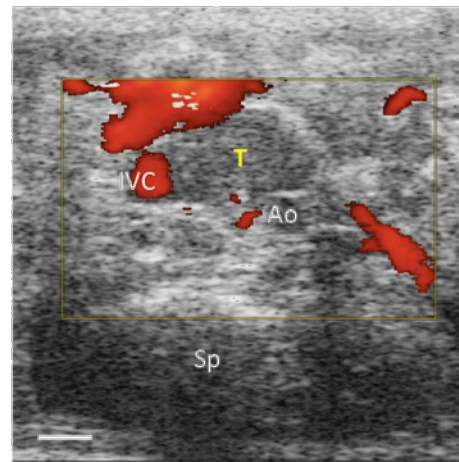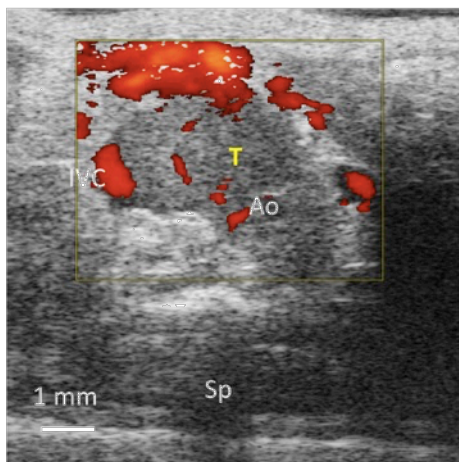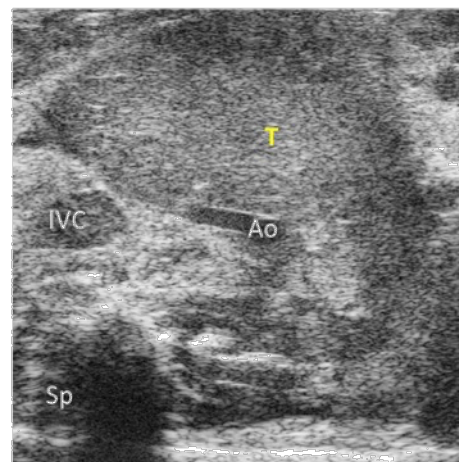by age and by days after treatment.

C
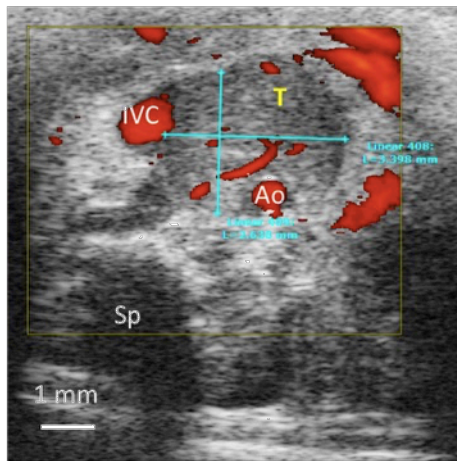
Day 0
18.9 mm³
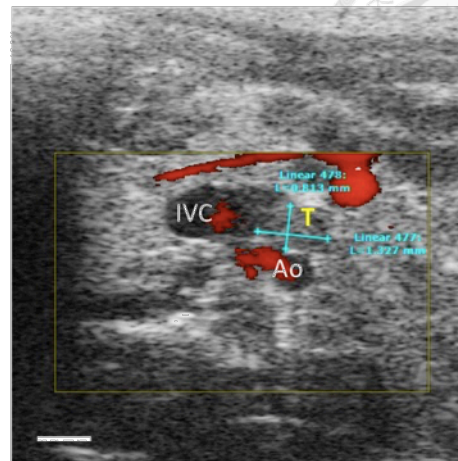
Day 7
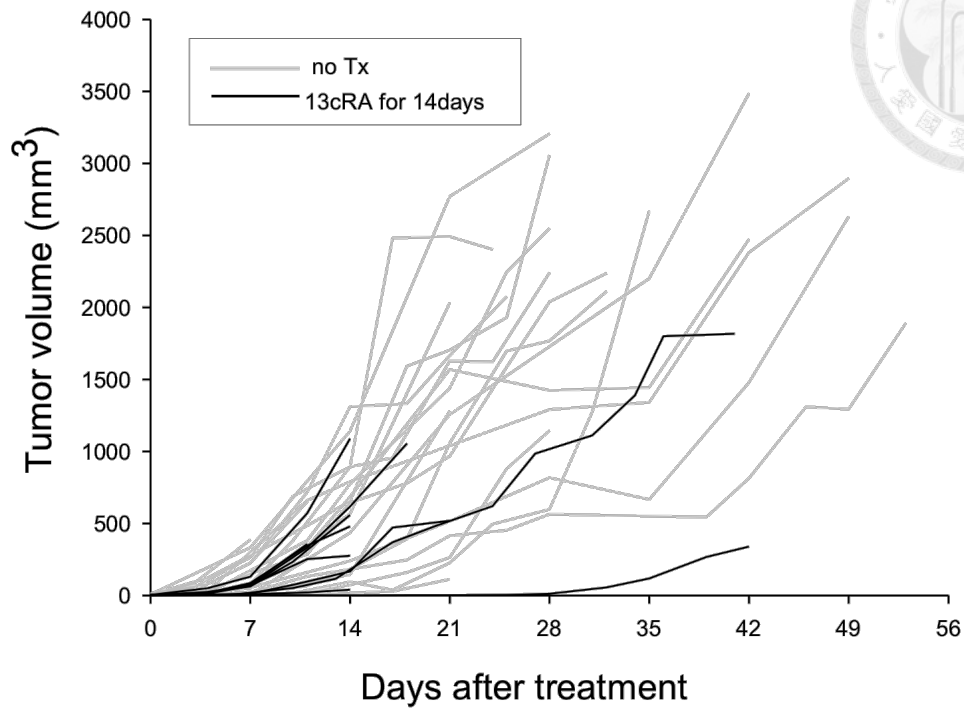0.9 mm³

Day 14
2.4 mm³

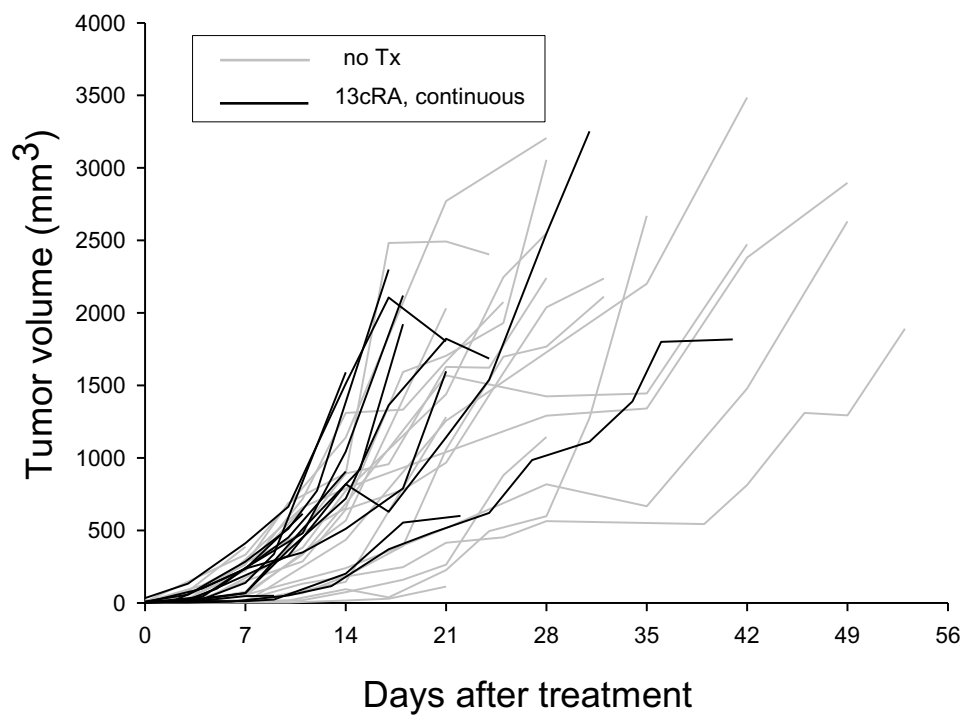Day 21
8.4 mm³

Day 28
28.2 mm³

Day 35
304.9 mm³

E

F

(**C**) Example of tumor volume change during JQ1 treatment for 28 days. The maximal effect was achieved during days 7–14 with diminished tumor vascularization. (**D** and **E**) By contrast, tumor growth curves of therapeutic (**D**) or prophylactic (**E**) use of 13-*cis*-retinoic acid dosing showed no efficacy.

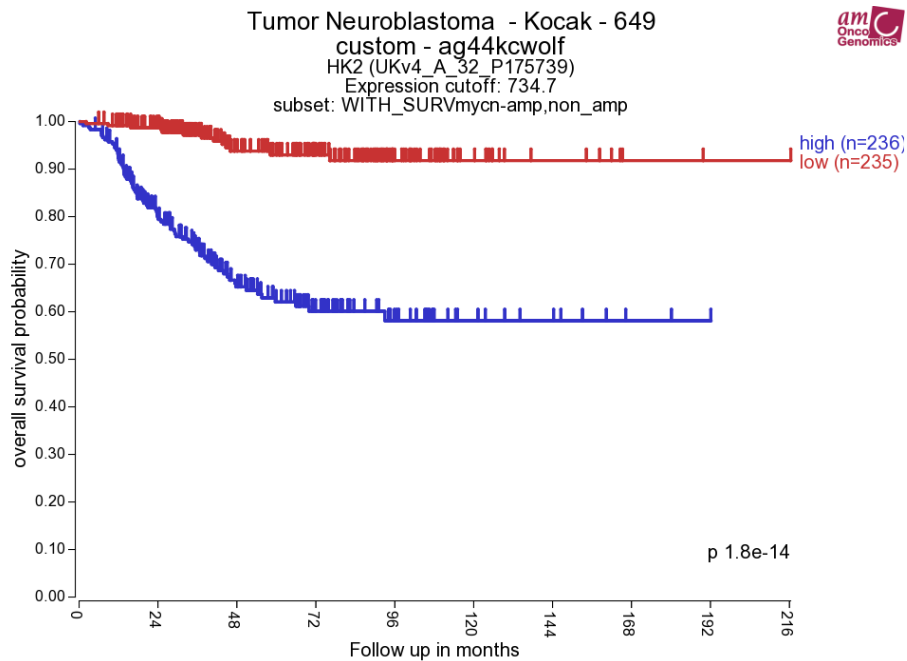Abbreviations: Ao = aorta; IVC = inferior vena cava; T = tumor.
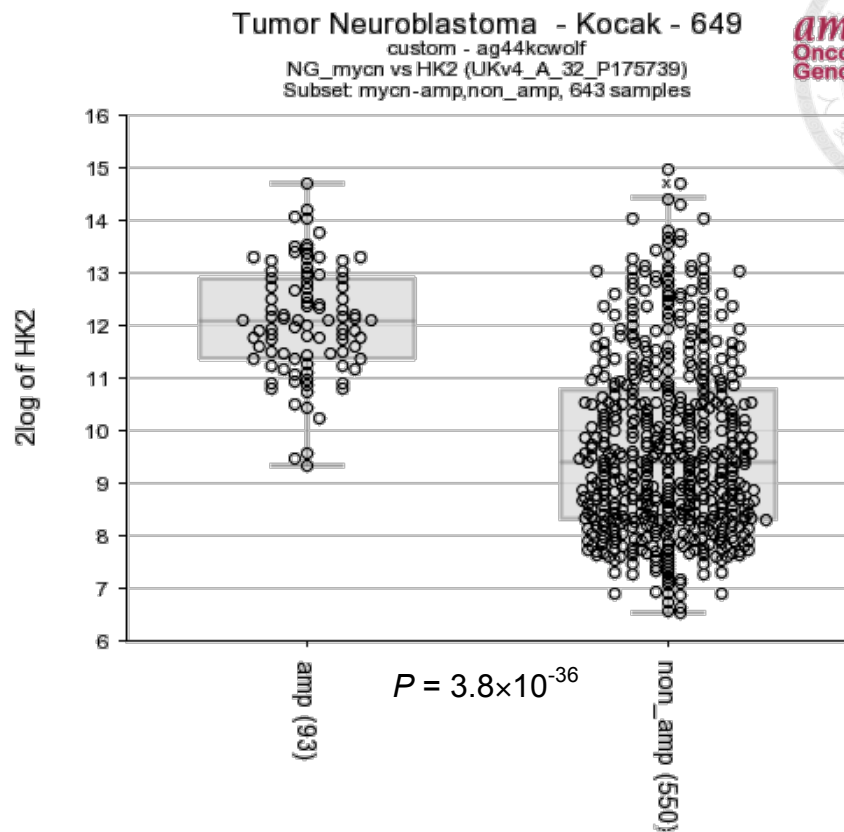
Figure 22. *HK2* expression, *MYCN* status, and prognosis in the Kocak dataset.
(**A**) Primary NB tumors with *MYCN* amplification (left panel) have significantly higher *HK2* expression. (**B**) Higher *HK2* expression (blue) is associated with worse survival outcome. Data are retrieved from the Kocak dataset[78] deposited at R2 (r2.amc.nl)[50,51].

A

Tumor Neuroblastoma - Kocak - 649
custom - ag44kcwolf
NG_mycn vs DDC (UKv4_A_23_P145644)
Subset: mycn-amp,non_amp, 643 samples

$P = 1.6 \times 10^{-65}$

B

Tumor Neuroblastoma - Kocak - 649
custom - ag44kcwolf
DDC (UKv4_A_23_P145644)
Expression cutoff: 60117.0
subset: WITH_SURVmycn-amp,non_amp
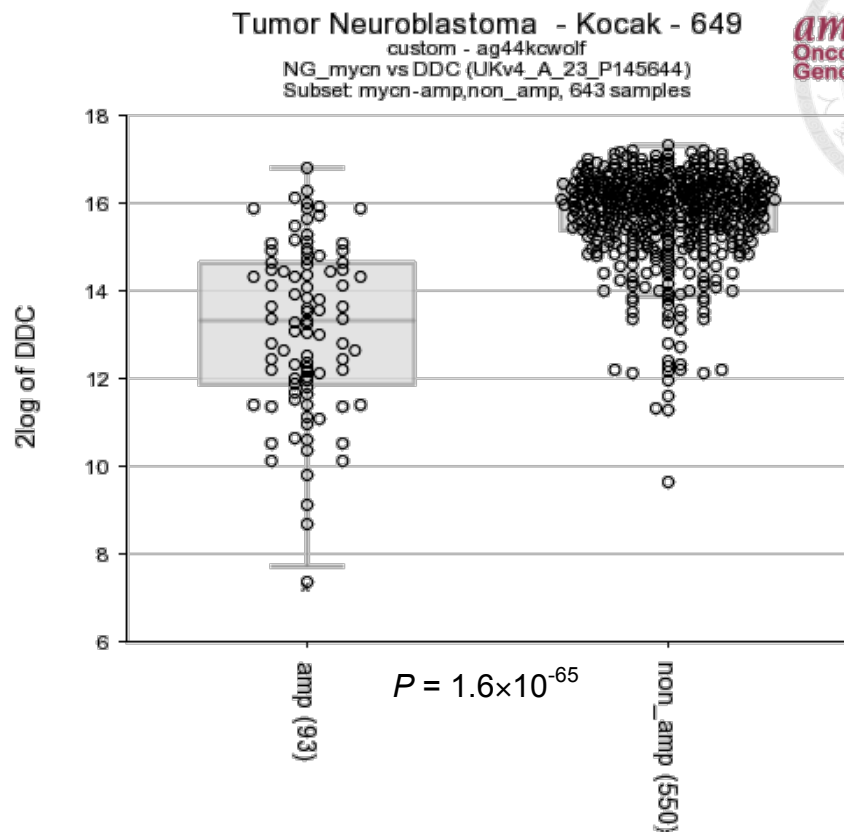
high (n=236)
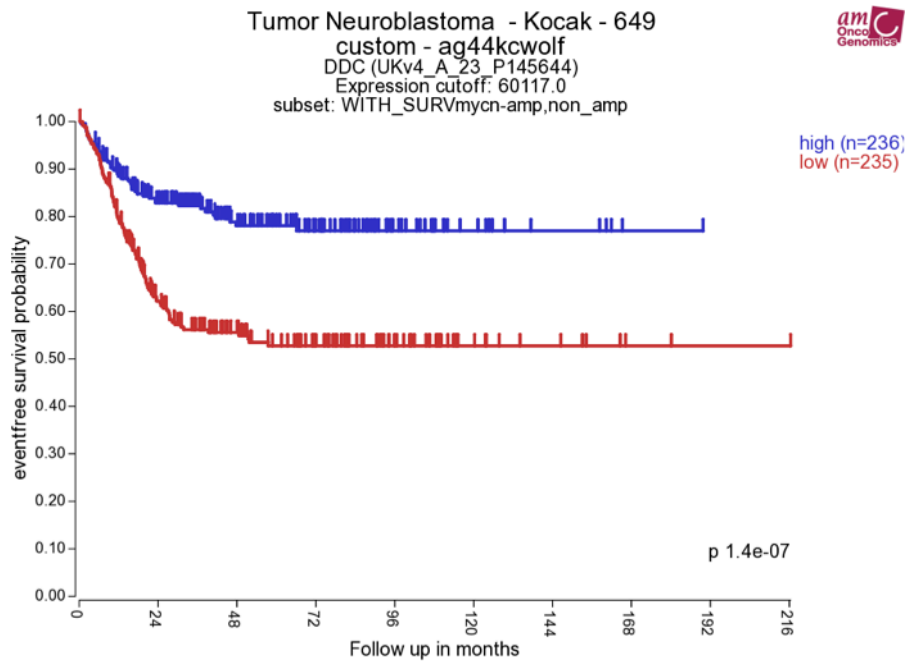low (n=235)

p 1.4e-07

Figure 23. *DDC* expression, *MYCN* status, and prognosis in the Kocak dataset.

(**A**) Primary NB tumors with *MYCN* amplification (left panel) have significantly lower *DDC* expression. (**B**) Lower *DDC* expression (red) is associated with worse survival outcome. Data are retrieved from the Kocak dataset[78] deposited at R2 (r2.amc.nl)[50,51].

8. Appendix: PhD Publications 修業期間發表之論文

Major Publications: († = Equal contribution; * = Corresponding author)

1. Lu MY†, **Liu YL**†, Chang HH, Jou ST, Yang YL, Lin KH, Lin DT, Lee YL, Lee H, Wu PY, Luo TY, Shen LH, Huang SF, Liao YF, Hsu WM*, Tzen KY*, National Taiwan University Neuroblastoma Study Group. Characterization of neuroblastic tumors using ^{18}F-FDOPA PET. *J Nucl Med*. 2013 Jan; 54(1):42–9. (SCI)

2. **Liu YL**†, Lu MY†, Chang HH, Lu CC, Lin DT, Jou ST, Yang YL, Lee YL, Huang SF, Jeng YM, Lee H, Miser JS, Lin KH, Liao YF, Hsu WM*, Tzen KY*. Diagnostic FDG and FDOPA positron emission tomography scans distinguish the genomic type and treatment outcome of neuroblastoma. *Oncotarget*. 2016 Mar; 7(14):18774–86. (SCI)

3. **Liu YL**, Miser JS, Hsu WM*. Risk-directed therapy and research in neuroblastoma. *J Formos Med Assoc*. Dec 2014; 113(12):887–9. (SCI)

4. **Liu YL**†, Lo WC†, Chiang CJ, Yang YW, Lu MY, Hsu WM, Ho WL, Li MJ, Miser JS, Lin DT*, Lai MS*. Incidence of cancer in children aged 0–14 years in Taiwan, 1996–2010. *Cancer Epidemiol*. 2015 Feb; 39(1):21-8. (SCI)

Other Publications:

5. **Liu YL**, Tung CL, Yang YL, Lin DT, Lin KH, Liao HL*. Precursor B-cell lymphoblastic lymphoma of the ear in a seven-year-old child. *J Clin Oncol*. 2012 Jul; 30(21):e184–7. (SCI)

6. Gupta S*, Yeh S, Martiniuk A, Lam CG, Chen HY, **Liu YL**, Tsimicalis A, Arora R, Ribeiro R, SIOP PODC Abandonment of Treatment Working Group. The magnitude and predictors of abandonment of therapy in paediatric acute leukaemia

in middle-income countries: A systematic review and meta-analysis. *Eur J Cancer*. 2013 Jul; 49(11):2555–64. (SCI)

7. Wu PY, Liao YF, Juan HF, Huang HC, Wang BJ, **Liu YL**, Yu IS, Shih YY, Jeng YM, Hsu WM*, Lee H*. Aryl hydrocarbon receptor down regulates *MYCN* expression and promotes cell differentiation of neuroblastoma. *PLoS One*. 2014 Feb; 9(2):e88795. (SCI)

8. Chen SH, **Liu YL**, Hsu WM, Miser JS*. Infants with cancer: A unique population. *J Exp Clin Med*. 2014 Feb; 6(1):1–9.

9. **Liu YL**, Wu PS, Tsai LP, Tsai WH*. Pediatric round pneumonia. *Pediatr Neonatol*. 2014 Dec; 55(6):491–4. (SCI)

10. Weaver MS, Arora RS, Howard SC, Salaverria CE, **Liu YL**, Ribeiro RC, Lam CG*. A practical approach to reporting treatment abandonment in pediatric chronic conditions. *Pediatr Blood Cancer*. 2015 Apr; 62(4):565–70. (SCI)

11. Chen SH, Fan CK, Miser JS, **Liu YL**, Huang YJ, Wang CY*. An infant boy with widespread ecchymoses and severe eosinophilia. *J Microbiol Immunol Infect*. 2015 Apr; 48(2):233–5. (SCI)

12. Kuo YT†, **Liu YL**†, Adebayo BO, Shih PH, Lee WH, Wang LS, Liao YF, Hsu WM, Yeh CT*, Lin CM*. JARID1B expression plays a critical role in chemoresistance and stem cell-like phenotype of neuroblastoma cells. *PLoS One*. 2015 May 7; 10(5):e0125343. (SCI)

13. Huang YY, Tzen KY*, **Liu YL**, Chiu CH, Tsai CL, Wen HP, Tang KH, Liu CC, Shiue CY. Impact of residual ^{18}F-fluoride in ^{18}F-FDOPA for the diagnosis of neuroblastoma. *Ann Nucl Med*. 2015 Jul; 29(6):489–98. (SCI)

14. Wong TT†*, **Liu YL**†, Ho DM†, Chang KP†, Liang ML, Chen HH, Lee YY, Chang FC, Lin SC, Hsu TR, Chen KW, Kwang WK, Hou WY, Wang CY, Yen SH,

Guo WY, Chen YW*. Factors affecting survival of medulloblastoma in children: the changing concept of management. *Childs Nerv Syst*. 2015 Oct; 31(10):1687–98. (SCI)

15. Yang TO, **Liu YL**, Huang WT, Chen MH, Chen PC. Specific and non-specific clinical presentations in the year before the diagnosis of childhood leukaemia. *Pediatr Blood Cancer*. 2016 Aug; 63(8):1387-93. (SCI)